Chapter 5

THIN-SKINNED DEFORMATION OF SEDIMENTARY ROCKS IN VALLES MARINERIS, MARS

Abstract

Deformation of sedimentary rocks is widespread within Valles Marineris, characterized by both plastic and brittle deformation identified in Melas, Candor and Ius Chasmata. We have identified four deformation styles using HiRISE and CTX images: km-scale convolute folds, detached slabs, folded strata and pull-apart structures. Convolute folds are detached rounded slabs of material with alternating dark and light-toned strata that show refolded folds with a fold wavelength of about one kilometer. The detached slabs are also isolated rounded blocks of material, but exhibit only highly localized evidence of stratification. The third style, folded strata, comprises continuously folded layers that are not detached. Finally, pull-apart structures are composed of stratified rock that has broken off into small irregularly-shaped pieces showing evidence of brittle deformation. Some areas exhibit multiple styles of deformation and grade from one type of deformation into another, both laterally and vertically. The deformed rocks are observed over thousands of kilometers, are limited to discrete stratigraphic intervals, and occur over a wide range in elevations. All deformation styles appear to be of likely thin-skinned origin. The orientation of fold axes is bimodal and exhibits northeast-southwest and southeast-northwest components. CRISM reflectance spectra show that some of the deformed sediments contain a component of mono- and polyhydrated sulfates.

Several possible mechanisms could be responsible for the deformation of sedimentary rocks in Valles Marineris, such as subaerial or subaqueous gravitational slumping or sliding and soft-sediment deformation, where the latter could include impact- or seismically-induced liquefaction. These mechanisms are evaluated based on their expected pattern, scale and areal extent of deformation. Deformation produced from slow subaerial or subaqueous landsliding and liquefaction is consistent with the deformation observed in Valles Marineris.

5.1 Introduction

The relative timing between the formation of the Valles Marineris canyon system and the various light-toned stratified deposits observed within the different chasmata remains an outstanding question for the geologic history of Mars. Some of this ambiguity arises from the fact that light-toned deposits with similar morphologic traits are observed in large mounds within the canyon (interior layered deposits, hereinafter referred to as ILDs), on the floor of the chasmata, and occasionally in rock outcrops in the walls of the canyon system. The issue is complicated further because the tectonic activity responsible for the formation of the Valles Marineris likely occurred as several episodes over a long period of time. Thus, it is unclear if the stratigraphy of deposits in one chasm can be directly correlated to the stratigraphy in other chasmata. Although individual light-toned units are not traceable throughout the entire canyon system, some of them exhibit clear evidence of deformation. The relative age of the strata within Valles Marineris, both in the mounds of light-toned layers and in the layers exposed on the surrounding floor, is still debated.

Understanding the mechanism(s) responsible for this deformation, both within and between chasmata, could provide insight into the relative timing of events within the Valles Marineris system.

The ILD are large mounds or mesas believed to be composed primarily of sedimentary rocks. The ILD are found within many of the chasmata in Valles Marineris as well as the peripheral chasmata such as Hebes, Juventae and Ganges (Scott and Tanaka 1986). Some authors have suggested that the ILD predate chasma formation, because layered materials are found in some chasma wall spurs (Malin and Edgett 2000; Montgomery and Gillespie 2005; Catling et al. 2006). Other studies based on geomorphology and structural relationships have suggested that the ILD accumulated on top of Noachian-aged bedrock during or after chasma formation (Scott and Tanaka 1986; Lucchitta 1990; Peulvast et al. 1993; Lucchitta et al. 1994; Schultz 1998; Okubo et al. 2008). Unfortunately, most locations lack unambiguous stratigraphic contacts between the ILD and canyon walls, making a definitive determination of the relative age of strata within the chasma difficult. Several lithologic interpretations of the ILD have been suggested, including lacustrine deposits (Nedell et al. 1987; Komatsu et al. 1993; Malin and Edgett 2000), eolian deposits (Nedell et al. 1987), volcanic (ash) deposits (Lucchitta 1990; Lucchitta et al. 1994; Chapman and Tanaka 2001), and lithified mass-wasted wall rock material (Nedell et al. 1987; Lucchitta et al. 1994).

The stages and timing of events in the evolution of Valles Marineris are also still debated, but the general framework that has emerged is as follows (Lucchitta et al. 1994;

Mege and Masson 1996; Schultz 1998; Peulvast et al. 2001; Okubo et al. 2008): 1. During Late Noachian to Early Hesperian time, there was dike emplacement radial to Syria Planum and the formation of graben and pit craters in the future region of Valles Marineris. 2. After Early Hesperian time, localized subsidence and sedimentary basin formation occurred in association with the earlier radial dikes, grabens and pit craters. Subsidence may have been related to melting of subsurface ice, dissolution of pre-existing chemical precipitates and formation of the chaotic terrain. The ILD were deposited in the subsiding basins. 3. Rifting during the Amazonian in the area of the ancestral basins and the ILD associated with deep-seated faults; rifting may have been driven by Tharsis-related stresses and may have connected the ancestral basins to one another. Following rifting, landslides and erosion further widened the ancestral basins and rifts to their present form.

An alternative model for the formation of Valles Marineris was proposed by Montgomery et al. (2009). They interpreted the formation of Valles Marineris and the Thaumasia plateau as a "mega-slide" characterized by thin-skinned deformation involving gravity sliding, extension, and broad zones of compression. The gentle slope of 1° in the region makes gravitational body forces too small to drive deformation of basalt, but slip along a detachment could have occurred if geothermal heating and topographic loading of salt or mixtures of salt and ice allowed for development of a layer-parallel zone of weakness (Montgomery et al. 2009). They proposed that the Valles Marineris reflects extension, collapse and excavation along fractures radial to Tharsis. They also suggest that deformation represented by compressional features in the highlands on the southern margin of the Thaumasia Plateau and the wrinkle ridges on the plateau imply décollements at multiple levels and several phases of deformation. Similar features are observed in terrestrial salt-based fold and thrust belts, which support regularly spaced folds of weak vergence and exhibit abrupt changes in deformational style at their margins (Davis and Engelder 1985).

Isolated occurrences of deformed strata were previously identified in western Melas and western Candor Chasmata and are thought to represent subaerial landslides of large interior layered deposits found in those chasmata (Okubo et al. 2008), subaqueous landslides of wallrock (Weitz et al. 2003), dry debris avalanches (Skilling et al. 2002), or gravity gliding of ILD (Lucchitta 2008). However, Context Camera (CTX) images provide nearly complete coverage of Valles Marineris and have revealed many more exposures of deformed strata that were identified and mapped during the course of this study. Recent High Resolution Imaging Science Experiment (HiRISE) images and HiRISE-based digital elevation models (DEMs) allowed a detailed look at the morphology of these deposits as well as their stratigraphic position.

In this study we identify many more occurrences of deformed strata on the floors of Ius, Melas and Candor Chasmata in Valles Marineris. The morphology and composition of these deposits are examined in detail to evaluate how the sediments were deformed and the relative timing of the deformation with respect to the formation of Valles Marineris.

5.2. Geologic Setting

Candor Chasma is a large depression (lowest elevation is approximately -5 kilometers) located in the northern part of Valles Marineris; it was mapped previously by Scott and Tanaka (1986) and Lucchitta (1999). Candor has several occurrences of ILD that have been studied using both spectral (Mangold et al. 2008b; Murchie et al. 2009; Roach et al. 2009a) and structural data (based on image-derived digital elevation models; Fueten et al. 2006; Fueten et al. 2008; Okubo et al. 2008). Lucchitta (1999) mapped the ILD as Hesperian or Amazonian in age, and Fueten et al. (2006) showed that the layers in the ILD (near the two white circles in Fig. 5.1A) dip away from the peak of the deposits and are subhorizontal in the surrounding plains. Fueten et al. (2006) interpreted this structural pattern as indicating that the ILD drape preexisting topography and lack evidence of large scale faulting indicative of chasma formation; this implies that the layers post-date chasma formation. Folded strata near the southern margin of Candor (locations C1 and C2 in Fig. 5.1A) generally dip towards the center of the chasma which is consistent with deposition in a preexisting basin (Okubo et al. 2008, Okubo 2010). Okubo et al. (2008) interpret the folds in this area as the result of southward-directed landsliding of the ILD.

Murchie et al. (2009) found that the lower and middle parts of the ILD in western Candor are dominated by monohydrated sulfate whereas the upper beds are dominated by polyhydrated sulfates. Roach et al. (2009a) found that the ILD in eastern Candor are composed of interlayered mono- and polyhydrated sulfates. Changes in the hydration state of these sulfates (mono or poly) have not been detected over several years of observations, which indicates that the monohydrated sulfates are not actively being altered to polyhydrated phases or polyhydrated phases dehydrated to monohydrated phases on short timescales (Roach et al. 2009a).

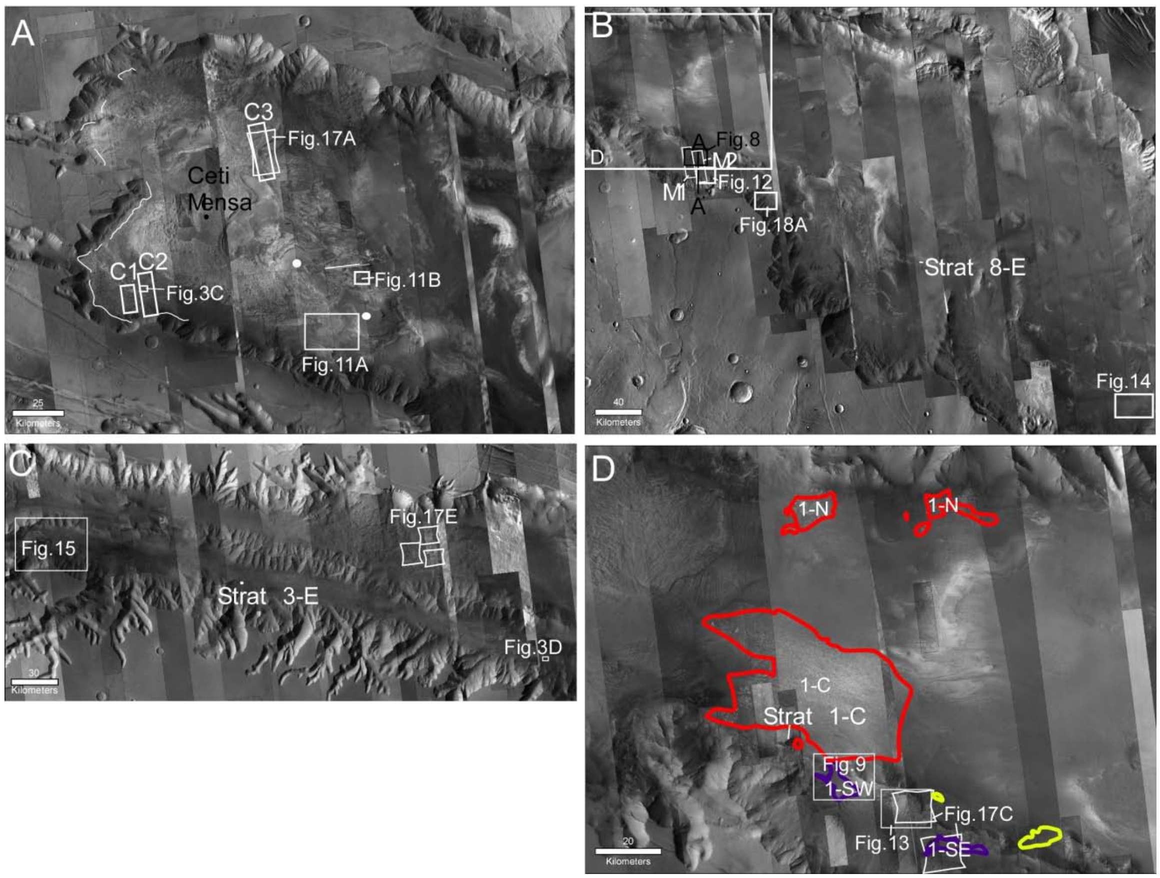

Fig 5.1. A.) Location map in Candor Chasma. White boxes labeled C1, C2 and C3 represent locations of DEM's discussed in the text. White boxes show locations of Figs. 5.11A and 5.11B and the CRISM image in Fig. 5.17A. White line traces out the topographic bench. Black circle indicates location of Ceti Mensa mound, and the two white circles indicate two other topographic highs in western Candor. B.) Location map in Melas Chasma with white boxes showing the locations of Figs. 5.1D, 5.12, 5.14 and 5.18A and black box showing location of Fig. 5.8. White rectangles labeled M1 and M2 represent locations of DEM's discussed in text. The black line shows the location where cross-section A-A' was measured and the white line where stratigraphic column 8-E was measured. White line shows location of cross-section A-A' from Fig. 5.6. C.) Location map in Ius Chasma with white boxes showing the locations of Figs. 5.3D, 5.15 and the CRISM images in 5.17E. The white circle shows where stratigraphic column 3-E was measured. D.) Zoomed in portion of Melas Chasma indicated in B. White boxes show locations of Figs. 5.9, 5.13 and the CRISM images from 5.17C. White line shows where

stratigraphic column 1-C was measured. Purple outlines show locations of outcrops showing convolute folds, yellow shows folded strata and red shows detached slabs. Outcrops are labeled with designations referred to in Table 5.1.

Melas Chasma is another deep depression (lowest elevation is approximately -5 km) that is located within central Valles Marineris. Several large ILD are located along the southern portion of Melas Chasma and OMEGA data of these ILD exhibit spectral signatures consistent with the presence of monohydrated (kieserite) and polyhydrated sulfates (Gendrin et al. 2005). Several interesting features have been discovered in a small basin in southwestern Melas Chasma (informally called southern Melas basin) including dense valley networks (Quantin et al. 2005), clinoforms (Dromart et al. 2007), and possible sublacustrine fans (Metz et al. 2009b). These features indicate the presence of liquid water and a potentially deep lake in the basin. Large exposures of detached slabs have been identified on the floor of western Melas Chasma (Skilling et al. 2002; Weitz et al. 2003) and have been interpreted to be the result of landsliding.

Ius Chasma is a large trough (lowest elevation is approximately -4.5 km) in western Valles Marineris that shows a regular, nearly rectangular geometry (Schultz 1991). This trough is thought to have formed by normal faulting and to postdate the ILD (Schultz 1998). No mounds of layered material are observed in Ius Chasma, but spectral signatures of kieserite, polyhydrated sulfates, clays and hydrated silica have been identified on the floor of eastern Ius Chasma (Gendrin et al. 2005; Roach et al. 2009b).

5.3. Methods

A mosaic of projected CTX (5 m/pixel) and HiRISE images (0.25-0.5 m/pixel) covering Valles Marineris was overlain onto a base map of THEMIS daytime IR images using ArcGIS®. CTX coverage over Valles Marineris is nearly complete, but HiRISE images cover only select locations. The entire Valles Marineris canyon was examined and areas showing deformation were identified and mapped (Fig. 5.2). Four primary styles of deformation were noted: large-scale convolute folds, detached slabs, folded strata and pull-apart structures (Fig. 5.3). Detached slabs are rounded blocks of detached material that only locally show evidence of layering (Fig. 5.3A), and convolute folds are defined similarly but are composed of alternating dark and light-toned strata that exhibit disharmonic folding (Fig. 5.3B). Folded strata are defined as laterally continuous layered materials, and the trend of their fold axial traces is not uniform (Fig. 5.3C). Pull-apart structures are composed of fragments of strata that have broken off into small irregularly-shaped pieces (Fig. 5.3D). Deformed areas were separated into eight regions as shown in Fig. 5.2. Regions are defined as groupings of nearby outcrops of various types of deformed strata, whereas outcrops are continuous exposures of one type of deformed strata.

The styles of deformation called detached slabs and convolute folds are composed of detached blocks. These blocks are inferred to have a sedimentary origin, though this is difficult to confirm with the exception of a few cases. Supporting a sedimentary origin are the observations that some of the blocks contain finely-stratified deposits and the spectroscopic signature of evaporite minerals, including kieserite and polyhydrated sulfates. In general, we regard these materials to now be (at least partly) lithified rocks; at the time of deformation they could have been strata formed of unconsolidated loose sediments, water-saturated sediments, loosely cemented sediments, or fine-grained sediments with high cohesion. The major and minor axes of the detached slabs and convolute folds were measured, and histograms of the size distributions for each region are shown in Figure 5.4. Many of the regions consist of several outcrops of deformed strata and in these cases the size distribution of blocks for each outcrop are reported separately (e.g. Fig 5.1D). The ratio of the major to minor axis of each block was computed and the areal size of each block was also measured. Statistics on the sizes of the blocks are shown in Table 5.1. In areas with only a few blocks exposed, the sizes of all blocks were measured. In areas with many blocks exposed, the size of blocks in areas with HiRISE coverage was measured.

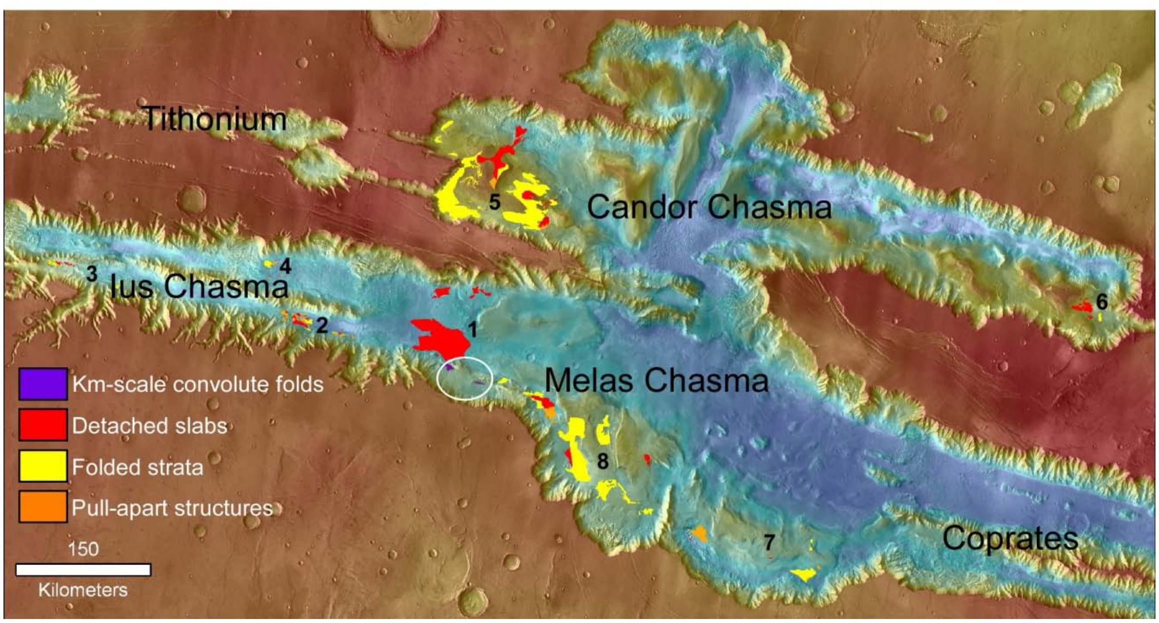

Fig 5.2. MOLA colorized elevation base map with eight regions of deformation mapped and labeled. Four styles of deformation were observed, km-scale convolute folds (purple), detached slabs (red), folded strata (yellow), and pull-apart structures (orange). Deformation was observed in Ius, Melas and Candor Chasmata, but not in Coprates or Tithonium Chasmata. White circle shows locations of km-scale convolute folded outcrops.

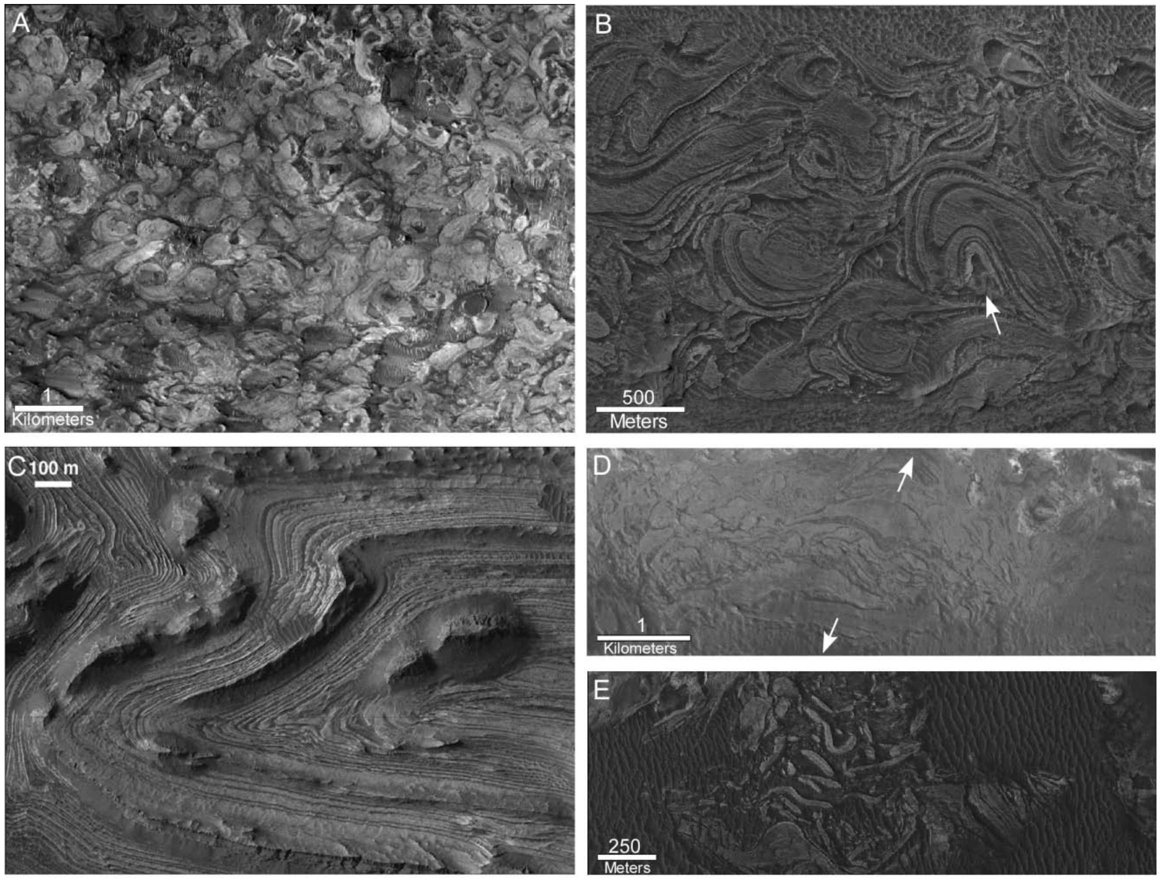

Fig 5.3. Four deformation styles were observed in Valles Marineris. A.) Detached slabs; this example is from Melas Chasma (P05_002828_1711). B.) Km-scale convolute folds which are observed only in two exposures in southern Melas basin (PSP_007087_1700). This example is from the easternmost exposure. White arrow shows location of disharmonic fold. C.) Folded strata; this example is from Candor Chasma (PSP_001918_1735). D.) Pull-apart structures; this example is from Ius Chasma (P07_003606_1727). Note how the strata look as if they have been pulled apart in the direction of the arrows. E.) Pull-apart structures; here the strata have been pulled apart to a greater extent than in d. The strata are expressed as irregularly shaped pieces (PSP_003593_1725).

Five Digital Elevation Models (DEMs) were constructed using the methods of Kirk et al. (2008) and cover three separate deformed areas (Fig. 5.1). These DEMs were evaluated to understand the three-dimensional geometry of the various deformation patterns. Three DEMs were produced based on images obtained in Candor Chasma. These consisted of the following stereo pairs (C1) PSP_001918_1735 (28.5 cm/pixel) and PSP_001984_1735 (26.2 cm/pixel) centered at –6.444˚ N, 283.221˚ E and with a vertical precision of 0.13 m; (C2) PSP_003474_1735 (27.5 cm/pixel) and PSP_003540_1735 (26.4 cm/pixel) centered at -6.433˚ N, 283.216˚ E and with a vertical precision of 0.12 m; (C3) PSP_008023_1745 (26.4 cm/pixel) and PSP_010238_1745 (27.3 cm/pixel) centered at -5.295° N, 284.166° E and with a vertical precision of 0.12 m. Two DEMs were in Melas Chasma and consisted of stereo pairs (M1) PSP_007087_1700 (26.7 cm/pixel) and PSP_007667_1700 (28.8 cm/pixel) centered at -9.816° N, 283.503° E and with a vertical precision of 0.13 m and (M2) PSP_007878_1700 (26.5 cm/pixel) and PSP_008735_1700 (28.9 cm/pixel) centered at -9.755° N, 283.4° E and with a vertical precision of 0.13 m. With a stereo convergence angle of 25° and assuming 1/5 pixel correlations, the vertical precision of the DEM is $x/(5\tan 25°)$ where x is the size of the pixel. The precision is limited by the DEM's 1 m postings in steep areas.

Two stratigraphic columns were measured in the southeastern outcrop exposure of convolute folds in region 1 (in Melas Chasma) using DEM's M1 and M2 (Fig. 5.1B, D and 5.5). A stratigraphic column was measured in the northern section of region 5 in Candor Chasma using DEM C3 (Fig. 5.1A and 5.5). The dips of bedding in these areas were obtained by using planar fits to bedding visible in the HiRISE images associated with the derived DEMs. Linear segments were traced out along well-exposed layers with some natural curvature to provide constraints on the three-dimensional geometry of the layer. We employed the method of Lewis et al. (2008b), which uses principal component analysis to ensure that the layers are well-fit by a plane. Additional stratigraphic columns in areas without DEM coverage were estimated using a combination of Mars Orbital Laser Altimeter (MOLA) data and visual images. This method was used for the stratigraphic columns measured in the southwest and central outcrops in region 1, the outcrops in region 3, and the outcrops in region 7 and 8 (Fig. 5.5). MOLA contour lines were used to estimate the thickness of stratigraphic units and elevations of contacts. True bed thicknesses in these columns are not known, because the dips of the bedding in these areas cannot be properly calculated without a high-resolution DEM. A cross-section was constructed for the southeastern outcrop in region 1 using a MOLA topographic profile from the north to the south end of southern Melas basin (Figs. 5.1B and 5.6). The DEM of this area was used to measure the true dips of beds shown in this section.

The exposed area of each deformed unit was measured in ArcGIS. For several of the areas, both lower and upper contacts for the deformed strata were visible and a thickness for the deformed units could be calculated. For other areas the thickness was estimated using gridded MOLA data. For regions where an upper or lower contact was not visible, a minimum thickness was estimated using MOLA data. The volume of each area was calculated by multiplying the measured area by the measured or estimated thickness. The length of each deformed area was measured in a direction perpendicular to the nearest chasma wall.

The axial traces of folds in the deformed regions were mapped wherever they were visible. The orientations of these folds with respect to north were measured, and rose diagrams of the directions were constructed (Fig. 5.7). Parts of the southern portion of region 5 were covered by DEM's C1 and C2, and the fold axes in these areas were mapped by Okubo et al. (2008) and (Okubo 2010), who measured the trend and plunge of fold axes in these areas and found the plunges were relatively shallow (~5°).

Region	Outcrop	Mean long dimension (m)	Mean short dimension (m)	Long dimension range (m)	Short dimension range (m)	Mean Area (m^2)	Mean Ratio	N
1	SE	647	451	394-1157	220-826	234,310	1.5	6
1	SW	459	247	160-1005	95-439	114,621	1.96	41
1	C	466	265	110-1086	64-665	124,507	1.81	107
2	E	192	107	91-298	51-175	17,740	1.91	21
2	W	349	209	92-777	55-557	74,139	1.81	63
3	E	-	-			-	-	-
3	W	397	249	143-796	106-369	94,531	1.63	18
4	C	135	83	80-214	41-118	9,849	1.68	15
1	N	413	272	119-686	84-514	100,299	1.56	40
5	E	347	195	80-993	59-599	89,632	1.79	18
5	W	-	-			-	-	-
5	N	265	146	63-815	29-307	44,882	1.82	37
5	C	581	269	204-867	96-544	114,325	2.22	38
6	C	208	123	90-464	55-229	24,320	1.73	35
7	E	-	-			-	-	-
7	W	-	-			-	-	-
8	E	470	259	171-847	98-538	113,051	1.98	22
8	W	394	254	159-823	113-442	86,089	1.62	33

Table 5.1. The mean sizes and the range in sizes of the blocks of material forming the detached slabs and convolute folds are listed for each region. Some regions have been subdivided into several outcrops (C-central, E-east, W-west, N-north, S-south). Ratio is the ratio of mean long dimension to mean short dimension. N is the number of blocks measured in each outcrop. Regions without entries did not have any exposures of detached slabs or convolute folds. Convolute folds are only observed in the SE and SW outcrops of region 1; all other measurements are for detached slabs.

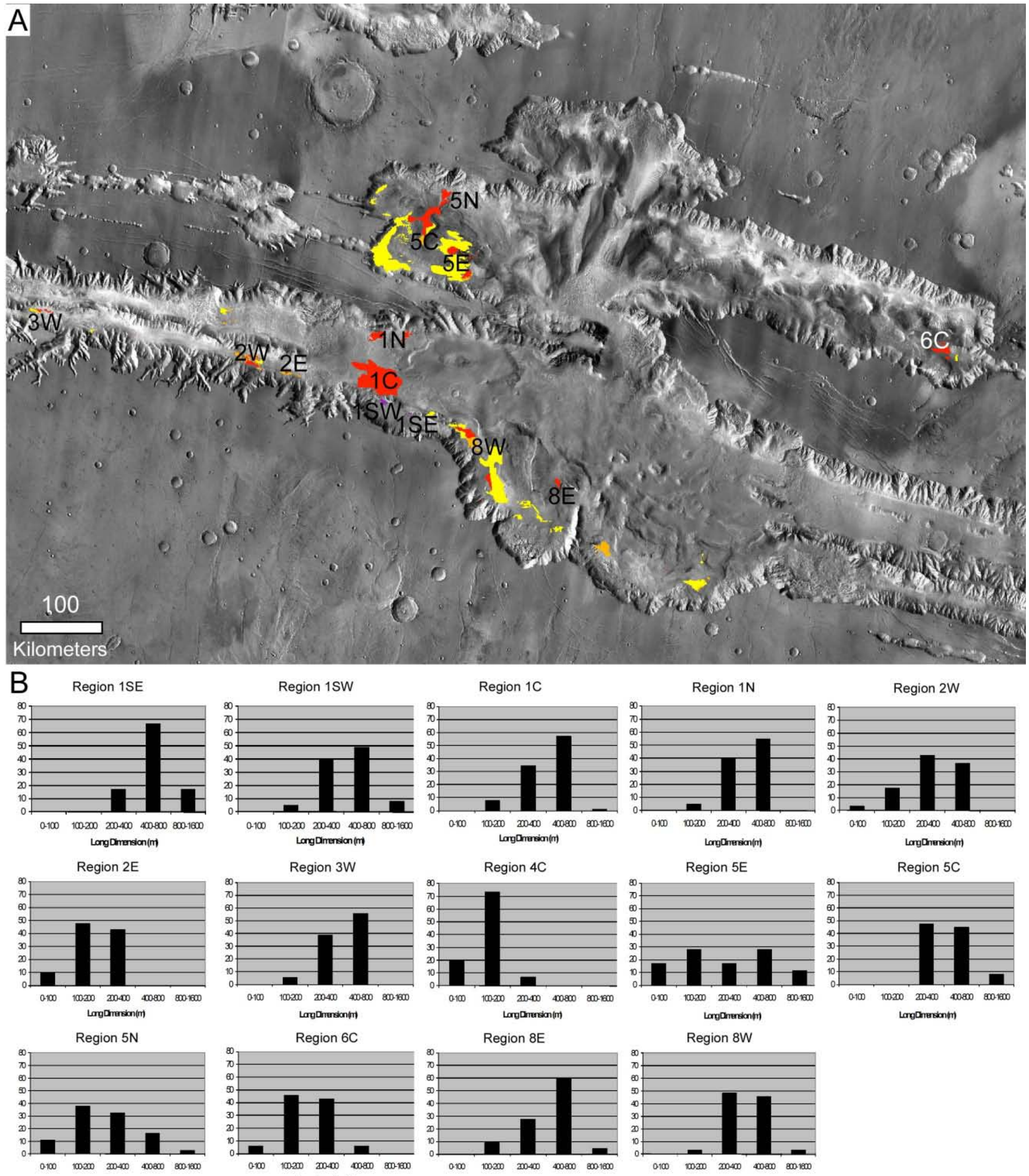

Fig 5.4. A.) THEMIS IR basemap with locations of outcrops labeled where block sizes were measured. B.) Histograms of the long dimension of the convolute folds and the detached slabs. The axes for each histogram are the same; the vertical axis is the percent of blocks that falls into a particular size range, and the horizontal axis are bins of long block dimension. Blocks are larger in Melas Chasma, smaller in Ius Chasma and show a more even distribution of size classes in Candor Chasma.

CRISM full-resolution target images (FRTs) exist for many of the deformed areas and were examined in this study to determine the composition of the beds (CRISM images listed in Table 5.2 and locations of key images shown in Fig. 5.1). These images have 544 spectral bands with 6.55 nm sampling and a resolution of ~18 m/pixel. The CRISM data were converted to I/F using the methods of Murchie et al. (2007, 2009). The data were corrected for photometric effects by dividing I/F values by the cosine of the solar incidence angle and atmospheric attenuation was accounted for by dividing by a scaled atmospheric transmission spectrum obtained during an observation crossing Olympus Mons (Mustard et al. 2008). The latter step corrects for atmospheric gases but does not account for aerosols. Map-projected CRISM images were imported into ArcGIS to integrate with HiRISE, CTX, and MOLA data. CRISM spectra presented here are I/F ratio spectra created by averaging pixels (spectra) corresponding to distinct geologic units and dividing those average spectra by an average of pixels (spectra) from a spectrally 'bland' area that usually corresponds to Mars dust (e.g., Milliken et al, 2008).

Melas Chasma	**Ius Chasma**	**Candor Chasma**
FRT000043C6	FRT00008950	FRT0000400F
FRT00006347	FRT00009445	FRT000039F3
FRT0000AC5C	FRT0000D5F8	FRT0000593E
FRT0000AD3D	FRT0000B347	HRL000033B7
FRT0000C00F	FRT0000CAE2	FRT000103C5
FRT0000A244	FRT0000873F	HRL00007C86
FRT0000AA51	FRT000027E2	FRT0000BE37
FRT0000A3E9	FRT0000905B	
FRT000061BD	FRT0000A396	
HRL000123C5		
FRT000136D3		
FRT0001070E		

Table 5.2. List of CRISM targeted images examined in this study.

5.4. Results

5.4.1 Deformation Styles

Mapping of deformed strata in Valles Marineris yields four primary deformation styles: km-scale convolute folds, detached slabs, folded strata, and pull-apart structures (Fig. 5.3). Some areas exhibit multiple styles of deformation and grade from one type of deformation into another, both laterally and vertically. Deformed strata have been identified in eight different regions throughout Ius, Melas and Candor Chasmata. Tithonium and Coprates Chasmata were also examined for this study, but deformed strata have not yet been observed in these locations. Regions are defined as groupings of nearby outcrops of various types of deformed strata. Outcrops are continuous exposures of one type of deformed strata.

Km-scale convolute folds were only observed in two exposures in Melas Chasma, both in relatively small outcrops in a small basin in southwestern Melas Chasma (SE and SW outcrops of region 1). The convolute folds are detached rounded slabs of alternating dark and light-toned strata that exhibit disharmonic folding with a fold wavelength of about one kilometer (Fig. 5.3A). The strata that appear dark-toned may be more friable and have been preferentially eroded out and filled in with dark-toned sand. Sequences of strata can be traced between some of the slabs (Fig. 5.8). Several fold geometries are observed

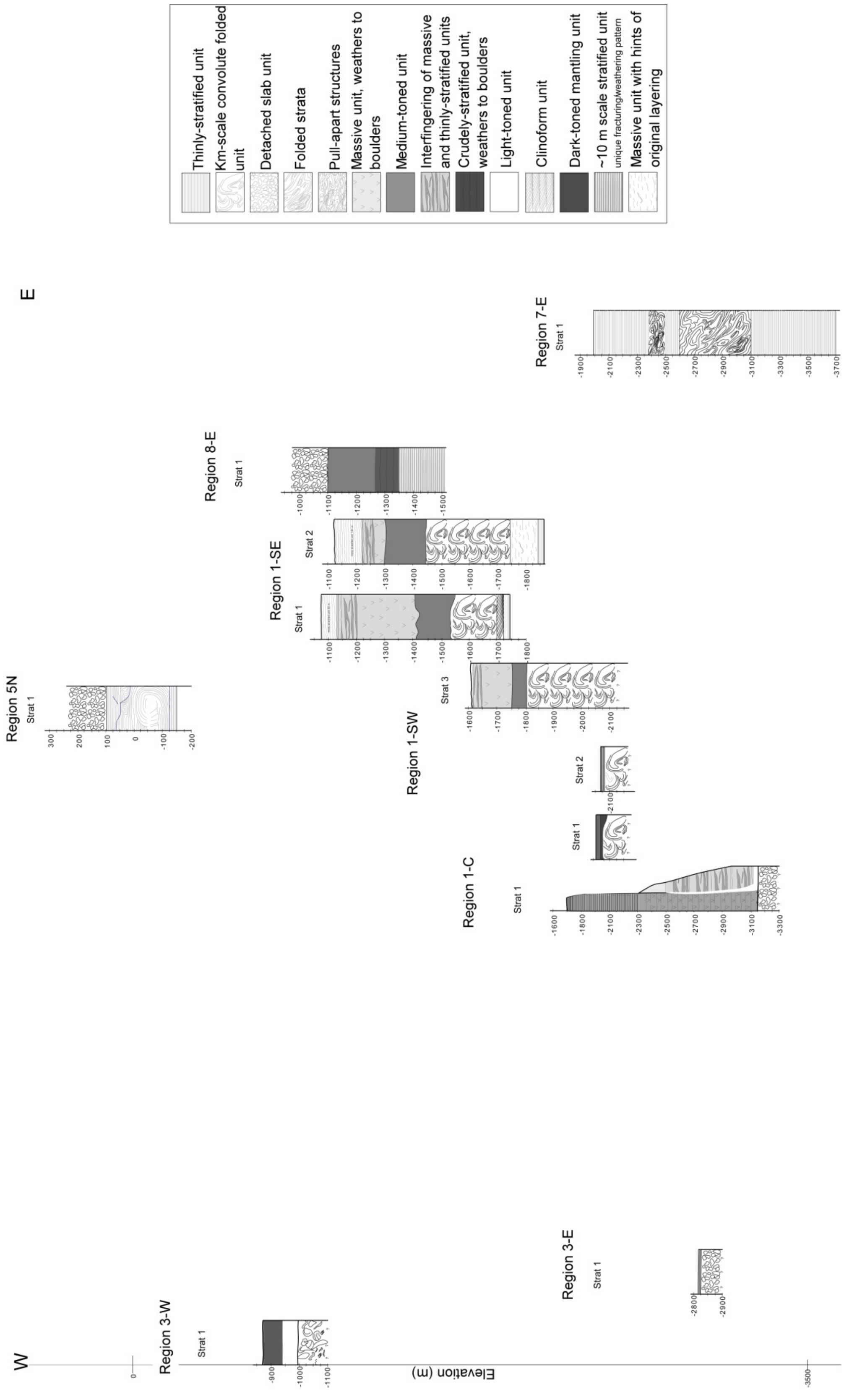
W
E
Elevation (m)
Region 3-W
Strat 1
Region 3-E
Strat 1
Region 1-C
Strat 1
Region 1-SW
Strat 1
Strat 2
Strat 3
Region 5N
Strat 1
Region 1-SE
Strat 1
Strat 2
Region 8-E
Strat 1
Region 7-E
Strat 1
Thinly-stratified unit
Km-scale convolute folded unit
Detached slab unit
Folded strata
Pull-apart structures
Massive unit, weathers to boulders
Medium-toned unit
Interfingering of massive and thinly-stratified units
Crudely-stratified unit, weathers to boulders
Light-toned unit
Clinoform unit
Dark-toned mantling unit
~10 m scale stratified unit
unique fracturing/weathering pattern
Massive unit with hints of original layering

Fig 5.5. Eleven stratigraphic columns were measured based on HiRISE DEM's and MOLA gridded data in Ius, Melas, and Candor Chasmata. Stratigraphic columns are labeled by region number and outcrop location and are arranged from west to east. Stratigraphic columns are arranged vertically such that relative elevations correlate (except for stratigraphic columns from regions 1-C and 7-E which are on a different vertical scale than the other sections - these two sections are correlated so that they line up at only at -2100 m, and the stratigraphic section from region 5N which occurs at a much higher elevation than the other sections).

including parallel, disharmonic and similar folds (Fig. 5.3A). In the southwestern outcrop of region 1, the km-scale convolute folds grade into detached slabs (Figs. 5.1D and 5.9). Table 5.1 shows the range and mean block sizes of the convolute folds as well as the mean ratio of the long to short dimension. Most blocks are elliptical in shape, and the convolute folds tend to be larger than the detached slabs.

The detached slabs are also rounded blocks of detached material, but they only locally show evidence of layering (Fig. 5.3B). These have previously been classified as 'blocky deposits' by Weitz et al. (2003). In most areas the slabs appear featureless, but in a few locations the slabs do show folded strata and appear to flow around each other (see Fig. 6 in Weitz et al. 2003). Some of the blocks show resistant edges (Fig. 5.10). Detached slabs are found in many exposures in Ius, Melas and Candor Chasma (Fig.5. 2). The mean and range of sizes of detached slabs are given in Table 5.1. Similar to the convolute folds, detached slabs tend to be elliptical, but the detached slabs have a larger range of sizes, including some small slabs (~30 m).

The folded strata are laterally continuous layered materials and the trend of their fold axial traces is not uniform (Fig. 5.3C). Folded strata exhibit many geometries including both similar folds and concentric folds, in addition to domes, basins, crescents, mushrooms and other interference patterns. Where fold axes can be determined in detail, they indicate non-cylindrical fold geometry (Okubo 2010). Fold wavelengths range in size from 250 m to 2700 m. There are large exposures of folded strata in Candor Chasma, some of which were studied by Okubo et al. (2008) and Okubo (2010). Folded strata also occur throughout Ius and Melas Chasmata.

The pull-apart structures are areas that show evidence of possible brittle deformation and appear to be composed of fragments of strata that have broken off into small irregularly-shaped pieces. In some areas the fragmented strata look as if they could be fit back together similar to puzzle pieces, whereas in other areas the fragmentation proceeded to a larger degree and only irregularly shaped fragments of strata remain (Fig. 5.3 D-E). It is possible that some of these structures may have originally been detached slabs that have experienced differential erosion to produce irregularly shaped blocks. Pull-apart structures occur in Ius, Melas and Candor Chasmata.

In some areas the different styles of deformation can be seen to grade into each other (Fig. 5.11). Thus, the four types appear to form a continuum of deformation styles that likely depend on the orientation of the principal stresses and the strain rate. The grading in deformation styles occurs laterally as well as vertically, with folded strata

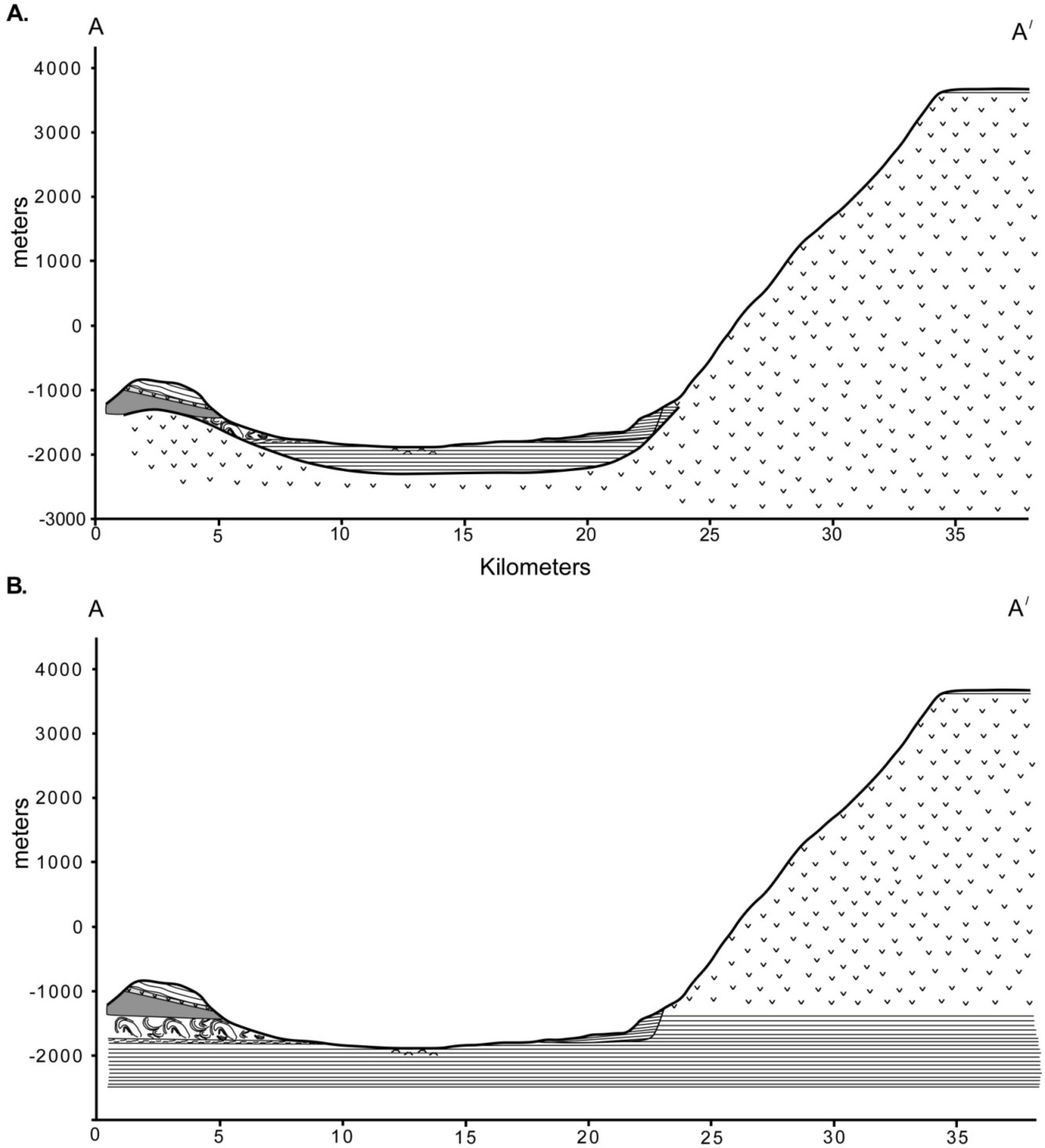

Fig 5.6. Cross-section constructed using MOLA topographic profile taken from A to A' in southern Melas basin (Fig. 5.1B) Vertical axis is in meters and horizontal axis is in kilometers. Two possible scenarios are shown. A.) Stratigraphy is shown assuming units currently exposed at surface were deposited in a pre-existing basin. It is not known how deep this pre-existing basin may have been nor to what elevation the northern basin wall might extend. In this case the strata should onlap the basin walls at the margins of the basin. B.) Stratigraphy is shown assuming units at surface were deposited before the formation of Valles Marineris and have been exposed due to subsequent erosion. In this case, the strata should not be observed to onlap the basin walls in any location.

transitioning into blocky deposits in several locations as one moves up the stratigraphic section (Fig. 5.11).

5.4.2 Map distribution and stratigraphy of deformed regions

5.4.2.1 Melas Chasma

Three regions of deformed strata occur in western and southern Melas Chasma (Fig 5.2). The two outcrops of convolute folds in region 1 occur on a slope near the northern ridge bounding southern Melas basin (Fig. 5.1D). The convolute folded strata in the southwestern outcrop of region 1 appear to extend over a low point in the ridgeline where

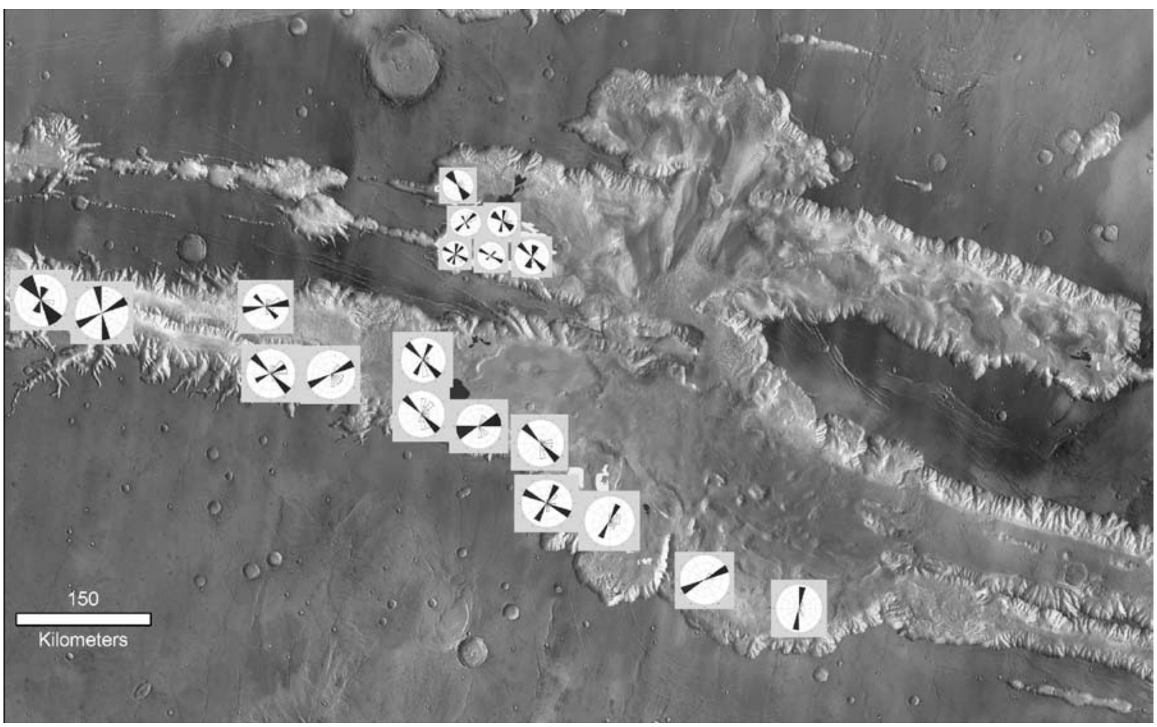

Fig 5.7. Rose diagrams of fold axial trace orientations plotted on deformation map in the locations they were measured. Fold axial trace orientations are bimodal with a component to the NE-SW and a component to the SE-NW.

they transition into a large outcrop of detached slabs in the central portion of region 1 (Fig. 5.9). There are two smaller outcrops of detached slabs at the base of the northern ridge bounding Melas Chasma (labeled 1-N in Fig. 5.1D). The central and northern outcrops in region 1 are likely part of a continuous outcrop of detached slabs, although no definitive exposures of detached slabs are identified in the area between them (Fig. 5.1D).

Regions 7 and 8 are exposed in the low areas near the chasma walls on the south wall of Melas Chasma (Fig. 5.2). Deformed strata are mostly located topographically below the interior layered deposits on materials previously mapped as interior massive deposits (Avm, Amazonian Valles Marineris younger massive material) and Avme (Amazonian Valles Marineris etched massive material) and interior floor materials (Avfr, Amazonian Valles Marineris rough floor material) by Scott and Tanaka (1986). Small areas of regions 7 and 8 do occur on the lower parts of the interior layered deposit mounds. The large southern outcrops of deformation in regions 7 and 8 appear to be close to the same stratigraphic horizon.

Two stratigraphic columns were measured in the southeastern outcrop of convolute folds in region 1 in southern Melas basin where DEMs were available (Fig. 5.8). The lowest portion of the basin is filled with a thinly-stratified unit with bedding dips between $0.6 \pm 0.1°$ and $1.4 \pm 1°$. Two features interpreted as sublacustrine fans occur in the topographic low of the basin, suggesting the basin was once filled with water (Metz et al. 2009). At the position of stratigraphic column 2, the thinly-stratified unit is overlain by a

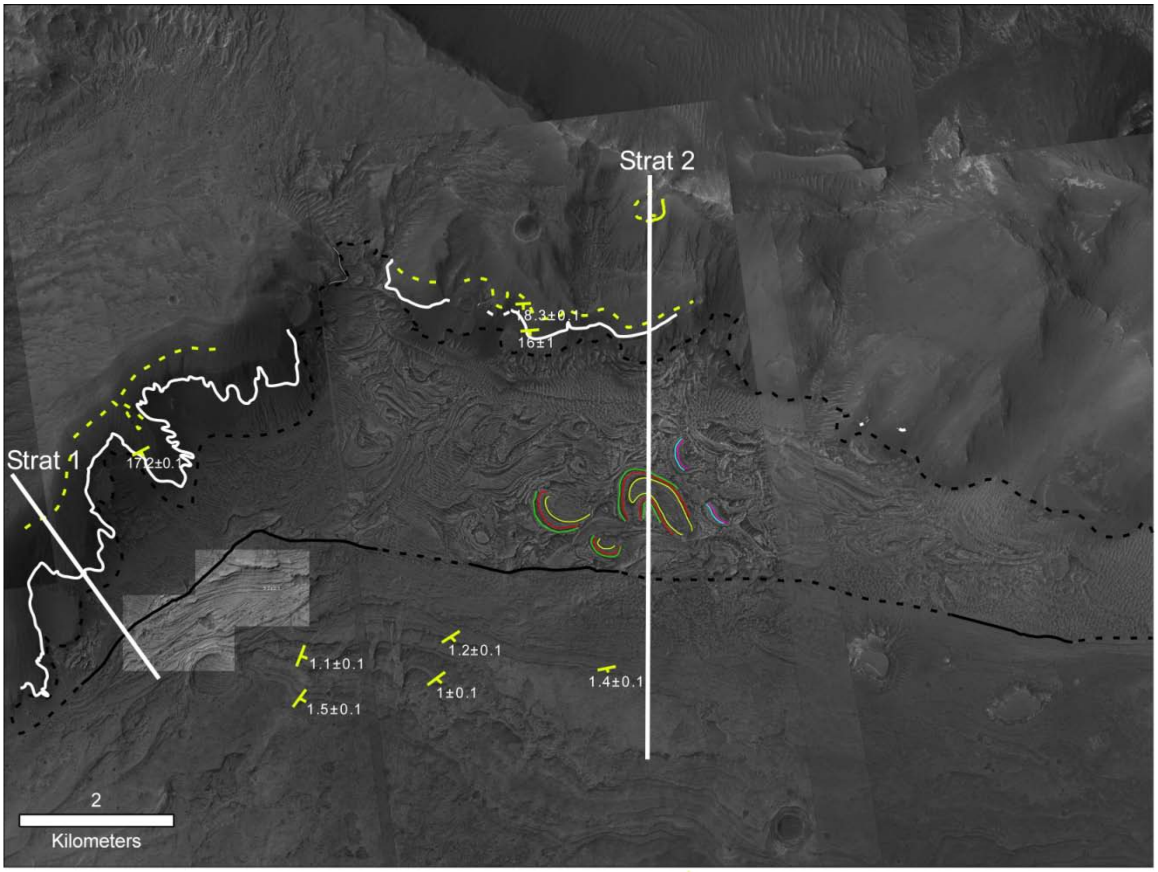

Fig 5.8. Map showing locations of stratigraphic sections measured in region 1-SE (labeled Strat 1 and Strat 2). Contacts between units identified in this region are also indicated: contact between flat-lying strata and km-scale convolute folds is mapped as a black line (lines are dashed where contact is inferred), contact between folds and medium toned unit is shown as a white line, and the contact between the massive unit that weathers to boulders and the thinly-stratified unit is shown as a dashed yellow line (gradational contact). Representative dips are shown in yellow. Several strata that are repeated through multiple fold blocks in the km-scale convolute folded unit are traced in various colors. Each color represents one bed that could be followed through multiple blocks.

96 m thick massive unit with hints of undisturbed layering. The massive unit is overlain by a 280 m thick convolute-folded unit. Further to the west at the position of stratigraphic column 1, a 23.9 m thick set of clinoforms lies above the thinly-stratified unit and is overlain by a 146 m thick convolute folded unit. No massive unit is observed below the

convolute folds in this location. The convolute folded unit may be a relatively thin unit deposited on a paleo-slope or it may fit conformably into the stratigraphy. However, there is no evidence for onlap of the slope by the convolute folded unit. Above the convolute folded unit is a 148 m-thick medium-toned unit that lacks signs of bedding. At the position of stratigraphic column 1, the medium-toned unit is overlain by a 44 m-thick massive unit that weathers into boulders, and this unit thickens to the west to 282 m at the position of stratigraphic column 1. The medium-toned unit interfingers and grades into a 131 m-thick thinly stratified unit that caps the ridge on the north side of southern Melas basin. On the west side of southern Melas basin this thinly-stratified unit is only 56 m thick and has been eroded via fluvial incision.

On the south chasma wall of southern Melas basin, a unit that appears to have slumped down the chasma wall is observed (Fig. 5.12). This unit contains bedding that dips to the north at ~7° which is steeper than the ~1° dips of strata present on the basin floor. A large section of rock appears to have slid away from the chasma wall, including a small stratified section of rock (Fig. 5.12B). An S-fold is observed where the section of 'sliding' rock has likely collided with the layered sediments on the basin floor (Fig. 5.12B). A set of isolated elliptical patterns is exposed in a several hundred meter long vertical exposure of rock near where the sliding block collided with the basin floor sediments (Fig. 5.12C).

A cross-section from the north to south end of southern Melas basin was measured at the location of stratigraphic column 2 (Figs. 5.1B and 5.6). This shows how the stratigraphy fits into the regional topography of the basin. There are at least two possible interpretations for the stratigraphy at depth in southern Melas basin as shown in Fig. 5.6A and B. The strata observed at the surface could onlap the side of an older buried depositional basin (Fig. 5.6A). One constraint that could favor this interpretation is that bedding in the northern wall of southern Melas basin dips at ~19° to the south. If these beds were deposited on a pre-existing slope, they would be expected to dip to the south. In the second possible interpretation, the strata observed at the surface are older than the wall-

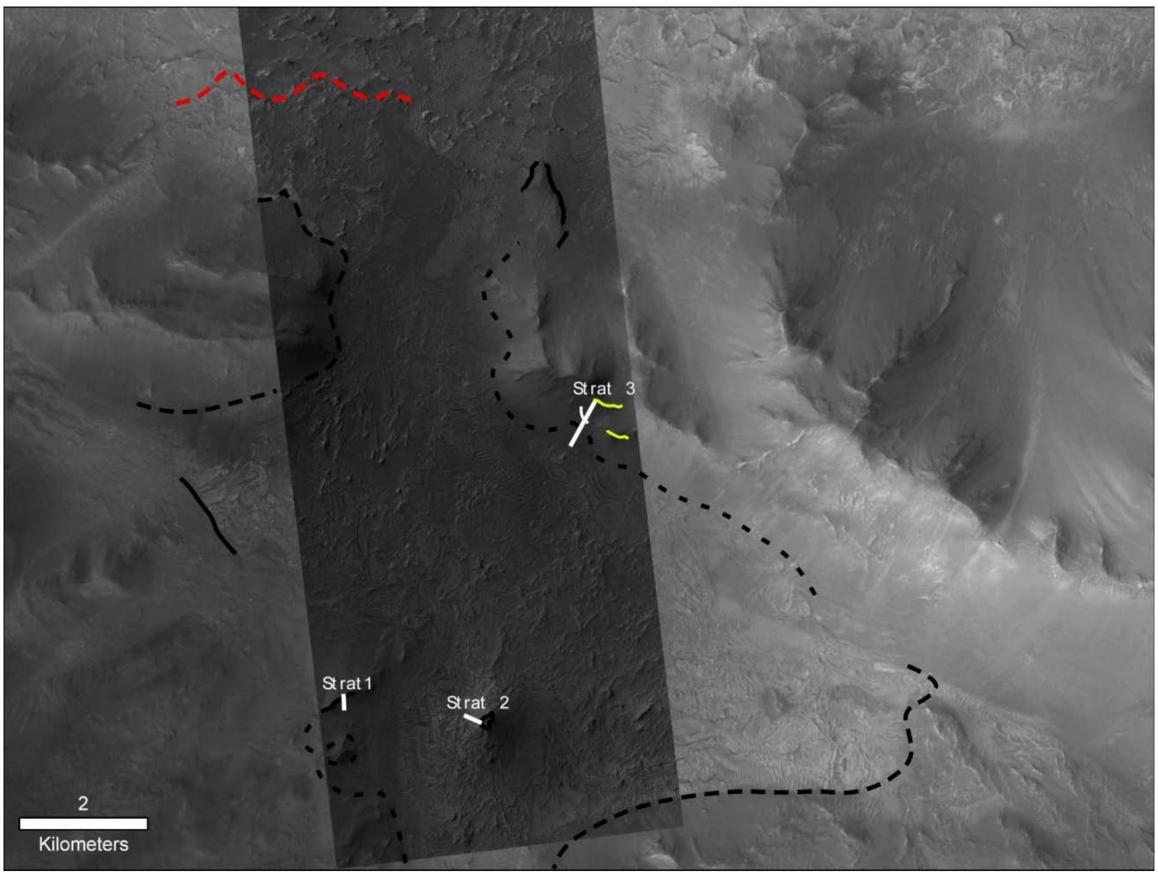

Fig 5.9. Map showing locations of stratigraphic sections measured in region 1-SW (labeled Strat 1-3). Contacts between units are indicated using the same color scheme as Fig 5.8. Dashed red line shows gradational contact between convolute folds and detached slabs.

rock composing the chasma walls of Valles Marineris and are exposed through erosion (Fig. 5.6B). The exposed stratigraphy and contacts within southern Melas basin do not allow discrimination between these two options. However, just to the east of southern Melas basin, layered sediments are observed to onlap the wall of the basin, suggesting at least some deposition of layered sediments occurred after the formation of the basin.

In the southwestern outcrop of convolute folds in region 1, which is ~27 km to the west of the southeastern outcrop (Fig. 5.1D), a similar stratigraphy to the southeastern outcrop was observed. Three stratigraphic columns were constructed for the southwestern outcrop using MOLA data (Fig. 5.9). At the position of stratigraphic column 3, a thick interval (~325 m) of km-scale convolute folds is observed. The deformed unit is overlain by the same three units observed to overlie the folds in region 1, a medium-toned unit, a massive unit and a laterally interfingering massive and thinly-stratified unit. The two other stratigraphic columns measured in the area show ~100 m thick exposures of convolute folds. In stratigraphic column 2, the folds are covered with a thin medium-toned unit that is overlain by a thin light-toned unit. In stratigraphic column 1, the folds are covered by a thin (~15 m thick), dark-toned stratified unit overlain by a thin (~15 m thick), medium-toned and stratified unit.

A stratigraphic column was estimated using MOLA data in the central outcrop of region 1 in western Melas Chasma (Fig. 5.1D). The lowest unit is a ~150 m-thick exposure of detached slabs. There is a thin, light-toned deposit that drapes the detached slabs and the ridge adjacent to the detached slabs. The light toned drape appears similar in tone and texture to a light-toned draping deposit seen on the ridge in the western part of southern Melas basin (Fig. 5.13). The light-toned drape also appears similar to the material composing the convolute folds. However, because the light-toned unit drapes detached slabs that can be seen to grade into the convolute folds, the light-toned unit must be stratigraphically younger.

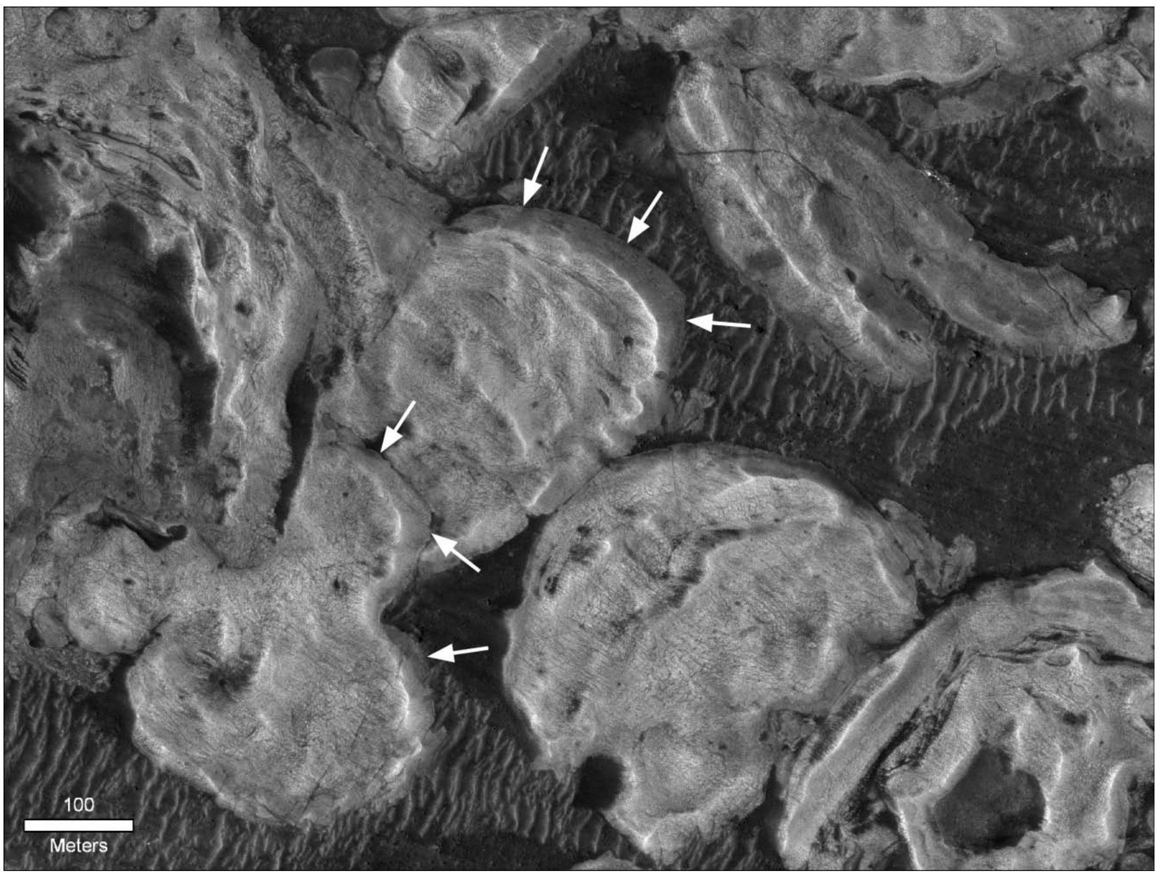

Fig 5.10. Some of the detached slabs show resistant edges as is illustrated by the white arrows (ESP_014339_1710).

A stratigraphic column was constructed for the southeastern outcrop of deformed strata in region 7 in southeastern Melas Chasma (Figs. 5.5 and 5.14). The base of the column consists of ~600 m of stratified deposits. A ~500 m thick unit with a weathering pattern that makes it difficult to determine the type of bedding occurs above the layered strata in the location where the stratigraphic column was measured. However, farther to the west at the same stratigraphic interval the deposits consist of folded strata (Fig. 5.14 A and B). These folds are largely elongated in a downslope direction. We have tentatively assumed the unit with the lattice-like weathering pattern also consists of folded strata. Above the unit with the lattice-like weathering pattern is another 100 m of stratified deposits. Above these are ~125 m of pulled-apart strata (Fig. 5.14 A and C). The eastern boundary of the areal exposure of the pulled-apart strata is very linear and may be a fault. At the top of the section are ~375 m of stratified deposits.

In the stratigraphic columns measured in the southeastern outcrops in region 1 and region 7, both the lower and upper contacts of the deformed units could be identified. In the other outcrops, either the lower or upper contact was observed, but not both in the location where the stratigraphic column was measured. However, in many regions these missing upper or lower contacts were observed in other outcrops within the region. The fact that both lower and upper contacts are observed in many areas implies that the deformation is restricted to a limited, relatively thin stratigraphic interval. The thickness of the deformed unit ranges

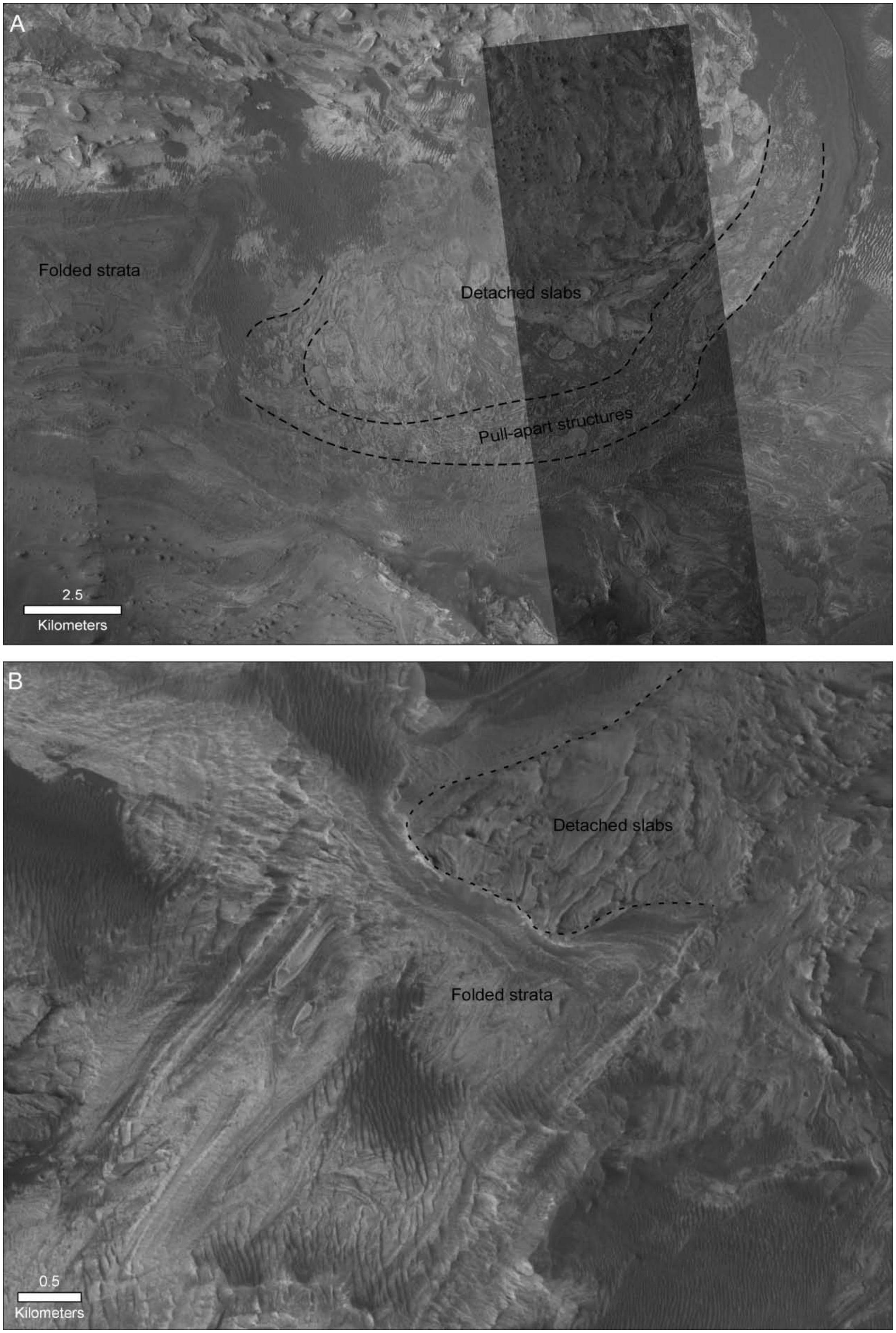
A
Folded strata
Detached slabs
Pull-apart structures
2.5
Kilometers
B
Detached slabs
Folded strata
0.5
Kilometers

Fig 5.11. Several styles of deformation can be seen to grade into each other. Dashed black lines show gradational contacts. A.) Lateral gradation between deformation types. Location of image shown in Fig. 5.1A. B.) Vertical transition between folded strata and detached slabs. Location of image shown in Fig. 5.1A.

from 100 m to 350 m thick, although in many areas only minimum thicknesses could be estimated, since both the lower and upper contacts were not observed.

5.4.2.2 Ius Chasma

Regions 2-4 occur in Ius Chasma. All of the outcrops in Ius occur on the floor of the chasma in areas previously mapped as interior floor (Avfr) and surface materials (Avsd (Amazonian Valles Marineris dark surface material)) by Scott and Tanaka (1986). There are no interior layered deposits or mounds near the deformed strata in Ius Chasma, suggesting the origin of the latter is not linked to the former. In region 2, the deformed strata are exposed in the lowest topographic areas, and in the eastern part of the region are covered by a terraced alluvial fan. Sediment eroded from the southern wall of Ius overlies the southern end of the deformed unit. In the western part of the region deformed strata are observed up to the level of a resistant bed in the northern wall of Ius. The areas above the resistant bed are mantled with eolian sediments. The southern portion of the deformed strata is covered with materials derived from erosion of the southern wall of Ius. Roach et al. (2009b) also examined the strata in this topographic low and found that they were composed of kieserite, polyhydrated sulfate and hydrated silicate with the polyhydrated sulfates found at higher elevations than the kieserite. In region 4 in the northern portion of

Ius Chasma, several types of deformed strata are observed and are partially covered by Amazonian landslide deposits. CRISM image FRT0000A396 examined by Roach et al (2009b) shows that the deformed strata in this area are composed of non-hydrated material.

Several different types of deformed strata are exposed in Region 3 at the bottom of the floor of western Ius Chasma (Fig. 5.15). Stratigraphic sections for this area are shown in Fig. 5.5. In the western outcrop of this region grading between detached slabs, pull-apart strata and folded strata is observed. The deformed strata occur in topographic lows and are exposed in an erosional window; several landslides overlie the deformed strata. A stratigraphic column was measured in this area and consists of ~100 m of deformed strata at the base overlain by a ~50 m thick light-toned unit (Fig. 5.15). At the top of the section is ~150 m of a dark toned mantling unit. The deformed strata are covered by eolian dunes in some of the low areas where the dark-toned unit has been eroded away.

5.4.2.3 Candor Chasma

Region 5 is located in western Candor Chasma and region 6 in eastern Candor Chasma. They occur in areas previously mapped as massive deposits (Avme), surface materials (Avsd), floor materials (Avfs, Amazonian Valles Marineris smooth floor material), and layered materials (Hvl, Hesperian Valles Marineris layered material) (Scott and Tanaka 1986). The deformed strata are observed up to the elevation of a topographic bench that runs around western Candor Chasma and is shown by the white line in Fig 5.1. The bench was interpreted by Lucchitta (2008) as a shoreline and by Okubo (2010) as forming through eolian erosion. Several large outcrops of the folded strata are found in the

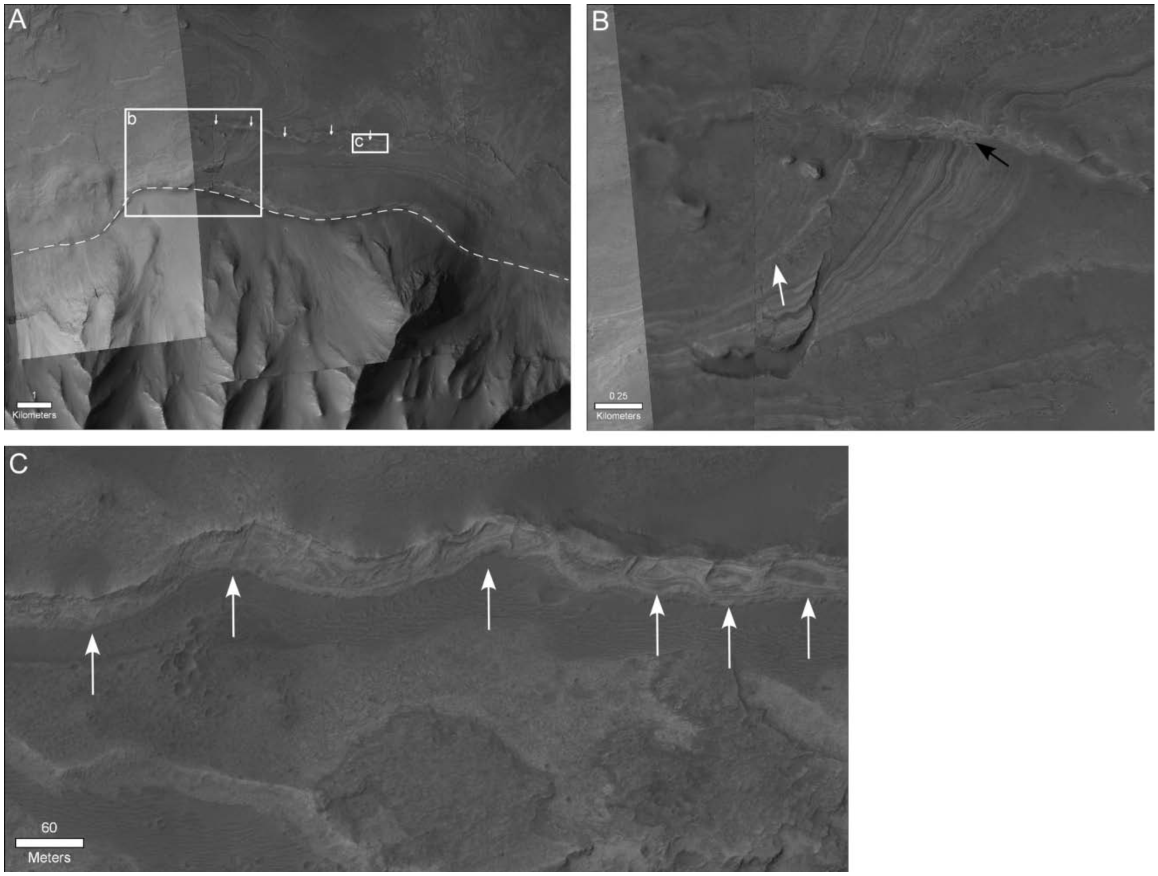

Fig 5.12. A.) Location of slump in southern Melas basin. Dashed line shows edge of slump. White arrows show where slump block slid into pre-existing basin floor strata. White boxes show locations of b and c. B.) Zoomed-in portion of slump showing a small stratified block that has pulled away from the main slump mass (white arrow). Black arrow shows S-fold where the slump collides with basin-floor strata. C.) Vertical section where hypothesized slump folds are shown in cross-section. White arrows highlight folds. B and C are from PSP_002828_1700.

western portion of region 5 in Candor at the base of the chasma wall and up to the level of the topographic bench. Another large exposure of deformed strata is found in the topographic low to the east of Ceti Mensa. In several areas in the eastern outcrops of region 5, detached slabs overlie folded strata (Fig. 5.11B). Much of the outcrop of deformed strata in the central portion of region 5 is located on the lower portion of Ceti

Mensa. A light-toned unit covers much of the central part of western Candor and appears to overlie the deformed strata. In some areas the deformed strata are exposed in erosional windows through the light-toned unit. Exposures of detached slabs cap elongated mesas in several areas. One example is shown in Fig. 5.16A.

A stratigraphic column was measured within a crater in the northern part of region 5 using DEM C3 (Figs. 5.5 and 5.16). At the base of the section is 25 m of undeformed sediments. At -125 m elevation, there is a low-angle fault and the layers above the fault were folded into an overturned concentric fold. There are several additional folds and many high-angle faults in the 225 m above the low-angle fault at -125 m (Fig 5.16). In the southwestern portion of the deformed unit is a potential interval of repeated stratigraphy. There is another 25 m of stratified sediments above the deformed interval. The top of the section is 125 m thick and consists of detached slabs that form a resistant cap. Faults were mapped in the crater wall and the orientations of the faults indicated in Fig. 5.16 B are shown in the equal-area stereonet in Fig. 5.16C.

5.4.3 Elevations of deformed strata

The deformed units are observed to occur at a variety of elevations, including as low as -4100 m in Melas Chasma and up to 3400 m in Candor Chasma. The elevations of the deformed strata range from -4200 to -1000 m in Ius Chasma, from -4100 to 400 m in Melas Chasma, and from -2500 to 3400 m in Candor Chasma. There does not seem to be a pattern in the elevations where deformed strata are observed.

Fig 5.13. Light-toned unit that drapes the ridge in the western part of southern Melas basin (PSP_009025_1705).

5.4.4 Fold orientations

Orientations of fold axial traces were measured wherever possible (i.e. for folded strata and convolute folds) and have largely bimodal trends as shown in Fig. 7. There is one set of fold axes with a NE-SW orientation and another set with a SE-NW orientation. This trend holds well for the folds in western Candor Chasma and for those in Ius Chasma. Folds in Melas Chasma exhibit more variation, with the fold axes in eastern Melas Chasma having primarily a NE-SW orientation, which is roughly perpendicular to the nearest chasma wall.

5.4.5 Composition of deformed strata inferred from CRISM spectra

CRISM images covering the deformed strata exhibit spectral signatures consistent with the presence of sulfates. Monohydrated sulfate (likely the Mg-variety kieserite) and polyhydrated sulfates are detected in spectra of deformed beds in Ius, Candor and Melas Chasmata (Fig. 5.17). Another type of material that does not show a good spectral match to any library spectra is detected in Ius and Melas Chasmata (Fig. 5.17 C, E). Ratio spectra of this unknown material has absorption bands at 1.4 µm, 1.91 µm and a 'doublet' near 2.21 and 2.27 µm (Fig. 5.17 D, F). Roach et al. (2009b) previously identified this material in Ius and Coprates Chasmata and Noctis Labrynthus and discuss its spectral characteristics in detail. We also note that the strength of the 1.4 µm band for this material is variable, and the relative strengths of the 2.21 and 2.27 bands also vary (Fig. 5.17 D, F). This suggests that the material is a mixture of at least two different phases, similar to the findings of Roach et al. (2009b). Laboratory experiments by Tosca et al. (2008b) formed a material which may be jarosite mixed with poorly crystalline clays or silica, and it has similar spectral properties to this unknown phase. The material precipitated in the Tosca et al. (2008b) experiments formed at a moderate pH of 6-7 and was XRD amorphous. This

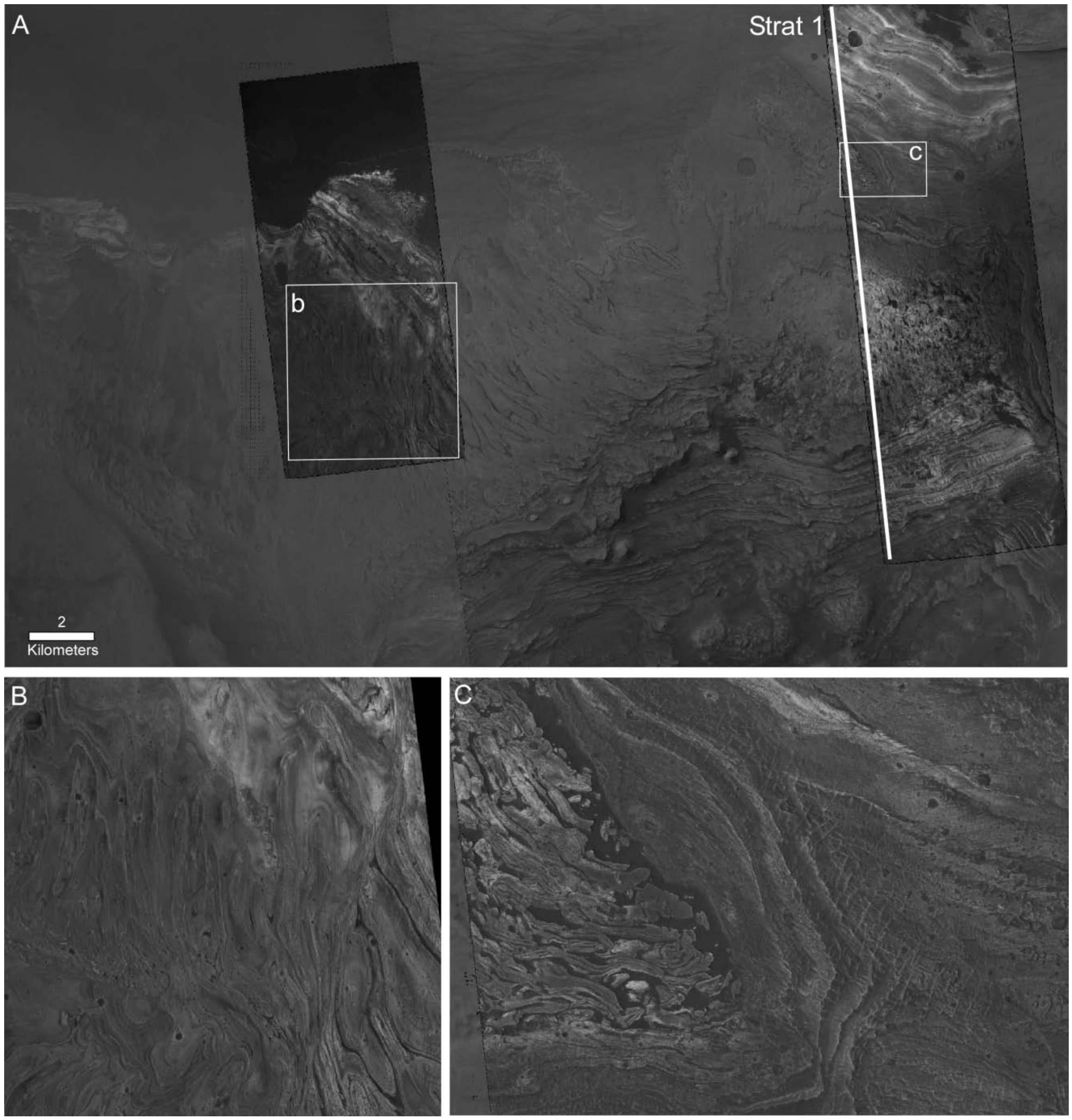

Fig. 5.14 A.) Multiple types of deformation exposed in region 7-W (P07_003909_1686, P17_007535_1688). White boxes show locations of b and c. White line shows location where stratigraphic column was estimated. B.) Folded strata (ESP_013719_1665). C.) Pull-apart strata (ESP_013508_1665).

material is also seen in layered material that onlaps the ridgelines to the west of region 8. This novel material is not identified in any of the ILD mesas in Candor or Melas Chasma, instead these ILD show strong spectral signatures consistent with the presence of kieserite and polyhydrated sulfates (Roach et al. 2009a). The deformed units in region 7 also do not show the novel material.

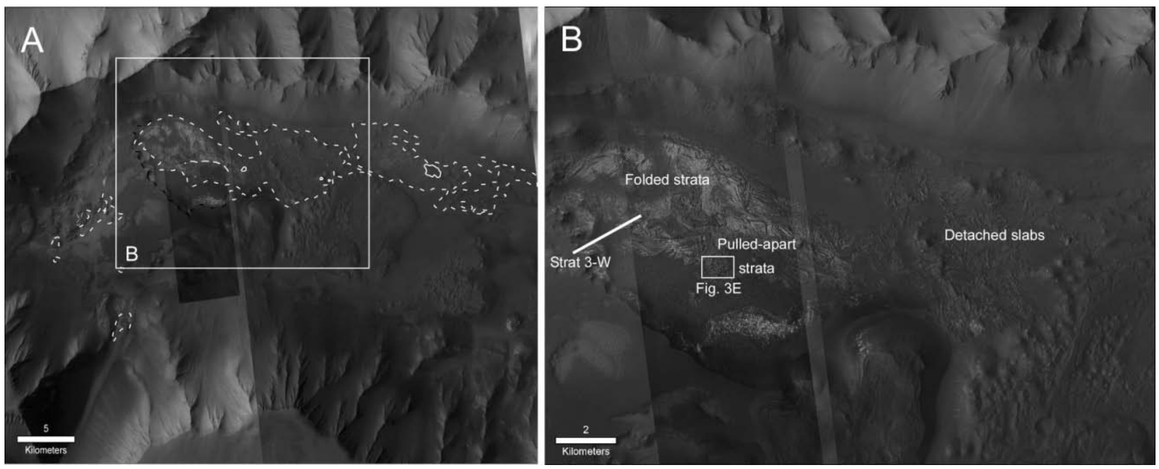

Fig 5.15. Deformation exposed in region 3. A.) White and black dashed lines show extent of deformed strata. White box shows location of B. B.) Grading between detached slabs, pull-apart strata and folded strata is observed. The white box shows the location of Fig. 5.3E. The location where stratigraphic column 1 was measured is shown by the white line.

5.5. Discussion

5.5.1 Rheology of deformed strata

The styles of deformation observed in Valles Marineris suggest that much of the deformation occurred in the plastic regime. The exception to this is the pull-apart structures that likely were deformed in the brittle regime. Because the deformed strata appear to be largely composed of several types of sulfates, including kieserite (ρ=2.57 g cm^{-3}) and polyhydrated sulfates, it is important to consider the deformational behavior of these minerals. Though published data on the material properties of sulfates is limited, the density of gypsum (ρ=2.32 g cm^{-3}) is less than that of most sedimentary and volcanic rocks, so given this flow-strength contrast it should theoretically deform in a fashion similar to halite at low strain rates (Williams-Stroud and Paul 1997). Halite is weak and easily mobilized by solid state flow and can flow at low temperatures and differential stresses (Jackson and Talbot 1986). Some work has been done on the deformation of gypsum which shows that at very slow strain rates the strength of gypsum approaches that of halite, which deforms plastically at shallow depths at strain rates of 10^{-8}-10^{-14} s^{-1} (Williams-Stroud and Paul 1997; Jackson and Talbot 1986). Gypsum undergoes creep at faster strain rates if water is present (de Meer and Spiers 1995). In order for water to be trapped with the gypsum during deformation, it would need to be covered with low permeability rock, such as clay-rich mudstones (Heard and Rubey 1966). The strength of these sulfates increases with water loss. Anhydrite requires two orders of magnitude larger differential stress than gypsum in order to attain diapiric strain rates (Williams-Stroud and Paul 1997).

The deformed sediments in Ius and Melas could also consist of volcanic ash that was deposited rapidly over a large area and became water saturated and subsequently altered. This interpretation could fit with the spectral detection of the material that may be jarosite mixed with poorly crystalline altered clays or silica. Studies of ash rheology show that the transition from brittle to ductile deformation occurs between 800-850 °C but shifts to lower temperatures with increasing water pressure or with lower rates of displacement (Robert et al. 2008).

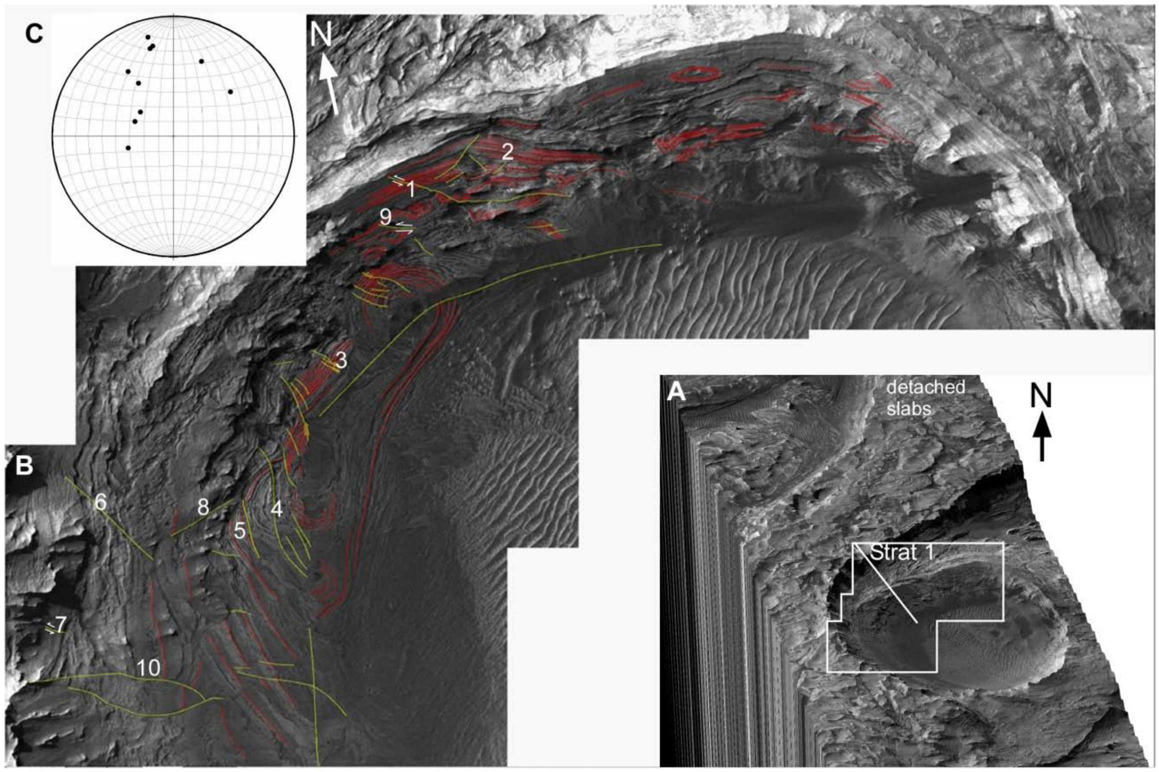

Fig 5.16. A.) Perspective view of DEM showing that the detached slabs form a resistant mesa. White box shows location of b. B.) Portion of crater wall in DEM with key strata to help visualize deformation mapped in red and faults in yellow. Faults whose orientation was measured are numbered 1-10. C.) Equal-angle stereonet of orientations of faults indicated in B (n=10).

5.5.2 Relative age of deformed strata

An important consideration is whether the strata on the floor of Valles Marineris, both the mounds of light-toned strata (ILD) and the surrounding sediments, pre- or post-date chasma formation. This question has been debated in the literature with several authors suggesting the light-toned layered rock predates chasma formation and is being exhumed from below the wallrock (Malin and Edgett 2000; Montgomery and Gillespie 2005; Catling et al. 2006) and most others suggesting the sediments postdate or were contemporaneous with chasmata formation (Lucchitta et al. 1992; Peulvast and Masson

1993; Lucchitta et al. 1994; Chapman and Tanaka 2001; Weitz et al. 2001; Komatsu et al. 2004; Fueten et al. 2006; Fueten et al. 2008; Okubo et al. 2008; Okubo 2010). Much of this controversy arises from the fact that there are very few clear, unambiguous contacts between the light-toned layered deposits, which are often near the centers of chasmata, and the canyon wallrock. Here we review the evidence presented in previous literature to support relative age interpretations for the ILD (cited images are listed in Table 5.3).

From the first images sent back by the Mariner and Viking spacecraft, the wallrock of Valles Marineris was seen as distinct from the light-toned layered rock found on the floors of the chasmata. Wallrock is described as showing 'spur and gully' morphology or smooth talus slopes and as giving rise to landslides, whereas the ILD are described as showing light-colored smooth surfaces with fluted topography distinctly different from wallrock (Lucchitta et al. 1992). An early study based on Viking images (Viking Orbiter 1 frames 913A11 and 913A13, 20-125 m/pixel) observed that the ILD in the divide between Ophir and central Candor Chasma onlap the spur and gully morphology of the canyon wall (Nedell et al. 1987). Lucchitta et al. (1994) observed that in east Candor, the ILD abuts and buries wallrock already eroded into spurs and gullies along the south part of the chasma. Witbeck et al. (1991) suggest that in Juventae and Ganges Chasmata layered deposits overlie conical hills that are similar to chaotic terrain farther west. In Melas Chasma, Peulvast and Masson (1993) state that 'no direct contact can be seen between the smooth

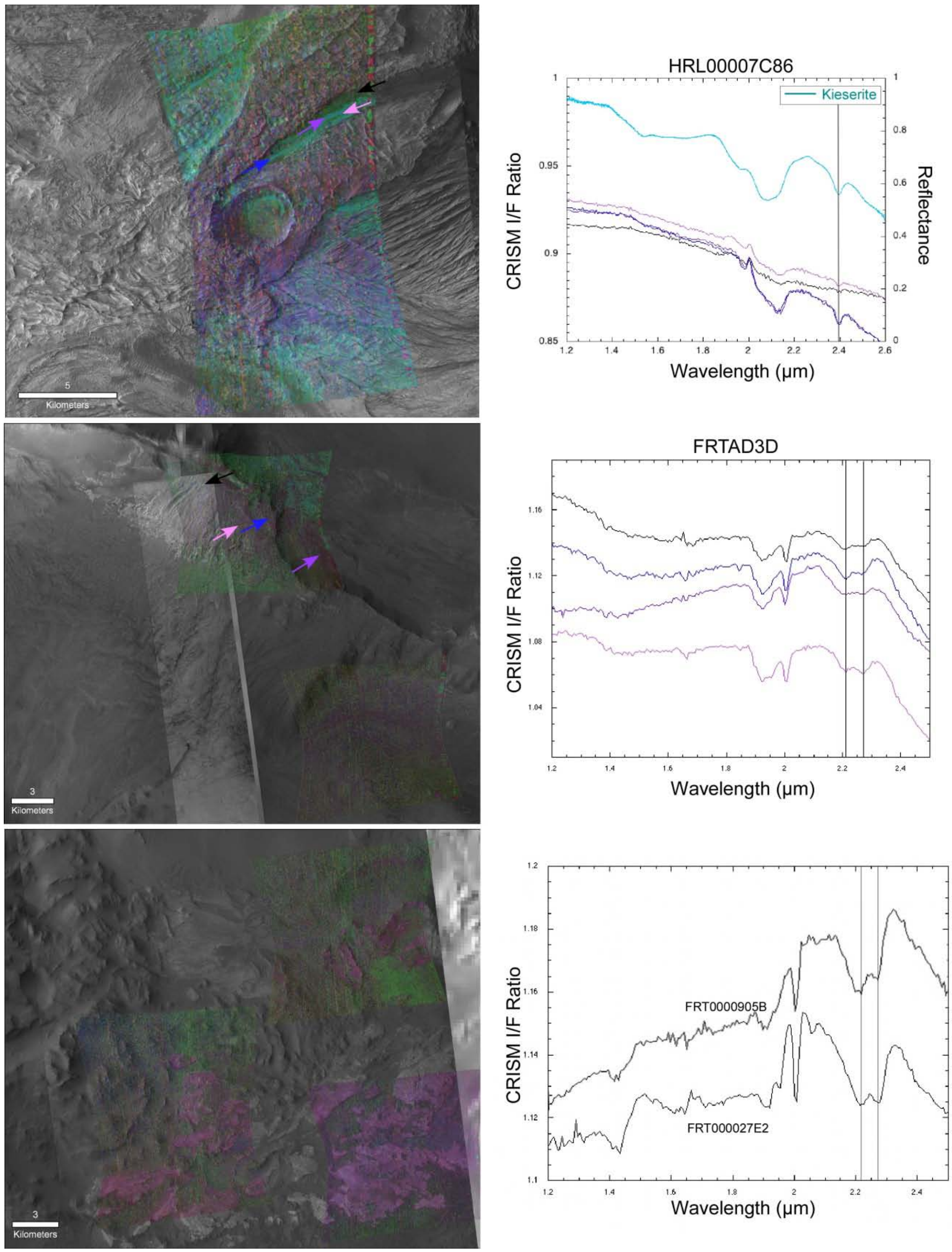

Fig 5.17. A.) Band parameter map from CRISM targeted image HRL00007C86 overlaid on CTX image from region 5 in Candor Chasma. Red channel is BD 2210, green channel is BD 2100 and blue channel is SINDEX. Green areas show kieserite. B.) Four CRISM

spectra (from areas indicated by arrows) show a good spectral match to the laboratory spectrum of kieserite. C.) Band parameter map from CRISM targeted image FRT0000AD3D overlayed on CTX image from region 1 in Melas Chasma. Red channel is BD 2210, green channel is BD 2100 and blue channel is SINDEX. D.) Four CRISM spectra (from areas indicated by arrows) show the unknown material with bands near 1.9 µm, and a doublet at 2.21 and 2.27µm. The drop in reflectance near 2.01 µm is due to incomplete removal of atmospheric CO_2 and is not a surface absorption. E.) Band parameter map from CRISM targeted images FRT0000905B, FRT000027E2 and FRT0000A396 overlayed on CTX image from region 4 in Ius Chasma. Purple areas show the unknown material. Red channel is BD 2210, green channel is BD 2100 and blue channel is BD 1900. F.) CRISM spectra from FRT0000905B and FRT000027E2 show the unknown material in the purple areas with bands at 1.43 µm, 1.91 µm and a doublet at 2.21 and 2.27 µm. The relative strength of the bands in the doublet varies. The drop in reflectance near 2.01 µm is due to incomplete removal of atmospheric CO_2 and is not a surface absorption.

surfaces (of the ILD) and the south Melas Chasma wall, as a 15-50 km 'moat' separates them.' They further note that landslides from the south Melas wallrock partly fill the moat and cover the base of the ILD bench, obscuring the contact. Peulvast and Masson (1993) suggest that the layered sediments in south Melas embay the wide reentrants and ridges, and thus formed in a basin whose walls already had their present outline.

When the Mars Orbiter Camera (MOC) on the Mars Global Surveyor began sending back images (4-10 m/pixel), new details of the ILD and wallrock were evident. Malin and Edgett (2000) suggest that several MOC images show that light-toned layered strata underlie the wallrock. They cite MOC images (M17-000468, M17-00467 and M20-01506) covering the eastern part of the wall of northwest Candor as evidence that the ILD continue under the chasma walls. While light-toned material can be seen high up on the wallrock in this location, a direct stratigraphic contact between the light-toned layered material and the wallrock is obscured by an eolian mantle, making the stratigraphic relationship ambiguous. It is possible the light-toned layers could underlie the wallrock here, but they could also onlap the wallrock. Additional images from west Candor (M14-00631, M-18-00099 and M19-00784) are cited as the best locations where layered units can be seen going into and under the chasm walls (Malin and Edgett 2000). In these areas, light-toned layered rocks are observed up to the level of a topographic bench, as described earlier in this paper. However, the direct stratigraphic contacts are also obscured here by eolian mantles and talus deposits. Their other examples from Coprates (M20-00380, M20-01760, M21-00103) and Ius (M08-07173) are also ambiguous with the actual contacts obscured by eolian mantle or talus deposits. Montgomery and Gillespie (2005) cite additional areas in Candor (R07-00897) and southwest Melas (R04-01897, R08-00286 and R08-00287) where they interpret wallrock as underlain by light-toned layered deposits. These areas also show ambiguous contacts that could represent onlap or wallrock underlain by light-toned strata.

Catling et al. (2006) examined many MOC images (Table 3) in Juventae Chasma which they state show that the ILD are older than the wallrock and chaos material. Many of these images do show promising contacts, and HiRISE images (PSP_005557_1755 and PSP_003790_1755, ~25 cm/pixel) confirm that light-toned strata do underlie wallrock near mound A of Catling et al. (2006). In this location, the HiRISE images resolve a relatively long exposure of a contact between the light-toned strata and the wallrock (Fig. 5.18B). This exposure occurs along a ridgeline in a spur and shows a sharp, irregular contact that cuts across elevation. The light-toned strata are less resistant to erosion than the dark-toned wallrock material which caps the ridge. The contact appears to be an erosional unconformity and shows that the local wallrock directly overlies the light-toned strata.

Other authors have described locations in MOC imagery where layered deposits appear to onlap chasma walls. Chapman and Tanaka (2001) observed layered deposits 'plastered onto' the chasma walls in Coprates (MOC image AB-106306). Komatsu et al. (2004) observed that an ILD mound overlaid the chaotic terrain in Juventae (MOC image M10-00466) and that the ILD are covered by younger landslides and eolian material. MOC image M10-00466 was later cited by Catling et al. (2006) to show that light-toned strata underlie the wallrock. Flauhaut et al (In Press) similarly observe ILD to overlie chaotic mounds in Capri. Chojnacki and Hynek (2008) suggest light-toned layers are 'pasted-on' to wallrock in Ophir Chasma (S04-01271). We regard these interpretations as ambiguous, because the contacts are mostly obscured by eolian mantles, talus deposits, and landslides; in areas where there may be direct contacts (such as Juventae), these contacts are not fully resolved in MOC imagery.

Structural relationships have also been used to argue the relative ages of the ILD. Using High Resolution Stereo Camera (HRSC)-derived DEMs, Fueten et al. (2006) measured the dips of layers in the ILD mounds of southwestern Candor Chasma and found that they were parallel to local slopes. Similar results were found for the ILD in Ophir (Zegers et al. 2006), Hebes (Hauber et al. 2006), Iani (Sowe et al. 2007), and Coprates Chasma (Hamelin et al. 2008). Okubo et al. (2008) and Okubo (In Press) used HiRISE DEMs to measure the dips of strata to the south of the ILD mounds in southwest Candor

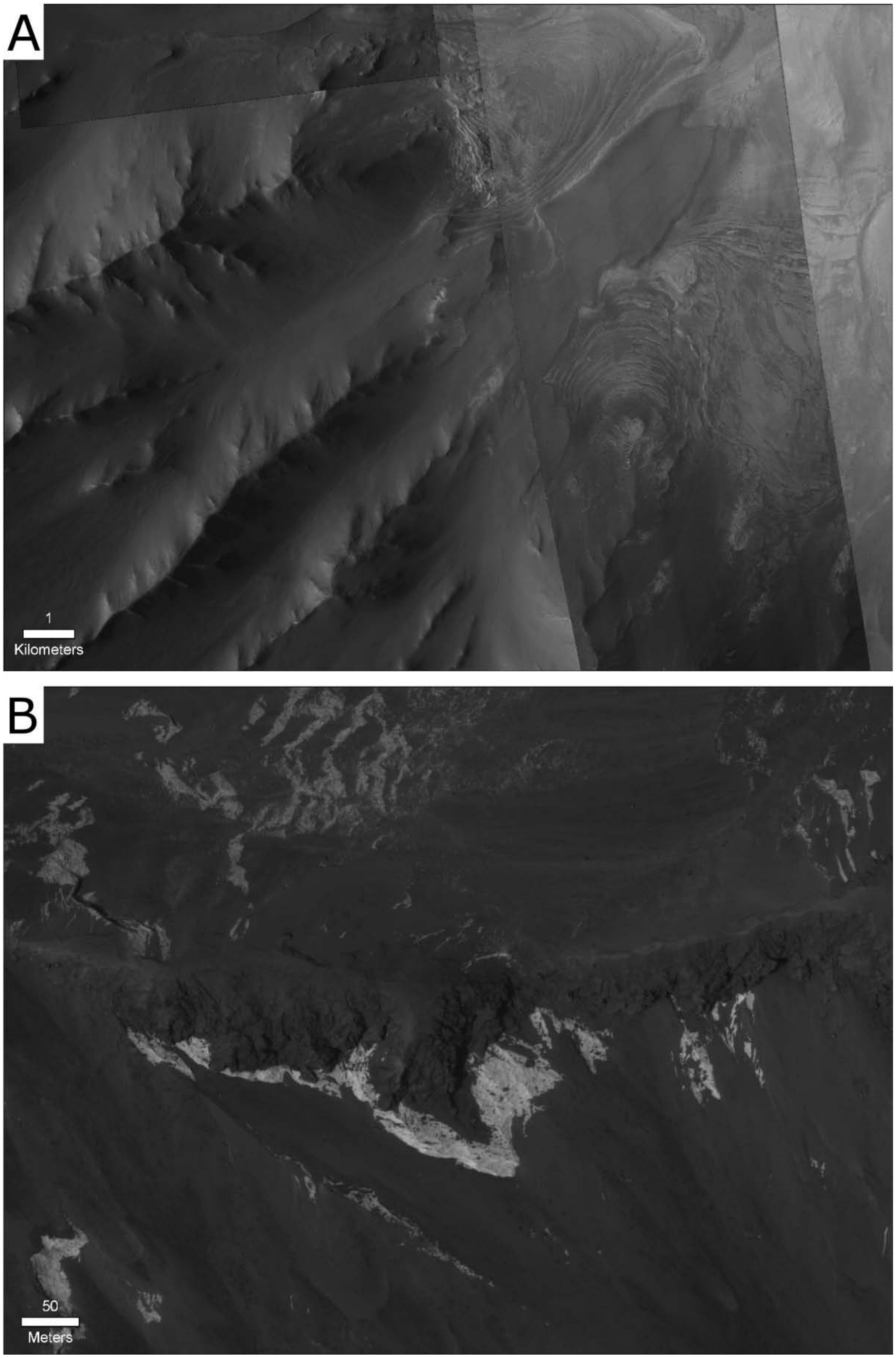
A
1
Kilometers
B
50
Meters

Fig. 5.18 A.) Onlap relationship between the light-toned stratified deposits and the wallrock in south Melas Chasma. The light toned layers fill in the topographic lows between the ridgelines (P05_002907_1706, PSP_004397_1695). B.) Contact between wallrock and light-toned layers in a ridgeline in Juventae Chasma (PSP_5557_1755).

and found that they generally dip toward the center of Candor, suggesting they postdate formation of the ancestral basin.

A search for unambiguous contacts between wallrock and light-toned stratified deposits was made in a separate effort by J. Metz and R. Milliken (unpublished analysis) using CTX and HiRISE imagery, but none were found in central Valles Marineris. In virtually every location, these contacts are obscured by eolian mantles, talus deposits, or landslides. In southern Melas Chasma, just to the east of southern Melas basin, there is a convincing area where the light-toned stratified deposits clearly onlap and fill in the topographic lows between ridges of wallrock (Fig. 5.18A). Structural data also seems to support a younger age for the light-toned deposits. The exception to this is in Juventae Chasma, where promising contacts showing wallrock overlying light-toned layers are observed. These few relatively unambiguous examples illustrate that the relative ages may differ in each chasma. Locally, light-toned layers may underlie wallrock, but in other locations the light-toned strata may have infilled pre- existing basins. Thus, resolving the controversy in the ages of the wallrock and light-toned layers may have to wait until landed missions can use absolute age-dating techniques in multiple chasmata.

Camera	Image	Location	Resolution	Reference
Candor				
Viking Orbiter 1	913A11	Ophir-Candor	63 m/pixel	Nedell et al. 1987
Viking Orbiter 1	913A13	Ophir-Candor	63 m/pixel	Nedell et al. 1987
MOC	M17-00468	5.56°S, 74.20°W	244 m/pixel	Malin and Edgett 2000
MOC	M17-00467	5.52°S, 74.56°W	5.8 m/pixel	Malin and Edgett 2000
MOC	M20-01506	5.17°S, 74.52°W	2.9 m/pixel	Malin and Edgett 2000
MOC	M14-00631	5.10°S, 77.1°W	5.71 m/pixel	Malin and Edgett 2000
MOC	M18-00099	4.98°S, 77.33°W	4.29 m/pixel	Malin and Edgett 2000
MOC	M19-00784	5.17°S, 77.36°W	4.29 m/pixel	Malin and Edgett 2000
MOC	R07-00897	4.90°S, 76.80°W	3.02 m/pixel	Montgomery and Gillespie 2005
Coprates				
MOC	M20-00380	14.64°S, 53.86°W	4.25 m/pixel	Malin and Edgett 2000
MOC	M20-01760	13.04°S, 65.13°W	5.68 m/pixel	Malin and Edgett 2000
MOC	M21-00103	14.64°S, 56.58°W	2.84 m/pixel	Malin and Edgett 2000
MOC	AB-106306	10.26°S, 69.31°W	5.97 m/pixel	Chapman and Tanaka 2001
Ius				
MOC	M08-07173	8.10°S, 84.30°W	5.7 m/pixel	Malin and Edgett 2000
Melas				
MOC	R04-01897	11.11°S, 75.45°W	5.96 m/pixel	Montgomery and Gillespie 2005
MOC	R08-00286	10.48°S, 75.77°W	4.48 m/pixel	Montgomery and Gillespie 2005
MOC	R08-00287	10.52°S, 75.40°W	250 m/pixel	Montgomery and Gillespie 2005
Juventae				
MOC	M10-00466	4.58°S, 63.43°W	2.87 m/pixel	Komatsu et al. 2004; Catling et al. 2006
MOC	E22-00455	2.31°S, 62.00°W	6.03 m/pixel	Catling et al. 2006
MOC	R03-00948	4.84°S, 63.50°W	2.87 m/pixel	Catling et al. 2006
MOC	E02-02546	4.15°S, 62.67°W	4.33 m/pixel	Catling et al. 2006
MOC	M11-02064	3.33°S, 62.01°W	1.43 m/pixel	Catling et al. 2006
MOC	E22-01273	2.46°S, 62.28°W	4.53 m/pixel	Catling et al. 2006
MOC	M10-00466	4.58°S, 63.43°W	2.87 m/pixel	Catling et al. 2006
MOC	E23-01035	4.47°S, 62.60°W	3.01 m/pixel	Catling et al. 2006
MOC	M04-00651	3.60°S, 61.98°W	4.3 m/pixel	Catling et al. 2006
MOC	E16-00591	2.37°S, 62.21°W	4.54 m/pixel	Catling et al. 2006
MOC	E11-02581	4.63°S, 63.39°W	3.02 m/pixel	Catling et al. 2006
MOC	E11-01370	4.28°S, 62.55°W	3.02 m/pixel	Catling et al. 2006
MOC	M21-00460	3.42°S, 61.93°W	5.75 m/pixel	Catling et al. 2006
MOC	E16-00591	2.37°S, 62.21°W	4.54 m/pixel	Catling et al. 2006

MOC	R02-00160	4.61°S, 63.30°W	3.01 m/pixel	Catling et al. 2006
MOC	M07-02818	3.37°S, 61.92°W	2.87 m/pixel	Catling et al. 2006
MOC	E14-01770	2.34°S, 62.15°W	3.02 m/pixel	Catling et al. 2006
MOC	E22-00892	2.28°S, 62.15°W	4.52 m/pixel	Catling et al. 2006
MOC	E22-00455	2.31°S, 62.00°W	6.03 m/pixel	Catling et al. 2006
MOC	R15-02329	2.27°S, 62.12°W	4.53 m/pixel	Catling et al. 2006
MOC	M08-04669	2.75°S, 61.70°W	5.74 m/pixel	Catling et al. 2006
MOC	E17-01902	2.85°S, 61.76°W	4.52 m/pixel	Catling et al. 2006
MOC	R05-00012	4.49°S, 64.07°W	3.01 m/pixel	Catling et al. 2006
MOC	R05-01255	4.44°S, 64.12°W	3.01 m/pixel	Catling et al. 2006
HiRISE	PSP_005557_1755	4.69°S, 63.20°W	27.1 cm/pixel	This paper
HiRISE	PSP_003790_1755	4.61°S, 63.10°W	26.7 cm/pixel	This paper
Ophir				
MOC	S04-01271	4.75°S, 73.43°W	3.01 m/pixel	Chojnacki and Hynek 2008

Table 5.3. Images cited in the literature as showing the contact between light-toned deposits and wallrock in Valles Marineris.

5.5.3 Possible causes of deformation

There are several possible mechanisms that could explain the observed deformation features in the strata of Valles Marineris. The salient features which need to be explained are (1) the lateral distribution pattern of deformation, including exposures as large as 1800 km^2 across spanning ~1000 km of Valles Marineris; (2) the deformational styles, including convolute folds, detached slabs, folded strata and pull apart structures and their gradations, both laterally and vertically, between different styles; (3) fold axis orientations which are largely bimodal with NE-SW and SE-NW orientations; (4) the scale of the deformation features, including km-scale convolute folds and 60 m to 1 km-sized detached slabs; (5) the thickness of the deformed intervals which range up to 350 m; (6) confinement of deformation to discrete stratigraphic intervals that occur at widely different elevations throughout the Valles Marineris system; and (7) composition of the deformed strata, which includes at least a component of sulfates.

Salt diapirism has been previously invoked to explain the folding in Candor and Melas Chasma (Beyer et al. 2000; Milliken et al 2007) . However, subsequent examination of new localities showed that undeformed strata are found directly beneath the folds in several areas in Candor and Melas and suggests that this mechanism is not consistent with all observations. Deformation caused by salt diapirism should show evidence of vertical motions, but the deformation observed in Valles Marineris does not show this, and where the orientations of fold axes can be measured, they are found to dip shallowly, consistent with subhorizontal shear. Due to this evidence, we will not consider salt diapirism any further.

Alternative mechanisms that may explain many of the observed features include liquefaction, landsliding, and gravity gliding.

5.5.3.1 Liquefaction

Liquefaction occurs when metastable, loosely packed grains become temporarily suspended in their pore fluid, and the drag exerted from the moving pore fluid exceeds the weight of the grains, lifting the grains and destroying the framework; this reduces the sediment strength to nearly zero (Lowe 1975). Liquefaction arises in unconsolidated sediments either before or soon after burial (Fernandes et al. 2007). On Earth, liquefaction is often triggered by seismic shaking associated with surface waves generated by large earthquakes; the deformed deposits that result are called "seismites" (Seilacher 1969). Seismic induced liquefaction typically occurs when a liquefiable sand layer is overlain by a thin, nonliquefiable stratum and the water table is shallow; this causes the pore fluid pressure to increase (Obermeier 1996). Other factors that increase the susceptibility of sediments to liquefaction include: (1) recent deposition; (2) rapid deposition; (3) water-saturation; (4) presence of homogenous fine-grained sediment; (4) shallow-burial; and (5) absence of cements (Allen 1986; Montenat et al. 2007). Sediments are commonly undeformed below the seismites, since these sediments have already been consolidated or cemented and are no longer susceptible to liquefaction (Pope et al. 1997).

Criteria that are used to recognize seismites include (1) restriction of deformation to a stratigraphic interval separated by undeformed beds; (2) occurrence in potentially liquefiable sediments; (3) zones of structures correlatable over large areas; and (4) presence of structures that suggest liquefaction (Sims 1975) . The deformation observed in Valles Marineris meets many of the criteria used to recognize seismites. The deformation is confined to a discrete interval with undeformed overlying and underlying beds. The deformation occurs over a large area and the deformational structures are consistent with those commonly reported to form from liquefaction. Seismites show a variety of deformational features including: ball-and-pillow structures, convoluted folded strata, sand blows, sand dikes, sedimentary breccias, homogenized beds, pull-apart structures, and slumps and slides (Davenport and Ringrose 1987; Roep and Everts 1992; Mohindra and Bagati 1996; Pope et al. 1997; Rodríguez-Pascua et al. 2000; Fernandes et al. 2007; Monentat et al. 2007). Earthquakes can cause strata to fail and shear on gently inclined slopes as low as 0.1-5% causing separation between individual slide blocks of as much as several meters (Obermeier 1996). The deformational structures observed in Valles Marineris are similar to many of those reported in seismites on Earth, such as convolute folded strata, detached slabs and pull-apart structures. The variation in seismite types is thought to be related to the stage of lithification, sediment characteristics and lithostatic pressure (Roep and Everts 1992; Monentat et al. 2007). The style of deformation can be seen to vary laterally in seismites, as is also observed in the deformation in Valles Marineris (Mohindra and Thakur 1998).

The cyclic shaking required to cause liquefaction is a horizontal acceleration of at least 0.1×g, and features caused by earthquake-induced liquefaction have been observed to occur from earthquakes greater than magnitude 5.5 (Obermeier 1996). The distance at which liquefaction features have been observed to occur from earthquakes of various magnitudes has been recorded. From Allen (1986) the relationship between earthquake magnitude (M) and distance (X) is

$$M = 0.499\ ln\left(\frac{X}{3.162 \times 10^{-5}}\right) \tag{1}$$

Because the deformation that we observe in Valles Marineris occurred across a distance of 1180 km, this implies that if this deformation was caused by earthquake-induced liquefaction then the 'marsquake' may have been at least magnitude 8.7, subject to the caveat that the effect of different crustal properties of Mars on this empirical relation is unknown. Another possibility is that the liquefaction was not caused by a marsquake, but by seismic energy generated from an impact event. Several seismites on Earth are suggested to have been induced from impact events, including deformation in the Carmel

Formation and Slickrock Member of the Entrada Sandstone in southeastern Utah (Alvarez et al. 1998); in the Cotham Member of Penarth Group in the United Kingdom (Simms 2003); and in the Alamo breccia in southern Nevada (French 2004). The Cretaceous-Tertiary impact is suggested to have generated a magnitude 13 earthquake which could have deformed unlithified sediments over several thousand kilometers (Collins et al. 2005). If an impactor was the source of the seismic energy that caused the deformation in Valles Mariners, it would likely have been at least 3 km in size to generate magnitude 8.7 marsquakes (calculated using Impact Effects Program from Collins et al. 2005). The crater formed by this impact would be about 36 km in size. There are several impact craters of this size or larger surrounding central Valles Marineris.

On Earth, liquefaction caused by earthquakes commonly arises at a depth ranging from a few meters to about 15 m and becomes increasingly difficult at depth; this is because the vertical stress applied by the overburden increases the resistance of the sediment to shearing and deformation (Obermeier 1996). The thickness of deformed sediments is thus limited by the maximum depth of sediments susceptible to liquefaction at the time of the earthquake (Simms 2003). On Earth, seismites are typically on the order of tens of centimeters to ten meters thick (Roep and Everts 1992, Mohindra and Bagati 1996, Pope et al. 1997, Mohindra and Thakur 1998, Jones and Omoto 2000, Rodríguez-Pascua et al. 2000, Simms 2003, Fernandes et al. 2007). This contrasts with the exposures of deformed beds in Valles Marineris which are up to 350 m thick. If these are seismites, it would require that sediments compact and lithify much more slowly on Mars. Sediments may not compact as easily on Mars due to the lower gravity; the mass of overburden would need to be about a third larger in order to have a similar weight of overburden with depth as on Earth. If seismites are indeed up to 350 m thick on Mars, it may also imply that cementation occurs more slowly there than on Earth. The degree of lithification would be lower if water in groundwater systems on Mars was less abundant on average than in groundwater systems on Earth. This is consistent with the evidence of incomplete lithification of the rocks observed in Meridiani Planum (McLennan et al. 2005).

Another challenge to interpreting the deformation in Valles Marineris as seismites is that the wavelength of folds in seismites on Earth is typically tens of centimeters to a couple of meters. The wavelength of folding observed on Mars is ~50 m to a kilometer. The factors controlling the wavelength of folding in seismites on Earth are uncertain, but Rodríguez-Pascua et al. (2000) suggest that folding is the result of the upward flow of liquefied sand at more or less regularly spaced sites. The wavelength may also depend on the thickness of the deforming layer or on the amplitude of the seismic waves. Pope et al. (1997) found that the fold axes of seismites were randomly oriented, although Simms (2003) found seismite fold axes had a strong preferred orientation. Simms (2003) suggests the preferred fold axes orientations are perpendicular to the direction of travel of seismic waves. Rodríguez-Pascua et al. (2000) observed that the axes of seismite convolute folds were bimodal with the two directions roughly perpendicular to each other. They suggest this is related to the directions of maximum compression and maximum stress from the paleostress ellipse.

Overall, many of the properties of the deformed sediments observed in Valles Marineris fit with a seismite interpretation. The observation of the deformation covering a broad region, the styles of deformation, and the confinement of the deformation to discrete intervals all fit well with an interpretation as seismites. However, the thickness of the deformed interval may be difficult to achieve in seismites and would imply an unusually thick stack of unlithified sediments on Mars. This would imply lithification occurred more slowly on Mars. The scale of the folding and the orientations of the fold axes are not well understood on Earth, and thus evaluating these constraints on Mars is difficult.

5.5.3.2 Landslides

Landslides deposits are common in Valles Marineris and represent some of the youngest geologic activity in this area (Late Hesperian to Amazonian) (Harrison and Grimm 2003; Quantin et al. 2004). These landslides were originally thought to be wet debris flows because of their long runout distances (Lucchitta 1979; Lucchitta 1987). However, recent work has suggested the role of interstitial fluid was negligible, and the runout distances are consistent with dry terrestrial landslides (McEwen 1989; Lajeunesse et al. 2006; Soukhovitskaya and Manga 2006). The morphology of these landslides includes slump blocks at the head, hummocky material farther out, and a vast apron of longitudinally ridged material extending to the toe (Lucchitta 1978).

Landslides are also suggested to have occurred at much earlier times in Valles Marineris. Okubo et al. (2008) suggests that folded strata in southwestern Candor Chasma are the result of a subaerial or subaqueous landslide that has been eroded such that the characteristic surface morphology is no longer present. They suggest that the folds reflect compression at the toe of a southward directed slide/slump from the nearby ILD. It has also been suggested that the detached slabs in Melas Chasma may be the result of landsliding (Skilling et al. 2002; Weitz et al. 2003).

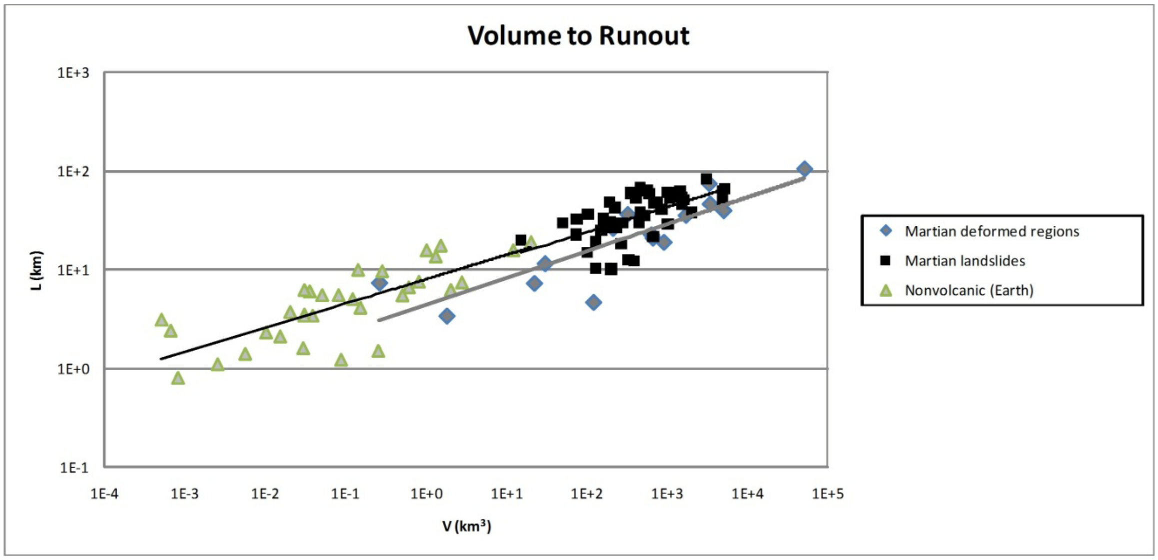

Fig 5.19. Plot showing landslide volume (V) on horizontal axis in km^3 and landslide runout (L) on vertical axis in km. Data for Martian landslides is taken from Quantin et al. 2004 (squares) and for terrestrial nonvolcanic landslides from Hayashi and Self 1992 (triangles). The volume to runout of the Martian deformed regions are from this study (diamonds).

Interpreting the deformed strata observed in Valles Marineris as the result of ancient landsliding does fit with the limited stratigraphic extent observed for the deformed strata. One would expect the beds stratigraphically below a landslide unit to be undeformed, because beds below the detachment surface of a landslide as well as beds below the surface over which the landslide runs out are not affected by the slide. The beds above a landslide deposit should also be undeformed, because they are deposited after the landslide occurs. The strata both underlying and overlying the deformed beds are undisturbed in Valles Marineris, as expected for a landslide origin. This interpretation also fits with the variety of elevations in which the deformation is observed to occur, because landslides could occur at any elevations in the chasma. The large size of the deformed units is also possible for landslide deposits. Fig. 5.19 shows the runout distance versus volume for recent Martian landslides, terrestrial nonvolcanic landslides, and the deformed units observed in Valles Marineris. The recent Martian landslides fit along the same trend as the terrestrial nonvolcanic landslides. The deformed regions in Valles Marineris fall close to the range of volume versus runout measurements from recent Martian landslides, although not along the same trend. The length for the deformed regions is actually the length of the deposit, not the runout length, because headscarp source regions for these deposits are not observed. Thus, if this deformation is the result of landsliding, the runout lengths would be expected to be longer than the values presented in Fig. 19, which would shift the fit for the deformed regions closer to the other Martian landslides.

The variety of deformational morphologies observed in Valles Marineris is also consistent with morphologies observed in large terrestrial submarine landslides (Lucente and Pini 2003; Lucente and Pini 2008). In the Miocene age Casaglia-Monte della Colonna landslide in the Northern Apennines, large detached stratified slabs and many types of folding, including overturned, recumbent, asymmetric, disharmonic, box, and refolded folds are identified (Lucente and Pini 2003). These are similar to the deformational morphologies of the detached slabs and folded strata observed in Valles Marineris. Detached slabs are observed in the upper part of terrestrial submarine slides, and these are commonly composed of undeformed strata but can also have folded strata (Lucente and Pini 2003). The slabs overlie a several meter thick strongly deformed set of beds that show isoclinal folds and overfolds; this unit acted as a shear zone (Lucente and Pini 2003). These characteristics are similar to the observation that detached slabs in Valles Marineris overlie folded strata in several areas in Candor Chasma (region 5) and in Melas Chasma (region 7). Lucente and Pini (2003) also found that the size of the slabs decreases towards the distal portion of the slide. The sizes of the slabs observed in Candor Chasma do show a decrease in average slab size on the northern and eastern part of the region. In the other regions, the size of the slabs shows no particular trend with location within a particular exposure, although the sizes of the slabs are a bit larger in Melas and a bit smaller in Ius.

The scale of the slabs observed in terrestrial submarine landslides can be hundreds of meters in size (Lucente and Pini 2003), which is of the same order as the slabs observed in Valles Marineris. The wavelength of the folding observed in terrestrial submarine landslide deposits is on the order of fifty centimeters to tens of meters in size (Lucente and Pini 2003), much smaller than the kilometer scale folds observed in Valles Marineris. However, this may in part be due to a sample bias, because it is difficult to observe kilometer scale folds in the terrestrial submarine slides.

Slabs that have an appearance similar to the detached slabs observed in Valles Marineris are also found in very slow landslides and are called 'block spreads'. Block spreads form when a thick layer of rock overlying a softer material fractures and separates due to liquefaction (Cruden and Varnes 1996). Blocks in spreads can be hundreds of meters thick and can occur over wide areas (Cruden and Varnes 1996). This type of feature would not require a body of water, but only enough pore water for liquefaction to be possible.

One of the challenges in interpreting the deformation as the result of landsliding is locating the source for each of the putative slides. The deformed regions in Ius Chasma are not adjacent to ILD, so if these are slides, the source must either be the sides of the chasma walls, or an ILD that has completely eroded away. There are ILD in Candor and Melas Chasma within ~100 km of the deformed units in those chasmata. The deformed strata are mostly topographically lower than the ILD, which means the ILD may have been able to serve as sources for potential slides. It could also mean that the deformed units are stratigraphically below the ILD and hence older. If the deformed strata were formed by landslides and these slides did originate from the ILD, then one might expect slides to have occurred around multiple sides of the ILD, which is not observed in Melas. One would also expect the orientation of the fold axes to be perpendicular to the direction of slide movement (or parallel to the walls of the ILD, if they were the source for the slides) (Lucente and Pini 2003). Also, some of the deformed strata are found on part of the Ceti Mensa ILD in Candor, so again the sources for these slides are unclear. The slides may have originated from the chasma walls of Valles Marineris, but if that were the case then no remnants of the layered material remains in many of the areas where the slides should have originated. Fold axes are oriented parallel to the chasma walls in many locations which would be expected if they were the source for the slides. However, some exceptions to this do occur and most areas exhibit a second set of fold axes that are perpendicular to the chasma walls. Although some dispersion of fold axes orientations are expected in slides due to rotation of fold hinges and sheath folds, fold axes are not typically bimodal (Lucente and Pini 2003).

Mechanisms that can trigger submarine landslides include volcanic activity; seismic activity, either faulting or impact induced; and fluid overpressurization, which occurs when rapid deposition of low permeability sediments traps pore fluid that cannot escape as the sediment compacts (Flemings et al. 2008; Lucente and Pini 2008). The same triggering mechanisms have been suggested to have caused the Amazonian landslides on Mars

(Quantin et al. 2004; Neuffer and Schultz 2006; Soukhovitskay and Manga 2006) and could have provided a triggering mechanism for potential ancient landslides.

5.5.3.3 Regional gravity gliding

Montgomery et al. (2009) suggest that the patterns of deformation surrounding the Thaumasia Plateau are indicative of a gravity-driven mega-slide. They suggest that extensional deformation in Syria Planum and Noctis Labryinthis connect to zones of transtension and strike-slip in Claritas Fossae and Valles Marineris and to compressional uplift along the Coprates Rise and Thaumasia highlands. They propose that the large-scale thin-skinned gravity spreading would have occurred above a detachment along a buried weak layer of salts or ice. In their model, Valles Marineris reflects extension, collapse, and excavation along fractures radial to Tharsis as part of one lateral margin of the Thaumasia gravity-spreading system. Their model predicts that a décollement or detachment should exist at some depth beneath the Thaumasia plateau. Because Valles Marineris is up to 8 km deep in some locations, this detachment surface might be exposed in some areas. Perhaps the deformation observed in Valles Marineris formed along the detachment surface as a result of shear from gravity gliding. This interpretation presupposes that the sediments exposed on the floor of Valles Marineris are older than the chasma itself.

If the deformation formed as a result of this potential mechanism, then one would expect that the deformation would be confined to a discrete slip surface. This surface need not correspond to a particular elevation and could have a complex 3D geometry. However, given a physically plausible geometry for the detachment, it might be expected to dip to the east near Syria Planum and dip to the west near the Thaumasia highlands, and the detachment surface might dip to the south at its northern boundary. This predicts that deformation within Valles Marineris would be located within the salt layer and should follow the detachment surface. We do find that the deformed strata in Valles Marineris have a component of salts, both mono- and polyhydrated sulfates, which could fit with the gravity-gliding model. In addition, sulfates should be easily deformed, because they are weak and prone to viscous creep. Deformation caused by gravity gliding should be confined to a limited stratigraphic interval as observed in Valles Marineris, but the elevations of the deformed strata in Valles Marineris do not convincingly delineate a discrete surface as might be expected for gravity gliding (Fig. 5.5).

The deformational morphologies expected from gravity gliding might be similar to a large landslide. Folding would be expected landward of the distal pinchout of the original salt layer as well as at the distal portion of the slide where the compressive stresses are greatest (Rowan et al. 2004). Irregular topography along the initial slide plane could cause convergent and divergent movement and cause broadly arcuate fold belts and dome and basin structures (Rowan et al. 2004). The trend of the folds may be highly variable (Rowan et al. 2004). Detached folds are observed to result from gravity gliding, but refolded folds (which could be indicative of one phase of disharmonic folding, similar to the convolute folds observed in Melas) are not documented (Rowan et al. 2004). The structural style of the folding that results from gravity gliding is highly dependent on the rheology and thickness of the décollement layer as well as the thickness of the overburden (Rowan et al. 2004). Thin overburden generally produces folds with shorter wavelengths and shorter amplitudes (Rowan et al. 2004). The wavelength of folding in Valles Marineris is somewhat smaller than for folds observed in terrestrial analog gravity glides, which would imply that the overburden on Mars was thinner than typical terrestrial glides. In gravity gliding , features somewhat similar to the detached slabs may result from many fault bounded blocks gliding down the detachment surface (Schultz-Ela 2001). Gravity-gliding would be expected to induce deformation over a broad area and this could explain the large areal exposures of deformation in Valles Marineris.

Overall, gravity gliding does fit several of the observations of deformation in Valles Marineris, including large areal extent of deformation, confinement to discrete stratigraphic interval, and some of the observed morphologies. However, the geometry of the surface defined by the deformation (at different elevations) is not consistent with what a detachment would predict. Also, the details of the deformational morphologies and grading between deformation types have not been described in terrestrial gravity-glide deposits.

6. Conclusions

Four styles of deformation including convolute folds, detached slabs, folded strata, and pull-apart structures were observed in Ius, Candor and Melas Chasmata. The deformed units are on the order of hundreds of meters thick, are underlain and overlain by undeformed strata, and occur in large exposures over broad areas and a wide range in elevation. Fold-axis orientations exhibit a bimodal distribution, with one set oriented NE-SW and another set oriented NW-SE. Visible-near infrared reflectance spectra of the deformed strata are consistent with the presence of a sulfate component, including mono- and polyhydrated varieties.

Overall, liquefaction and landsliding both provide the most parsimonious explanations for the cause of deformation observed in Valles Marineris. The morphology, limited stratigraphic interval, and large aerial distribution of the deformation fit well with liquefaction, but the scale of the features is much larger than similar features observed on Earth. Submarine or slow subaerial landsliding fits with the morphology, limited stratigraphic interval, and scale of the slabs observed in Valles Marineris, but the details of the areal distribution make identifying a source for the slides challenging. It is possible that a combination of liquefaction and landsliding may have been responsible for the formation of these features, possibly induced by local tectonic activity or a large impact. If sediments were deposited fairly rapidly in a submarine setting, then an impact could have triggered liquefaction and submarine landsliding over a broad region in Valles Marineris. Gravity gliding was considered but does not appear to be as good of a fit to the observations as the other mechanisms.

The only mechanism considered that requires the deformed strata to be deformed before the formation of Valles Marineris is gravity gliding, and this mechanism is not a good fit to our observations. If landsliding of ILD mounds was responsible for forming the deformed strata, then this could have occurred anytime after the deposition of the ILD and before the Amazonian landslides which overlie the deformed beds. If the strata deformed as a result of liquefaction, then this would imply the deformation happened soon after deposition of the sediments since liquefaction occurs in water-saturated unlithified sediments.

REFERENCES

Aharonson, O., M. T. Zuber, and D. H. Rothman (2001), Statistics of Mars' topography from the Mars Orbiter Laser Altimeter: Slopes, correlations, and physical models, J*ournal of Geophysical Research*, *106*, 23723-23735.

Ahlbrandt, T. S. ,and S. G. Fryberger (1981), Sedimentary features and significance of interdune deposits, in *Recent and Ancient Non-Marine Depositional Environments: Models for Exploration: SEPM, Special Publication 31*, edited by Flores, R.M. , 293-314.

Albarède, F., and J. Blichert-Toft, (2007), The split fate of the early Earth, Mars, Venus, and Moon, *Comptes Rendus Geoscience*, *339*, 917-927.

Allen, J. R. L. (1986), Earthquake magnitude-frequency, epicentral distance, and soft-sediment deformation in sedimentary basins, *Sedimentary Geology, 46*, 67-75.

Allen, P. A. (2008), From landscapes into geological history, *Nature*, *451*, 274-276.

Allison, M. A., S. A. Kuehl, T. C. Martin, A. Hassan (1998), Importance of flood-plain sedimentation for river sediment budgets and terrigenous input to the oceans; insights from the Brahmaputra-Jamuna River *Geology*, *26*, 175-178.

Alvarez, W., E. Staley, D. O'Connor, and M. A. Cham (1998), Synsedimentary deformation in the Jurassic of southeastern Utah- A case of impact shaking?, *Geology, 26*, 579-582.

Andrews-Hanna, J. C., R. J. Phillips, and M. T. Zuber (2007), Meridiani Planum and the global hydrology of Mars, *Nature, 446*, 163-166.

Andteron, R. (1976), Tidal-shelf sedimentation: An example from the Scottish Dalradian, *Sedimentology, 23,* 429-458.

Are, F., and E. Reimnitz (2000), An overview of the Lena River delta setting: geology, tectonics, geomorphology, and hydrology, *Journal of Coastal Research*, *16*, 1083–1093.

Arvidson, R. E., F. P. Seelos, K. S. Deal, W. C. Koeppen, N. O. Snider, J. M. Kieniewicz, B. M. Hynek, M. T. Mellon, and J. B. Garvin (2003), Mantled and exhumed terrains in Terra Meridiani, Mars, *Journal of Geophysical Research, 108,* 8073.

Arvidson, R. E., R. C. Anderson, P. Bartlett, J. F. Bell, P. R. Christensen, P. Chu, K. Davis, B. L. Ehlmann, M. P. Golombek, S. Gorevan, E. A. Guiness, A. F. C. Haldemann, K. E. Herkenhoff, G. Landis, R. Li, R. Lindemann, D. W. Ming, T. Myrick, T. Parker, L. Richter, F. P. Seelos, L. A. Soderblom, S. W. Squyres, R. J. Sullivan, and J. Wilson (2004), Localization and physical property experiments conducted by opportunity at Meridiani Planum, *Science, 306,* 1730-1733.

Arvidson, R. E., F. Poulet, R. V. Morris, J. P. Bibring, J. F. Bell, S. W. Squyres, P. R. Christensen, G. Bellucci, B. Gondet, B. L. Ehlmann, W. H. Farrand, R. L. Fergason, M. Golombek, J. L. Griffes, J. Grotzinger, E. A. Guiness, K. E. Herkenhoff, J. R. Johnson, G. Klingelhöfer, Y. Langevin, D. Ming, K. Seelos, R. J. Sullivan, J. G. Ward, S. M. Wiseman, and M. Wolff (2006), Nature and origin of the hematite-bearing plains of Terra Meridiani based on analyses of orbital and Mars Exploration rover data sets, *Journal of Geophysical Research, 111,* E12S08, doi:10.1029/2006JE002728.

Ashley, G. M., J. B. Southard, and J. C. Boothroyd (1982), Deposition of climbing-ripple beds: a flume simulation, *Sedimentology*, *29*, 67-79.

Back, S., M. de Batist, P. Kirillov, M. R. Strecker, P. Vanhauwaert (1998), The Frolikha Fan: A large Pleistocene glaciolacustrine outwash fan in northern Lake Baikal, Siberia, *Journal of Sedimentary Research*, *68*, 841-849.

Bagnold, R. A. (1941), *The Physics of Blown Sand and Desert Dunes*, London, Chapman & Hall, 265 p.

Baker, V. R. (2001), Water and the Martian landscape, *Nature*, *412*, 228-236.

Baker, V. R., (2006), Geomorphological evidence for water on Mars, *Elements, 2*, 139-143.

Bal, A., and D. W. Lewis (1994), A Cretaceous-early Tertiary macrotidal estuarine-fluvial succession: Puponga Coal Measures in Whanganui Inlet, onshore Pakawau Sub-basin, northwest Nelson, New Zealand, *New Zealand Journal of Geology and Geophysics*, *37*, 287.

Beales, F. W. (1972), Dolomitic mottling in Palliser (Devonian) limestone, Banff and Jasper National Parks, Alberta, in *Carbonate Rocks I: Classifications--Dolomite--Dolomitization*, AAPG Reprint Series no 4.

Beaubouef, R. T., J. C. Van Wagoner, N. L. Adair (2003), Ultra-High Resolution 3-D Characterization of Deep-Water Deposits-II: Insights into the Evolution of a Submarine Fan and Comparisons with River Deltas, extended abstract *AAPG Annual Meeting*, Salt Lake City, UT.

Behrmann, J. H., et al. (2006), Rapid Sedimentation, Overpressure, and Focused Fluid Flow, Gulf of Mexico Continental Margin, *Scientific Drilling, 3*, 12-17.

Bell, J. F., S. W. Squyres, K. E. Herkenhoff, J. N. Maki, H. M. Arneson, D. Brown, S. A. Collins, A. Dingizian, S. T. Elliot, E. C. Hagerott, A. G. Hayes, M. J. Johnson, J. R.

Johnson, J. Joseph, K. Kinch, M. T. Lemmon, R. V. Morris, L. Scherr, M. Schwochert, M. K. Shepard, G. H. Smith, J. N. Sohl-Dickstein, R. J. Sullivan, W. T. Sullivan, and M. Wadsworth (2003), Mars Exploration Rover Athena Panoramic Camera (Pancam) investigation, *Journal of Geophysical Research, 108*, E12.

Beyer, R. A., H. J. Melosh, A. McEwen, and R. D. Lorenz (2000), Salt diapirs in Candor Chasma, Mars?, LPSC XXXI abstract, League City, TX.

Bhattacharya, J. P., and R. G. Walker (1991), River- and wave-dominated depositional systems of the Upper Cretaceous Dunvegan Formation, northwestern Alberta, *Bulletin of Canadian Petroleum Geology, 39*(2), 165-191.

Bhattacharya, J. P., and R. G. Walker (1992), Deltas, in *Facies Models: A Response to Sea Level Change*, edited by R. G. Walker and N. P. James, pp. 157-177, Geological Association of Canada, Stittsville, Ontario.

Bhattacharya, J. P., T. H. D. Payenberg, S. C. Lang, and M. C. Bourke (2005), Dynamic river channels suggest a long-lived Noachian crater lake on Mars. *Geophysical Research Letters*, *32*, L10201, doi:10.1029/2005GL022747.

Blair, T. C., and J. G. McPherson (1994a), Alluvial fan processes and forms, in *Geomorphology of Desert Environments*, edited by A. D. Abrahams and A. J. Parsons, pp. 354-402, Chapman & Hall, London.

Blair, T. C., and J. G. McPherson (1994b), Alluvial fans and their natural distinction from rivers based on morphology and, hydraulic processes, sedimentary processes and facies assemblages, *Journal of Sedimentary Research*, *A64*, 450-489.

Blondel, P., and B. J. Murton (1997), *Handbook of Seafloor Sonar Imagery*, Chichester, England, John Wiley & Sons, 314 p.

Bouma, A. H. (1962), *Sedimentology of Some Flysch Deposits; A Graphic Approach to Facies Interpretation*, 168 pp., Elsevier, Amsterdam.

Branney, M. J., and P. Kokelaar (2002), *Pyroclastic density currents and the sedimentation of ignimbrites*, Geological Society of London Memoir 27, 143 p.

Breuer, D., and T. Spohn (2003), Early plate tectonics versus single-plate tectonics on Mars: Evidence from magnetic field history and crust evolution, *Journal of Geophysical Research, 108*, 5072.

Bristow, C. S. (1993), *Sedimentary structures exposed in bar tops in the Brahmaputra River, Bangladesh*, Geological Society of London Special Publications, 75, 277-289.

Britter, R. E., and P. F. Linden (1980), The motion of the front of a gravity current traveling down an incline, *Journal of Fluid Mechanics*, *99*, 531-543.

Brookfield, M. E. (1977), Origin of bounding surfaces in ancient aeolian sandstones, *Sedimentology, 24,* 303-332.

Bullen, S. B., and D. F. Sibley (1984), Dolomite selectivity and mimetic replacement, *Geology, 12*, 655-658.

Catling, D. C., S. E. Wood, C. Leovy, D. R. Montgomery, H. M. Greenberg, C. R. Glein, and J. M. Moore (2006), Light-toned layered deposits in Juventae Chasma, Mars, *Icarus*, *181*, 26-51, doi:10.1016/j.icarus.2005.10.020.

Chakraborty, C., and P. K. Bose (1992), Ripple/dune to upper stage plane bed transition: some observations from the ancient record, *Geological Journal*, *27*, 349-359.

Chapman, M. G., and K. L. Tanaka (2001), Interior trough deposits on Mars: Subice volcanoes?, *Journal of Geophysical Research*, *106*, 10087-10100.

Cheel, R. J., and G. V. Middleton (1986), Horizontal laminae formed under upper flow regime plane bed conditions, *Journal of Geology, 94,* 489-504.

Chojnacki, M., and B. M. Hynek (2008), Geological context of water-altered minerals in Valles Marineris, Mars, *Journal of Geophysical Research, 113*, E12005, doi:10.1029/ 2007JE003070.

Christensen, P. R., J. L. Bandfield, R. N. Clark, K. S. Edgett, V. E. Hamilton, T. Hoefen, H. H. Kieffer, R. O. Kuzmin, M. D. Lane, M. C. Malin, R. V. Morris, J. C. Pearl, R. Pearson, T. L. Roush, S. W. Ruff, and M. D. Smith (2000), Detection of crystalline hematite mineralization on Mars by the Thermal Emission Spectrometer: Evidence for near-surface water, *Journal of Geophysical Research*, 105, 9623-9642.

Clark, B. C., R. V. Morris, S. M. McLennan, R. Gellert, B. Joliff, A. H. Knoll, S. W. Squyres, T. K. Lowenstein, D. W. Ming, N. J. Tosca, A. Yen, P. R.Christensen, S. Gorevan, J. Bruckner, W. Calvin, G. Dreibus, W. Farand, G. Klingelhöfer, H. Waenke, J. Zipfel, J. F. Bell, J. P. Grotzinger, H. Y. McSween, and R. Rieder (2005), Chemistry and mineralogy of outcrops at Meridiani Planum, *Earth and Planetary Science Letters, 240*, 73-94.

Clark, J. D., N. H. Kenyon, K. T. Pickering (1992), Quantitative analysis of the geometry of submarine channels: Implications for the classification of submarine fans, *Geology*, *20*, 633-636.

Clark, J. D., and K. T. Pickering, (1996), Architectural elements and growth patterns of submarine channels: Applications to hydrocarbon exploration. *AAPG Bulletin, 80,* 194-221.

Clemmensen, L. B., H. Olsen, and R. C. Blakey (1989), Erg-margin deposits in the Lower

Jurassic Moenave Formation, Wingate Sandstone, south Utah, *GSA Bulletin*, *101*, 759-773.

Coleman, J. M., and L. D. Wright (1975), Modern river deltas: Variability of processes and sand bodies, in *Deltas: Models for exploration*, edited by M. L. Broussard, Houston Geological Society, Houston, 99-149.

Coleman, J. M., D. B. Prior, J. F. Lindsay (1983), Deltaic influences on shelf-edge instability processes, in *The Shelfbreak: Critical Interface on Continental Margins*, edited by D. J. Stanley and G. T. Moore, Society of Economic Paleontologists and Mineralogists, Tulsa, 121-137.

Collins, G. S., H. J. Melosh, and R. A. Marcus (2005), Earth impact effects program: A web-based computer program for calculating the regional environmental consequences of a meteoroid impact on Earth, *Meteoritics & Planetary Science, 40*, 817-840.

Covault, J. A., W. R. Normark, B. W. Romans, S. A. Graham (2007), Highstand fans in the California boderland: The overlooked deep-water depositional systems, *Geology*, *35*, 783-786.

Cruden, D. M., and D. J. Varnes, (1996), Landslide types and processes, in *Landslides: Investigation and Mitigation*, edited by Turner, A.K., and Schuster, R.L., Special Report 247, Washington, DC, National Academy Press, 36-75.

Dalrymple, R. W. (1992), Tidal depositional systems, in *Facies Models: Geological Society of Canada*, edited by R. G. Walker and N. P. James, N.P., St. John's, 195-218.

Damuth, J. E., V. Kolla, R. D. Flood, R. O. Kowsmann, M. C. Monteiro, M. Gorini, J. J. C. Palma, R. H. Belderson (1983a), Distributary channel meandering and bifurcation patterns on the Amazon deep-sea fan as revealed by long-range side-scan sonar (GLORIA). *Geology*, *11*, 94-98.

Damuth, J. E., R. O. Kowsmann, R. D. Flood, R. H. Belderson, M. A. Gorini (1983b), Age relationships of distributary channels on Amazon deep-sea fan: Implications for fan growth pattern, *Geology*, *11*, 470-473.

Damuth, J. E., and R. D. Flood (1984), Morphology, sedimentation processes, and growth pattern of the Amazon deep-sea fan, *Geo-Marine Letters*, *3*, 109-117.

Dardis, G. F. (1985), Genesis of Late Pleistocene cross-valley moraine ridges, south-central Ulster, Northern Ireland, *Earth Surface Processes and Landforms*, *10*, 483-495.

Dasgupta, P. (2003), Sediment gravity flow- the conceptual problems, *Earth-Science Reviews*, *62*, 265-281.

Davenport, C. A., and P. S. Ringrose (1987), Deformation of Scottish Quaternary sediment sequences by strong earthquake motions, in *Deformation of Sediments and Sedimentary Rocks*, edited by M. E. Jones, and R. M. F. Preston, Geological Society Special Publication No. 29, 299-314.

Davis, D. M., and T. Engelder, (1985), The role of salt in fold and thrust belts, *Tectonophyics.*, *119*, 67-88.

de Meer, S., and C. J. Spiers, (1995), Creep of wet gypsum aggregates under hydrostatic loading conditions, *Tectonophysics*, *245*, 171-183.

De Pater, I., and J. J. Lissauer (2001), *Planetary Sciences*, Cambridge University Press, Cambridge, U. K., 568 p.

Demicco, R. V., and L. Hardie (1994), *Sedimentary Structures and Early Diagenetic Features of Shallow Marine Carbonate Deposits*, SEPM, Atlas, v. 1.

Deptuck, M. E., Z. Sylvester, C. Pirmez, and C. O'Byrne, (2007), Migration-aggradation history and 3-D seismic geomorphology of submarine channels in the Pleistocene Benin-major Canyon, western Niger Delta slope. *Marine and Petroleum Geology*, *24*, 406-433.

Dickson, J. L., J. W. Head, M. Kreslavsky (2007), Martian gullies in the southern mid-latitudes of Mars: Evidence for climate-controlled formation of young fluvial features based upon local and global topography, *Icarus*, *188*, 315-323.

Dietrich, W. E. and P. J. Whiting (1989), Boundary shear stress and sediment transport in river meanders of sand and gravel, in *River Meandering*, edited by K. Ikeda and G. Parker, American Geophysical Union Water Resources Monograph 12, 1-50.

Dromart, G., C. Quantin, O. Broucke (2007), Stratigraphic architectures spotted in southern Melas Chasma, Valles Marineris, Mars, *Geology*, *35*, 363-366.

Droz, L., R. Kergoat, P. Cochonat, S. Berné (2001), Recent sedimentary events in the western Gulf of Lions (western Mediterranean), *Marine Geology*, *176*, 23–37.

Droz, L., A. T. dos Reis, M. Rabineau, S. Berne, G. Bellaiche (2006), Quaternary turbidite systems on the northern margins of the Balearic Basin (Western Mediterranean): a synthesis, *Geo-Marine Letters, 26*, 347-359.

Edgett, K. (2005), The sedimentary rocks of Sinus Meridiani: Five key observations from data acquired by the Mars Global Surveyor and Mars Odyssey orbiters, *Mars, 1*, 5-58.

Edgett, K. S., and M. C. Malin (2002), Martian sedimentary rock stratigraphy: Outcrops and interbedded craters of northwest Sinus Meridiani and southwest Arabia Terra, *Geophysical Research Letters, 29*, 2179.

Edmonds, D. A., and R. L. Slingerland, (2007), Mechanics of river mouth bar formation: Implications for the morphodynamics of delta distributary networks, *Journal of Geophysical Research, 112*, F02034, doi:10.1029/2006JF000574.

Edmonds, D. A., D. C. J. D. Hoyal, B. A. Sheets, and R. L. Slingerland (2009), Predicting avulsions: Implications for coastal wetland restoration, *Geology, 37,* 759-762, doi: 10.1130/G25743A.

EEZ-SCAN Scientific Staff (1991), Atlas of the U.S. Exclusive Economic Zone, Bering Sea: U.S. Geological Survey Miscellaneous Investigations, I-2053, 145 p.

Ehlmann, B. L., J. Mustard, C. I. Fassett, S. C. Schon, J. W. Head, D. J. Des Marais, J. Grant, S. Murchie (2008), Clay minerals in delta deposits and organic preservation potential on Mars, *Nature Geoscience, 1*, 355-358.

Fassett, C. I., and J. W. Head (2005), Fluvial sedimentary deposits on Mars: Ancient deltas in a crater lake in the Nili Fossae region, *Geophysical Research Letters, 32*, L14201, doi:10.1029/2005GL023456.

Fernandes, L. A., A. B. de Castro, and G. Basilici (2007), Seismites in continental sand sea deposits of the Late Cretaceous Caiua Desert Bauru Basin, Brazil, *Sedimentary Geology, 199*, 51-64.

Fischer, A. G. (1964), The Lofer Cyclothems of the Alpine Triassic, in *Symposium on Cyclic Sedimentation*, edited by D. F. Merriam, Kansas State Geological Survey, Bulletin 169, 107-149.

Flauhaut, J., C. Quantin, P. Allemand, and P. Thomas, *In Press*, Morphology and geology of the ILD in Capri/Eos Chasma (Mars) from visible and infra-red data, *Icarus*, 10.1016/j.icarus.2009.11.019.

Flemings, P. B., and J. P. Grotzinger (1996), STRATA: Freeware for analyzing classic stratigraphic problems *GSA Today*, *6*, 1-7.

Flemings, P. B., H. Long, B. Dugan, J. Germaine, C. M. John, J. H. Behrmann, D. Sawyer, and I. E. Scientists (2008), Erratum to "Pore pressure penetrometers document high overpressure near the seafloor where multiple submarine landslides have occurred on the continental slope, offshore Louisiana, Gulf of Mexico", *Earth and Planetary Science Letters*, *274*, 269-283, 10.1016/j.epsl.2008.06.027.

Flood, R. D., and J. E. Damuth (1987), Quantitative characterisitcs of sinuous distributary channels on the Amazon Seep-Sea Fan, *GSA Bulletin*, *98*, 728-739.

Frederiksen, K. S., L. B. Clemmensen, H. S. Lawaetz (1998), Sequential architecture and cyclicity in Permian desert deposits, Brodick Beds, Arran, Scotland, *Journal of the Geological Society of London*, *155*, 677-683.

French, B. M. (2004), The importance of being cratered: The new role of meteorite impact as a normal geological process, *Meteoritics & Planetary Science*, *39*, 169-197.

Fryberger, S. G., and C. J. Schenk (1988), Pin stripe lamination - a distinctive feature of modern and ancient eolian sediments, *Sedimentary Geology*, *55*, 1-15.

Fryberger, S. G., T. S. Ahlbrandt, and S. Andrews (1979), Origin, sedimentary features, and significance of low-angle eolian "sand sheet" deposits, Great Sand Dunes National Monument and vicinity, Colorado, *Journal of Sedimentary Petrology*, *49*, 733-746.

Fryberger, S. G., A. M. Al-Sari, and T. J. Clishamp (1983), Eolian dune, interdune, sand sheet and siliciclastic sabkha sediments of an offshore prograding sand sea, Dhahran Area, Saudi Arabia, *AAPG Bulletin*, *67*, 280-312.

Fueten, F., R. Stesky, P. MacKinnon, E. Hauber, K. Gwinner, F. Scholten, T. Zegers, G. Neukum (2006), A structural study of an interior layered deposit in southwestern Candor Chasma, Valles Marineris, Mars, using high resolution stereo camera data from Mars Express, *Geophysical Research Letters*, *33*, L07202, doi:10.1029/ 2005GL025035.

Fueten, F., R. Stesky, P. MacKinnon, E. Hauber, T. Zegers, K. Gwinner, F. Scholten, and G. Neukum (2008), Stratigraphy and structure of interior layered deposits in west Candor Chasma, Mars, from High Resolution Stereo Camera (HRSC) stereo imagery and derived elevations, *Journal of Geophysical Research*, *113*, E10008, doi:10.1029/2007JE003053.

Galloway, W. E. (1975), Process framework for describing the morphologic and stratigraphic evolution of deltaic depositional systems, in *Deltas: Models for Exploration*, edited by M. L. Broussard, Houston Geological Society, Houston.

Gardner, J. V., M. E. Field, H. Lee, and B. E. Edwards (1991), Ground-truthing 6.5-kHz side scan sonographs': What are we really imaging? *Journal of Geophysical Research*, *96*, 5955-5974.

Gardner, J. V. (2007), Law of the Sea Mapping Program, http://www.ccom-jhc.unh.edu/index.php?p=39|46&page=law_of_the_sea.php, edited.

Glotch, T. D., and P. R. Christensen (2005), Geologic and mineralogic mapping of Aram Chaos: Evidence for a water-rich history, *Journal of Geophysical Research*, *110*.

E09006, doi:10.1029/2004JE002389.

Goodbred, S. L., and S. A. Kuehl (1998), Floodplain processes in the Bengal Basin and the storage of Ganges–Brahmaputra river sediment: an accretion study using ^{137}Cs and ^{210}Pb geochronology *Sedimentary Geology*, *121*, 239-258.

Grant, J. A., R. P. Irwin, J. P. Grotzinger, R. E. Milliken, L. L. Tornabene, A. S. McEwen, C. M. Weitz, S. W. Squyres, T. D. Glotch, B. J. Thomson (2008), HiRISE imaging of impact megabreccia and sub-meter aqueous strata in Holden Crater, Mars, *Geology*, *36*, 195-198.

Griffes, J. L., J. P. Grotzinger, and R. E. Milliken (2010), Working towards a classification scheme for sedimentary rocks on Mars, Lunar and Planetary Science Conference, abstract, Woodlands, TX.

Grotzinger, J. P., R. E. Arvidson, J. F. Bell, W. Calvin, B. C. Clark, D. A. Fike, M. Golombek, R. Greeley, A. Haldemann, K. E. Herkenhoff, B. L. Jolliff, A. H. Knoll, M. Malin, S. M. McLennan, T. Parker, L. Soderblom, J. N. Sohl-Dickstein, S. W. Squyres, N. J. Tosca, and W. A. Watters (2005), Stratigraphy and sedimentology of a dry to wet eolian depositional system, Burns formation, Meridiani Planum, Mars, *Earth and Planetary Science Letters*, *240*, 11-72.

Grotzinger, J. P., J. Bell, K. Herkenhoff, J. Johnson, A. Knoll, E. McCartney, S. McLennan, J. Metz, J. Moore, S. Squyres, R. Sullivan, A. Aharonson, R. Arvidson, B. Joliff, M. Golombek, K. Lewis, T. Parker, and L. Soderblom (2006), Sedimentary textures formed by aqueous processes, Erebus crater, Meridiani Planum, Mars, *Geology, 34*, 1085-1088.

Hamelin, N., H. Racher, F. Fueten, R. Stesky, P. MacKinnon, E. Hauber, K. Gwinner, F. Scholten, and T. Zegers, (2008), Structural analysis of an interior layered deposit in northern Coprates Chasma, Mars, Lunar and Planetary Science Conference XXXIX, Abstract 1424, Woodlands, TX.

Harrison, K. P., and R. E. Grimm (2003), Rheological constraints on Martian landslides, *Icarus*, *163*, 347–362.

Hartmann, W. K. (2005), Martian cratering 8: Isochron refinement and the chronology of Mars, *Icarus*, *174*, 294-320.

Harvey, A. M. (1984), Debris flow and fluvial deposits in Spanish Quaternary alluvial fans: Implications for fan morphology, in *Sedimentology of Gravels and Conglomerates, Memoir 10,* edited by E. H. Koster and R. J. Steel, Candian Society of Petroleum Geologists, Calgary, 123-132.

Harvey, A. M. A. E. Mather, M. Stokes (2005), Alluvial fans: geomorphology, sedimentology, dynamics, *Geological Society of London, Special Publications 251*, 1-7.

Hashimoto, A., T. Oguchi, Y. Hayakawa, Z. Lin, K. Saito, T. A. Wasklewicz (2008), GIS analysis of depositional slope change at alluvial-fan toes in Japan and the American Southwest, *Geomorphology, 100,* 120-130.

Hauber, E., K. Gwinner, A. Gendrin, F. Fueten, R. Stesky, S. M. Pelkey, H. Wulf, D. Reiss, T. Zegers, P. MacKinnon, G. Michael, R. Jaumann, J. P. Bibring, G. Neukum, and H. C. -I. Team (2006), An integrated study of interior layered deposits in Hebes Chasma, Valles Marineris, Mars, using MGS, MO and MEX data, Lunar and Planetary Science Conference XXXVII, Abstract 2022, League City, TX.

Hayashi, J. N., and S. Self (1992), A comparison of pyroelastic flow and debris avalanche mobility, *Journal of Geophysical Research, 97*, 9063-9071.

Head, J. W., D. R. Marchant, M. C. Agnew, C. I. Fassett, and M. A. Kreslavsky (2006), Extensive valley glacier deposits in the northern mid-latitudes of Mars: Evidence for Late Amazonian obliquity-driven climate change, *Earth and Planetary Science Letters*, *241*, 663-671.

Heard, H. C., and W. M. Rubey (1966), Tectonic implications of gypsum dehydration, *GSA Bulletin, 77*, 741-760.

Heldmann, J. L., E. Carlsson, H. Johansson, M. T. Mellon, O. B. Toon (2007), Observations of Martian gullies and constraints on potential formation mechanisms II. The northern hemisphere, *Icarus, 188*, 324-344.

Herman, A. K., P. R. Carlson, J. V. Gardner (1996), Aleutian Basin of the Bering Sea: Styles of sedimentation and canyon development, in *Geology of the United States Seafloor: The view from GORIA*, edited by J. V. Gardner, et al., Cambridge University Press, Cambridge, 305-332.

Hernandez-Molina, F. J., E. Llave, D. A. V. Stow, M. Garcia, L. Somoza, J. T. Vazqueze, F. J. Lobof, A. Maestrob, V. Dıaz del Rıog, R. Leonb, T. Medialdeab, J. Gardnerh (2006), The contourite depositional system of the Gulf of Ca´diz: A sedimentary model related to the bottom current activity of the Mediterranean outflow water and its interaction with the continental margin, *Deep-Sea Research II*, *53*, 1420-1463.

Hodgson, D. M., S. S. Flint, D. Hodgetts, N. J. Drinkwater, E. P. Johannessen, S. M. Luthi (2006), Stratigraphic evolution of fine-grained submarine fan systems, Tanqua Depocenter, Karoo Basin, South Africa, *Journal of Sedimentary Research, 76*, 20-

40.

Hummel, G., and G. Kocurek (1984), Interdune areas of the back-island dune field, North Padre Island, Texas, *Sedimentary Geology, 39,* 1-26.

Hunter, R. E. (1977a), Basic types of stratification in small eolian dunes, *Sedimentology*, *24*, 361-387.

Hunter, R. E. (1977b), Terminology of cross-stratified sedimentary layers and climbing-ripple structures, *Journal of Sedimentary Petrology*, *47*, 697-706.

Hunter, R. E. (1981), Stratification styles in eolian sandstones: some Pennsylvanian to Jurassic examples from the western interior U.S.A., in *Recent and Ancient Nonmarine Depositional Environments: Models for Exploration*, edited by F. G. Ethridge, and R. M. Flores, SEPM, Special Publication 31, 315-329.

Hynek, B. M. (2004), Implications for hydrologic processes on Mars from extensive bedrock outcrops throughout Terra Meridiani, *Nature*, *431*, 156-159.

Jackson, B. A. (2004), Seismic evidence for gas hydrates in the North Makassar Basin, Indonesia, *Petroleum Geoscience*, *10*, 227-238.

Jackson, M. P. A., and C. J. Talbot (1986), External shapes, strain rates, and dynamics of salt structures, *GSA Bulletin.*, *97*, 305-323.

Jerolmack, D. J., D. Mohrig, M. T. Zuber, S. Byrne (2004), A minimum time for the formation of Holden Northeast fan, Mars, *Geophysical Research Letters*, *31*, L21701, doi:10.1029/2004GL021326.

Jerolmack, D. J., D. Mohrig, J. P. Grotzinger, D. A. Fike, and W. A. Watters (2006), Spatial grain size sorting in eolian ripples and estimation of wind conditions on planetary surfaces: Application to Meridiani Planum, Mars, *Journal of Geophysical*

Research, *111*, E12S02, doi:10.1029/2005JE002544.

Jerolmack, D., and D. Mohrig (2007), Conditions for branching in depositional rivers, *Geology, 35,* 463-466, doi: 10.1130/G23308A.1.

Johnson, K. S. (2005), Subsidence hazards due to evaporite dissolution in the United States, *Environmental Geology, 48*, 395-409.

Jones, A. P., and K. Omoto (2000), Towards establishing criteria for identifying trigger mechanisms for soft-sediment deformation: a case study of Late Pleistocene lacustrine sands and clays, Onikobe and Nakayamadaira Basins, northeastern Japan, *Sedimentology, 47*, 1211-1226.

Jones, G. H. S. (1978), Coherently overturned flaps surrounding craters, *Nature*, *273*, 211-213.

Kane, I. A., W. D. McCaffrey, J. Peakall (2008), Controls on sinuosity evolution within submarine channels, *Geology*, *36*(4), 287-290.

Karl, H. A., M. A. Hampton, N. H. Kenyon (1989), Lateral migration of Cascadia deep-sea channel in response to accretionary tectonics, *Geology, 17*, 144-147.

Kenyon, N. H., and J. Millington (1995), Contrasting deep-sea depositional systems in the Bering Sea., in *Atlas of deep water environments: architectural style in turbidite systems*, edited by K. T. Pickering, et al., Chapman and Hall, London, 196–202.

Kirk, R. L., E. Howington-Krause, M. R. Rosiek, J. A. Anderson, B. A. Archinal, K. J. Becker, D. A. Cook, D. M. Galuszka, P. E. Giessler, T. M. Hare, I. M. Holmberg, L. P. Keszthelyi, B. L. Redding, W. A. Delamere, D. Gallagher, J. D. Chapel, E. M. Eliason, R. King, and A. S. McEwen (2008), Ultrahigh resolution topographic mapping of Mars with MRO HiRISE stereo images: Meter-scale slopes of candidate Phoenix landing sites, *Journal of Geophysical Research, 113*, E00A24, doi: 10.1029/2007JE003000.

Klaucke, I., D. G. Masson, N. H. Kenyon, J. V. Gardner (2004), Sedimentary processes of the lower Monterey Fan channel and channel-mouth lobe, *Marine Geology*, *206*, 181-198.

Knauth, L. P., D. M. Burt, and K. H. Wohletz (2005), Impact origin of sediments at the opportunity landing site on Mars, *Nature, 438*, 1123-1128.

Kneller, B. C., and C. Buckee (2000), The structure and fluid mechanics of turbidity currents: a review of some recent studies and their geological implications, *Sedimentology*, *47*, 62-94.

Knoll, A., B. Joliff, W. Farrand, J. Bell, B. Clark, R. Gellert, M. Golombek, J. Grotzinger, K. Herkenhoff, J. Johnson, S. McLennan, R. Morris, S. Squyres, R. Sullivan, N. Tosca, A. Yen, and Z. Learner (2008), Veneers, Rinds, and Fracture Fills: Relatively Late Alteration of Sedimentary Rocks at Meridiani Planum, Mars, *Journal of Geophysical Research, 113*, E06S16, doi:10.1029/2007JE002949.

Kocurek, G. (1981), Significance of interdune deposits and bounding surfaces in aeolian dune sands, *Sedimentology, 28*, 753-780.

Kocurek, G. (1991), Interpretation of ancient eolian sand dunes, *Annual Reviews of Earth and Planetary Science, 19*, 43-75.

Kocurek, G., and J. Nielson (1986), Conditions favourable for the formation of warm-climate aeolian sand sheets, *Sedimentology, 33*, 795-816.

Kolla, V. H. W. Posamentier, and L. J. Wood (2007), Deep-water and fluvial sinuous channels – Characteristics, similarities and dissimilarities, and modes of formation, *Marine and Petroleum Geolology, 24*, 388-405.

Komatsu, G., P. E. Geissler, R. G. Strom, and R. B. Singer (1993), Stratigraphy and erosional landforms of layered deposits in Valles Marineris, Mars, *Journal of Geophysical Research, 98*, 11105-11121.

Komatsu, G., G. G. Ori, P. Ciarcelluti, Y. D. Litasov (2004), Interior layered deposits of Valles Marineris, Mars: analogous subice volcanism related to Baikal Rifting, Southern Siberia, *Planetary and Space Science*, *52*, 167-187.

Konyukhov, A. I. (2009), Geological structure, sedimentation conditions, and petroleum potential of sedimentary basins in Southeast Asia, *Lithology and Mineral Resources*, *44*, 427-440.

Kraal, E. R., E. Asphaug, J. M. Moore, A. Howard, A. Bredt (2008a), Catalogue of large alluvial fans in Martian impact craters, *Icarus*, *194*, 101-110.

Kraal, E. R., M. van Dijk, G. Postma, M. G. Kleinhans (2008b), Martian stepped-delta formation by rapid water release, *Nature*, *451*, 973-976.

Labourdette, R. (2007), Integrated three-dimensional modeling approach of stacked turbidite channels, *AAPG Bulletin*, *91*, 1603-1618, doi: 10.1306/06210706143.

Lajeunesse, E., C. Quantin, P. Allemand, and C. Delacourt (2006), New insights on the runout of large landslides in the Valles-Marineris canyons, Mars, *Geophysical Research Letters*, *33*, L04403.

Lane-Serff, G. F., L. M. Beal, and T. D. Hadfield (1995), Gravity current flow over obstacles, *Journal of Fluid Mechanics, 292,* 39-53

Langford, R. P. (1989), Fluvial-aeolian interactions part 1, modern systems, *Sedimentology*, *36*, 1023-1035.

Langford, R., and B. Bracken (1987), Medano Creek, Colorado, a model for upper flow-regime fluvial deposition, *Journal of Sedimentary Petrolology, 57*, 863-870.

Lawson, D. E. (1983), Erosion of perennially frozen streambanks, US Army Corps of Engineers, Cold Regions Research & Engineering Laboratory, CRREL Report 83-29.

Leclair, S. F. (2002), Preservation of cross-strata due to the migration of subaqueous dunes: an experimental investigation, *Sedimentology, 49*, 1157-1180.

Leeder, M. R. (1999), *Sedimentology and Sedimentary Basins,* Blackwell, Oxford, 592 pp.

Lewis, K. W., and O. Aharonson (2006), Stratigraphic analysis of the distributary fan in Eberswalde crater using stereo imagery, *Journal of Geophysical Research, 111*, doi:10.1029/2005JE002558.

Lewis, K. W., O. Aharonson, J. P. Grotzinger, R. L. Kirk, A. S. McEwen, and T. A. Suer (2008a), Quasi-periodic bedding in the sedimentary rock record of Mars, *Science, 322*, 1532-1535.

Lewis, K. W., O. Aharonson, J. P. Grotzinger, S. W. Squyres (2008b), Structure and stratigraphy of Home Plate from the Spirit Mars Exploration Rover, *Journal of Geophysical Research, 113*, E12S36, doi:10.1029/2007JE003025.

Link, M. H. (2003), Depositional systems and sedimentary facies of the Miocene-Pliocene Ridge Basin Group, Ridge Basin, southern California, in *Evolution of Ridge Basin, Southern California*, edited by J. C. Crowell, The Geological Society of America, Boulder, Colorado, 17-87.

Lowe, D. R. (1975), Water escape structures in coarse-grained sediments, *Sedimentology*, *22*, 157-204.

Lozinsky, R. P. (1994), Cenozoic stratigraphy, sandstone petrology, and depositional history of the Albuquerque Basin, central New Mexico, in *Basins of the Rio Grande Rift: Structure, Stratigraphy, and Tectonic Setting*, edited by G. R. Keller and S. M. Cather, GSA, Boulder, 73-81.

Lucchitta, B. K. (1978), A large landslide on Mars, *GSA Bulletin, 89*, 1601-1609.

Lucchitta, B. K. (1979), Landslides in Valles Marineris, Mars, *Journal of Geophysical Research,84*, 8097-8113.

Lucchitta, B. K. (1987), Valles Marineris, Mars: Wet debris flows and ground ice, *Icarus, 72*, 411-429.

Lucchitta, B. K. (1990), Young volcanic deposits in the Valles Marineris, Mars? *Icarus*, *86*(2), 476-509.

Lucchitta, B. K., A. S. McEwen, G. D. Clow, P. E. Geissler, R. B. Singer, R. A. Schultz, and S. W. Squyres (1992), The canyon system on Mars, in *Mars*, edited by H. H. Kieffer, B. M. Jakosky, C. W. Snyder, and M. Matthews, Tucson, University of Arizona Press, 453-492.

Lucchitta, B. K., N. K. Isbell, and A. Howington-Kraus (1994), Topography of Vallis Marineris: Implications for erosional and structural history, *Journal of Geophysical Research, 99*, 3783-3798.

Lucchitta, B. K. (1999), Geologic map of Ophir and central Candor Chasmata (MTM–05072) of Mars, U.S. Geological Survey Investment Series, I-2568, Denver, USGS Information Services.

Lucchitta, B. K. (2008), HiRISE images of layered deposits in west Candor Chasma, Mars (II): Unconformities and possible gravity tectonics, Lunar and Planetary Science

XXXIX, League City, TX, 2317.

Lucente, C. C., and G. A. Pini, (2003), Anatomy and emplacement mechanism of a large submarine landslide within a Miocene foredeep in the northern Apennine, Italy: A field perspective. *American Journal of Science*, *303*, 565-602.

Lucente, C. C., and G. A. Pini (2008), Basin-wide mass-wasting complexes as markers of the Oligo-Miocene foredeep-accretionary wedge evolution in the Northern Apennines, Italy. *Basin Research, 20*, 49-71, doi: 10.1111/j.1365-2117.2007.00344.x.

MacNaughton, R. B., R. W. Dalrymple, G. M. Narbonne (1997), Early Cambrian braid-delta deposits, MacKenzie Mountains, north-western Canada, *Sedimentology*, *44*, 587-609.

Malin, M. C., and K. S. Edgett (2000), Sedimentary rocks of early Mars, *Science*, *290*, 1927-1937.

Malin, M. C., and K. S. Edgett (2001), Mars Global Surveyor Mars Orbiter Camera: Interplanetary cruise through primary mission, *Journal of Geophysical Research*, *106*, 23429-23570.

Malin, M. C., and K. S. Edgett (2003), Evidence for persistent flow and aqueous sedimentation on early Mars, *Science*, *302*, 1931-1934.

Malin, M. C., G. E. Danielson, A. P. Ingersoll, H. Masursky, J. Veverka, M. A. Ravine, and T. A. Soulanille (1992), The Mars Observer Camera, *Journal of Geophysical Research*, *97*, 7699-7718.

Malin, M., K. S. Edgett, L. V. Posiolova, S. M. McColley, E. Z. N. Dobrea (2006), Present-day impact cratering rate and contemporary gully activity on Mars, *Science*, *314*, 1573-1577.

Malin, M., J. F. Bell, B. A. Cantor, M. A. Caplinger, W. M. Calvin, R. T. Clancy, K. S. Edgett, L. Edwards, R. M. Haberle, P. B. James, S. W. Lee, M. A. Ravine, P. C. Thomas, and M. J. Wolff (2007), Context Camera Investigation on board the Mars Reconnaissance Orbiter, *Journal of Geophysical Research*, *112*, E05S04, doi:10.1029/2006JE002808.

Mallarino, G., R. T. Beaubouef, A. W. Droxler, V. Abreu, L. Labeyrie (2006), Sea level influence on the nature and timing of a minibasin sedimentary fill (northwestern slope of the Gulf of Mexico), *AAPG Bulletin*, *90*, 1089-1119.

Mangold, N., C. Quantin, V. Ansan, C. Delacourt, P. Allemand (2004), Evidence for precipitation on Mars from dendritic valleys in the Valles Marineris area, *Science*, *305*, 78-81.

Mangold, N., V. Ansan, P. Masson, C. Quantin, and G. Neukum (2008a), Geomorphic study of fluvial landforms on the northern Valles Marineris Plateau, Mars, *Journal of Geophysical Research, 113*, E08009, doi:10.1029/2007JE002985.

Mangold, N., A. Gendrin, B. Gondet, S. LeMouelic, C. Quantin, V. Ansan, J. P. Bibring, Y. Langevin, P. Masson, and G. Neukum (2008b), Spectral and geologic study of the sulfate-rich region of West Candor Chasma, Mars, *Icarus, 194*, 519-543.

McCollom, T. M., and B. M. Hynek (2005), A volcanic environment for bedrock diagenesis at Meridiani Planum on Mars, *Nature*, *438*, 1129-1131.

McEwen, A. S. (1989), Mobility of large rock avalanches: Evidence from Valles Marineris, Mars, *Geology*, *17*, 1111-1114.

McEwen, A. S., E. M. Eliason, J. W. Bergstrom, N. T. Bridges, C. J. Hansen, W. A.

Delamere, J. A. Grant, V. G. Gulick, K. E. Herkenhoff, L. P. Keszthelyi, R. L. Kirk, M. T. Mellon, S. W. Squyres, N. Thomas, and C. M. Weitz (2007), Mars Reconnaissance Orbiter's High Resolution Imaging Science Experiment (HiRISE), *Journal of Geophysical Research, 112*, E05S02, doi:10.1029/2005JE002605.

McLennan, S. (2003), Sedimentary silica on Mars, *Geology, 31*, 315-318.

McLennan, S. M., and J. P. Grotzinger (2008), The sedimentary rock cycle of Mars, in *The Martian Surface: Composition, Mineralogy, and Physical Properties*, edited by J. F. Bell, Cambridge University Press, 541-577.

McLennan, S. M., J. F. Bell, W. M. Calvin, P. R. Christensen, B. C. Clark, P. A. De Souza, J. Farmer, W. H. Farrand, D. A. Fike, R. Gellert, A. Ghosh, T. D. Glotch, J. P. Grotzinger, B. Hahn, K. E. Herkenhoff, J. A. Hurowitz, J. R. Johnson, S. S. Johnson, B. Jolliff, G. Klingelhöfer, A. H. Knoll, Z. Learner, M. C. Malin, H. Y. McSween, J. Pocock, S. W. Ruff, L. A. Soderblom, S. W. Squyres, N. J. Tosca, W. A. Watters, M. B. Wyatt, and A. Yen (2005), Provenance and diagenesis of the evaporite-bearing Burns formation, Meridiani Planum, Mars, *Earth and Planetary Science Letters, 240,* 95-121.

Mege, D., and P. Masson (1996), Amounts of crustal stretching in Valles Marineris, Mars, *Planetary and Space Science, 44,* 749-782.

Melosh, H. J. (1989), *Impact Cratering: A Geologic Process*, Oxford Monographs on Geology and Geophysics, Oxford University Press, New York, 245 p.

Metz, J. M., J. P. Grotzinger, D. M. Rubin, K. W. Lewis, S. W. Squyres, J. F. Bell (2009a), Sulfate-rich eolian and wet interdune deposits, Erebus crater, Meridiani Planum, Mars, *Journal of Sedimentary Research*, 79, 247-264.

Metz, J. M., J. P. Grotzinger, D. Mohrig, A. McEwen, C. Weitz, C. Pirmez, B. Prather (2009b), Sublacustrine depositional fans in Melas Chasma, *Journal of Geophysical Research 114,* E10002, doi:10.1029/2009JE003365.

Miall, A. D. (1992), Alluvial deposits, in *Facies Models: Geological Society of Canada*, edited by R. G. Walker, and N. P. James, St. John's, 119-142.

Middleton, G. V. (1993), Sediment deposition from turbidity currents, *Annual Reviews of Earth and Planetary Science*, *21,* 89-114.

Milliken, R. E., J. Grotzinger, R. A. Beyer, S. Murchie, and A. McEwen (2007), Evidence for salt tectonics in Valles Marineris, Mars, Seventh International Conference on Mars, Pasadena, CA.

Milliken, R. E., G. A. Swayze, R. E. Arvidson, J. L. Bishop, R. N. Clark, B. L. Ehlmann, R. O. Green, J. P. Grotzinger, R. V. Morris, S. L. Murchie, J. F. Mustard, C. M. Weitz (2008), Opaline silica in young deposits on Mars, *Geology*, *36*, 847-850.

Mohindra, R., and T. N. Bagati (1996), Seismically induced soft-sediment deformation structures (seismites) around Sumdo in the lower Spiti valley (Tethys Himalaya), *Sedimentary Geology,101*, 69-83.

Mohindra, R., and V. C. Thakur (1998), Historic large earthquake-induced soft sediment deformation features in the Sub-Himalayan Doon valley, *Geology Magazine, 135*, 269-281.

Montenat, C., P. Barrier, P. Ott d'Estevou, and C. Hilbsch (2007), Seismites: An attempt at critical analysis and classification, *Sedimentary Geology, 196*, 5-30, doi:10.1016/ j.sedgeo.2006.08.004.

Montgomery, D. R., and A. Gillespie (2005), Formation of Martian outflow channels by catastrophic dewatering of evaporite deposits, *Geology, 33*, 625-628.

Montgomery, D. R., M. Som, M. P. A. Jackson, B. C. Schreiber, A. R. Gillespie, J. B. Adams (2009), Continental-scale salt tectonics on Mars and the origin of Valles Marineris and associated outflow channels, *GSA Bulletin*, *121*, 117-133.

Moore, J. M., and A. D. Howard (2005), Large alluvial fans on Mars, *Journal of Geophysical Research*, *110*, E04005.

Mountney, N. P., and B. D. Thompson (2002), Stratigraphic evolution and preservation of aeolian dune and damp/wet interdune strata: an example from the Triassic Helsby Sandstone Formation, Cheshire Basin, UK, *Sedimentology, 49*, 805-833.

Murchie, S., R. Arvidson, P. Bedini, K. Beisser, J. P. Bibring, J. L. Bishop, J. Boldt, P. Cavender, T. Choo, R. T. Clancy, E. H. Darlington, D. J. Des Marais, R. Espiritu, D. Fort, R. Green, E. Guinness, J. Hayes, C. Hash, K. Heffernan, J. Hemmler, G. Heyler, D. Humm, J. Hutcheson, N. Izenberg, R. Lee, J. Lees, D. Lohr, E. Malaret, T. C. Martin, J. A. McGovern, P. McGuire, R. Morris, J. Mustard, S. M. Pelkey, E. Rhodes, M. Robinsson, T. L. Roush, E. Schaefer, G. Seagrave, F. Seelos, P. Silvergate, S. Slavney, M. Smith, W. -J. Shyoong, K. Strobehn, H. Taylor, P. Thompson, B. Tossman, M. Wirzburger, and M. Wolff (2007), Compact Reconnaissance Imaging Spectrometer for Mars (CRISM) on Mars Reconnaissance Orbiter (MRO), *Journal of Geophysical Research*, *112*, E05S03, doi:10.1029/ 2006JE002682.

Murchie, S. L., J. F. Mustard, B. L. Ehlmann, R. E. Milliken, J. L. Bishop, N. K. McKeown, E. Z. N. Dobrea, F. P. Seelos, D. L. Buczkowski, S. M. Wiseman, R. E. Arvidson, J. J. Wray, G. Swayze, R. N. Clark, D. J. D. Marais, A. S. McEwen, and

J. -P. Bibring (2009), A synthesis of Martian aqueous mineralogy after 1 Mars year of observations from the Mars Reconnaissance Orbiter, *Journal of Geophysical Research, 114*, E00D06, doi:10.1029/2009JE003342.

Mustard, J. F., C. D. Cooper, and M. K. Rifkin (2001), Evidence for recent climate change on Mars from the identification of youthful near-surface ground ice, *Nature, 412*, 411-414.

Mustard, J., S. L. Murchie, S. M. Pelkey, B. L. Ehlmann, R. E. Milliken, J. A. Grant, J. -P. Bibring, F. Poulet, J. Bishop, E. N. Dobrea, L. Roach, F. Seelos, R. E. Arvidson, S. Wiseman, R. Green, C. Hash, D. Humm, E. Malaret, J. A. McGovern, K. Seelos, T. Clancy, R. Clark, D. D. Marais, N. Izenberg, A. Knudson, Y. Langevin, T. Martin, P. McGuire, R. Morris, M. Robinson, T. Roush, M. Smith, G. Swayze, H. Taylor, T. Titus, and M. Wolff (2008), Hydrated silicate minerals on Mars observed by the Mars Reconnaissance Orbiter CRISM instrument, *Nature, 454*, 305-309, doi:10.1038/nature07097.

Mutti, E., R. Tinterri, G. Benevelli, D. di Biase, G. Cavanna (2003), Deltaic, mixed and turbidite sedimentation of ancient foreland basins, *Marine and Petroleum Geology*, *20*, 733-755.

Nedell, S. S., S. W. Squyres, and D. W. Anderson (1987), Origin and evolution of the layered deposits in the Valles Marineris, Mars, *Icarus, 70*, 409-441.

Nelson, C. H., D. C. Twitchell, W. C. Schwab, H. J. Lee, N. H. Kenyon (1992), Upper Pleistocene turbidite sand beds and chaotic silt beds in the channelized, distal, outer fan lobes of the Mississippi fan, *Geology*, *20*, 693-696.

Nelson, C. H., E. B. Karabanov, S. M. E. Colman (1999), Tectonic and sediment supply control of deep rift lake turbidite systems: Lake Baikal, Russia, *Geology*, *27*, 163-166.

Neuffer, D. P., and R. A. Schultz (2006), Mechanisms of slope failure in Valles Marineris, Mars. *Quarterly Journal of Engineering Geology & Hydrogeology*, *39*, 227-240.

Normark, W. R., and F. H. Dickson (1976a), Sublacustrine fan morphology in Lake Superior, *AAPG Bulletin*, *60*, 1021-1036.

Normark, W. R., and F. H. Dickson (1976b), Man-made turbidity currents in Lake Superior, *Sedimentology*, *23*, 815-831.

Obermeier, S. F. (1996), Use of liquefaction-induced features for paleoseismic analysis - An overview of how seismic liquefaction features can be distinguished from other features and how their regional distribution and properties of source sediment can be used to infer the location and strength of Holocene paleo-earthquakes, *Engineering Geology*, *44*, 1-76.

Okubo, C. H., K. W. Lewis, A. McEwen, R. L. Kirk (2008), Relative age of interior layered deposits in southwest Candor Chasma based on high-resolution structural mapping, *Journal of Geophysical Research*, *113*, E12002, doi:10.1029/2008JE003181.

Okubo, C. H., 2010, Structural geology of Amazonian-aged layered sedimentary deposits in southwest Candor Chasma, Mars, *Icarus*, doi: 10.1016/j.icarus.2009.11.012.

Olariu, C., and J. P. Bhattacharya (2006), Terminal distributary channels and delta front architecture of river-dominated delta systems, *Journal of Sedimentary Research*, *76*, 212-233.

O'Neill, C., A. M. Jellinek, and A. Lenardic (2007), Conditions for the onset of plate tectonics on terrestrial planets and moons, *Earth and Planetary Science Letters, 261*, 20-32.

Orange, D. L., J. Decker, P. A. Teas, R. D. Schneider, A. H. Saller, A. Heffernan, N. Maher, and M. Levey (2006), A modern basin-floor fan imaged in the Makassar Straits, Indonesia: Insights from high-resolution multibeam bathymetry and backscatter, sub-bottom profiler data and USBL-navigated cores, AAPG Annual Convention, Houston TX., April 9-12, 2006.

Parker, G., C. Paola, K. X. Whipple, D. Mohrig (1998), Alluvial fans formed by channelized fluvial and sheet flow. I: Theory, *Journal of Hydraulic Engineering-Asce*, *124*, 985-995.

Parker, G., and O. Sequeiros (2006), Large scale river morphodynamics: Application to the Mississippi Delta, in *RiverFlow 2006 Conference*, edited by R. M. L. Ferreria, Lisbon, Taylor and Francis, New York, 1067–1076.

Pattison, S. A. J. (2005), Storm-influenced prodelta turbidite complex in the lower Kenilworth Member at Hatch Mesa, Book Cliffs, Utah, USA: Implications for shallow marine facies models, *Journal of Sedimentary Research*, *75*, 420-439.

Pelkey, S. M., and B. M. Jakosky (2002), Surficial geologic surveys of Gale crater and Melas Chasma, Mars: integration of remote-sensing data, *Icarus, 160*, 228-257.

Pelkey, S. M., B. M. Jakosky, P. R. Christensen (2003), Surficial properties in Melas Chasma, Mars, from Mars Odyssey THEMIS data, *Icarus*, *165*, 68-89.

Pelkey, S. M., J. F. Mustard, S. Murchie, R. T. Clancy, M. Wolff, M. Smith, R. E. Milliken, J. P. Bibring, A. Gendrin, F. Poulet, Y. Langevin, and B. Gondet (2007), CRISM multispectral summary products: Parameterizing mineral diversity on Mars from reflectance, *Journal of Geophysical Research, 112*, E08S14, doi:10.1029/ 2006JE002831.

Pelletier, J. D., K. J. Kolb, A. S. McEwen, R. L. Kirk (2008), Recent bright gully deposits on Mars:Wet or dry flow? *Geology*, *36*, 211-214.

Peulvast, J. P., and P. L. Masson (1993), Melas Chasma: Morphology and tectonic patterns in central Valles Marineris (Mars), *Earth, Moon, and Planets*, *61*, 219-248.

Peulvast, J. P., D. Mege, J. Chiciak, F. Costard, P. Masson (2001), Morphology, evolution and tectonics of Valles Marineris wall slopes (Mars), *Geomorphology*, *37*, 329–352.

Pickering, K. T. et al. (1986), A high-sinuosity, laterally migrating submarine fan channel-levee-overbank: Results from DSDP Leg 96 on the Mississippi Fan, Gulf of Mexico, *Marine and Petroleum Geology, 3,* 3-18.

Plint, A. G., and J. A. Wadsworth (2003), Sedimentology and palaeogeomorphology of four large valley systems incising delta plains, western Canada Foreland Basin: implications for mid-Cretaceous sea-level changes, *Sedimentology*, *50*, 1147-1186.

Pope, M. C., J. F. Read, R. Bambach, and H. J. Hofmann (1997), Late Middle to Late Ordovician seismites of Kentucky, southwest Ohio and Virginia: Sedimentary recorders of earthquakes in the Appalachian basin, *GSA Bulletin, 109*, 489-503.

Quantin, C., P. Allemand, and C. Delacourt (2004), Morphology and geometry of Valles Marineris landslides, *Planetary and Space Science*, *52*, 1011-1022.

Quantin, C., P. Allemand, N. Mangold, G. Dromart, C. Delacourt (2005), Fluvial and lacustrine activity on layered deposits in Melas Chasma, Valles Marineris, Mars, *Journal of Geophysical Research*, *110*, E12S19, doi:10.1029/2005JE002440.

Roach, L. H., J. F. Mustard, S. L. Murchie, J. -P. Bibring, F. Forget, K. W. Lewis, O. Aharonson, M. Vincendon, and J. L. Bishop (2009a), Testing evidence of recent hydration state change in sulfates on Mars, *Journal of Geophysical Research, 114*, doi:10.1029/2008JE003245.

Roach, L. H., J. F. Mustard, G. A. Swayze, R. E. Milliken, J. L. Bishop, S. L. Murchie, and K. Lichtenberg (2009b), Hydrated mineral stratigraphy of Ius Chasma, Valles Marineris, *Icarus*, doi:10.1016/j.icarus.2009.09.003.

Robert, G., J. K. Russell, and D. Giordano (2008), Rheology of porous volcanic materials: High-temperature experimentation under controlled water pressure, *Chemical Geology*, *256*, 216-230.

Rodriguez, J. A. P., J. S. Kargel, D. A. Crown, L. F. Bleamaster, K. L. Tanaka, V. R. Baker, H. Miyamoto, J. M. Dohm, S. Sasaki, G. Komatsu (2006), Headward growth of chasmata by volatile outbursts, collapse, and drainage; Evidence from Ganges chaos, Mars, *Geophysical Research Letters*, *33*, L18203, doi:10.1029/ 2006GL026275.

Rodríguez-Pascua, M. A., J. P. Calvo, G. De Vicente, and D. Gómez-Gras (2000), Soft-sediment deformation structures interpreted as seismites in lacustrine sediments of the Prebetic Zone, SE Spain, and their potential use and indicators of earthquake magnitudes during Late Miocene, *Sedimentary Geology*, *135*, 117-135.

Røe, S. -L. (1987), Cross-strata and bedforms of probable transitional dune to upper-stage plane-bed origin from a Late Precambrian fluvial sandstone, northern Norway, *Sedimentology*, *34*, 89-101.

Roep, T. B., and A. J. Everts (1992), Pillow-beds: a new type of seismites? An example from an Oligocene turbidite fan complex, Alicante, Spain, *Sedimentology, 39*, 711-72.

Rothman, D. H., J. Grotzinger, P. B. Flemings (1994), Scaling in Turbidite Deposition, *Journal of Sedimentary Research, A64*, 59-67.

Rowan, M. G., F. J. Peel, and B. C. Vendeville (2004), Gravity-driven fold belts on passive margins, in *Thrust Tectonics and Hydrocarbon Systems*, edited by K. R. McClay, AAPG Memoir 82, 157-182.

Rubin, D. (1987), *Cross-Bedding, Bedforms, and Paleocurrents*, SEPM, Concepts in sedimentology and paleontology, 1, 187 p.

Rubin, D. M., and R. E. Hunter (1982), Bedform climbing in theory and nature, *Sedimentology, 29*, 121-138.

Sadler, P. M. (1981), Sediment accumulation rates and the completeness of stratigraphic sections, *Journal of Geology, 89*, 569-584.

Scherer, C. M. S., and E. L. C. Lavina (2005), Sedimentary cycles and facies architecture of aeolian-fluvial strata of the Upper Jurassic Guara Formation, southern Brazil, *Sedimentology, 52*, 1323-1341.

Scholz, C. A., and B. R. Rosendahl (1990), Coarse-clastic facies and stratigraphic sequence models from Lakes Malawi and Tanganyika, East Africa, in *Lacustrine Basin Exploration: Case Studies and Modern Analogs, Memoir 50*, edited by B. J. Katz, American Association of Petroleum Geologists, Tulsa, 151-168.

Schwartz, R. K. (1982), Bedform and stratigraphic characteristics of some modern small-scale washover sand bodies, *Sedimentology, 29*, 835-849.

Schultz, R. A. (1998), Multiple-process origin of Valles Marineris basins and troughs, Mars, *Planetary and Space Science*, *46*, 827-834.

Schultz-Ela, D. D. (2001), Excursus on gravity gliding and gravity spreading, *Journal of Structural Geology*, *23*, 725-731.

Schumm , S. A. (1963), Sinuosity of alluvial rivers on the Great Plains, *GSA Bulletin*, *74*, 1089-1099.

Schumm, S. A. (1977), *The Fluvial System*, John Wiley and Sons, Inc., New York.

Schwab, W. C., H. J. Lee, D. C. Twitchell, J. Locat, C. H. Nelson, W. G. McArthur, N. H. Kenyon (1996), Sediment mass-flow processes on a depositional lobe, outer Mississippi fan, *Journal of Sedimentary Research*, *66*, 916-927.

Scott, D. H., and K. L. Tanaka (1986), Geologic map of the western equatorial region of Mars, USGS, Reston VA.

Seilacher, A. (1969), Fault-graded beds interpreted as seismites, *Sedimentology*, *13*, 155-159.

Sharp, R. P. (1973), Mars: Fretted and chaotic terrains, Journal of *Geophysical Research, 78*, 4073–4083.

Shaw, J. (1972), Sedimentation in the ice-contact environment, with examples from Shropshire (England), *Sedimentology*, *18*, 23-62.

Simms, M. J. (2003), Uniquely extensive seismite from the latest Triassic of the United Kingdom: Evidence for bolide impact? *Geology*, *31*, 557-560.

Sims, J. D. (1975), Determining earthquake recurrence intervals from deformational structures in young lacustrine sediments, *Tectonophysics*, *29*, 141-152.

Skilling, I. P., M. G. Chapman, and B. K. Lucchitta (2002), Young, blocky flows in east Ius/west Melas and west Candor Chasmata, Mars: Debris avalanche deposits derived from interior layered deposits (ILD) mounds? Lunar and Planetary Science Conference XXXIII: League City, Texas, 1361.

Slingerland, R.L., and N. D. Smith (2004), River avulsions and their deposits, *Annual Reviews of Earth and Planetary Science 32*, 257–285, doi:10.1146/annurev.earth. 32.101802.120201.

Sohn, Y. K., C. W. Rhee, and B. C. Kim (1999), Debris flow and hyperconcentrated flood-flow deposits in an alluvial fan, northwestern part of the Cretaceous Yongdong Basin, central Korea, *Journal of Geology, 107*, 111-132.

Sowe, M., E. Hauber, R. Jaumann, K. Gwinner, F. Fueten, R. Stesky and G. Neukum (2007), Interior layered deposits in the eastern Valles Marineris and chaotic terrains on Mars, Lunar and Planetary Science Conference XXXVIII, Abstract 1568, League City, TX.

Soukhovitskaya, V. and M. Manga (2006), Martian landslides in Valles Marineris: Wet or dry? *Icarus, 180*, 348–352.

Smith, D. E., M. T. Zuber, H. V. Frey, J. B. Garvin, J. W. Head, D. O. Muhleman, G. H. Pettengill, R. J. Phillips, S. C. Soloman, H. J. Zwally, W. B. Banerdt, T. C. Duxbury, M. P. Golombek, F. G. Lemoine, G. A. Neumann, D. D. Rowlands, O. Aharonson, P. G. Ford, A. B. Ivanov, C. L. Johnson, P. J. McGovern, J. B. Abshire, R. S. Afzal, and X. Sun (2001), Mars Orbiter Laser Altimeter: Experiment summary after the first year of global mapping of Mars, *Journal of Geophysical Research*, *106*, 23689-23722.

Spencer, J. R., and F. P. Fanale (1990), New models for the origin of Valles Marineris closed depressions, *Journal of Geophysical Research*, *95*, 14301-14313.

Squyres, S. W., R. E. Arvidson, E. T. Baumgartner, J. F. Bell, P. R. Christensen, S. Gorevan, K. E. Herkenhoff, G. Klingelhofer, M. B. Madsen, R. V. Morris, R. Rieder, and R. A. Romero (2003), Athena Mars rover science investigation, *Journal of Geophysical Research, 108,* E12, doi:10.1029/2003JE002121.

Squyres, S. W., J. P. Grotzinger, R. E. Arvidson, J. F. Bell, C. W. Calvin, P. R. Christensen, B. C. Clark, J. A. Crisp, W. H. Farrand, K. E. Herkenhoff, J. R. Johnson, G. Klingelhöfer, A. H. Knoll, S. M. McLennan, H. Y. McSween, R. Morris, J. W. Rice, R. Rieder, and L. A. Soderblom (2004), In situ evidence for an ancient aqueous environment at Meridiani Planum, Mars, *Science, 306,* 1709-1714.

Squyres, S. W., A. H. Knoll, R. E. Arvidson, B. C.Clark, J. P. Grotzinger, B. L. Jolliff, S. M. McLennan, N. J. Tosca, J. F. Bell, W. M. Calvin, W. H. Farrand, T. D. Glotch, M. P. Golombek, K. E. Herkenhoff, J. R. Johnson, G. Klingelhöfer, H. Y. McSween, and A. S. Yen (2006), Two years at Meridiani Planum: Results from the Opportunity Rover, *Science, 313*, 1403-1407.

Squyres, S., O. Aharonson, B. Clark, B. A. Cohen, L. Crumpler, P. A.De Souza, W. H. Farrand, R. Gellert, J. Grant, J. P. Grotzinger, A. F. Haldemann, J. R. Johnson, G. Klingelhöfer, K. Lewis, R. Li, T. McCoy, A. S. McEwen, H. Y. McSween, D. W. Ming, J. M. Moore, R. V. Morris, T. J. Parker, J. W. Rice, S. W. Ruff, M. Schmidt, C. Schröder, L. A. Soderblom and A. Yen (2007), Pyroclastic activity at Home Plate in Gusev Crater, Mars, *Science, 316*, 738-742.

Stanistreet, I. G., T. S. McCarthy (1993), The Okavango Fan and the classification of subaerial fan systems, *Sedimentary Geology, 85*, 115-133.

Stolper, D., M. Kennedy, and J. Grotzinger (2007), Scale of lamination in sedimentary rocks as a guide to depositional process on Mars (Abstract), Geological Society of America.

Straub, K. M., D. Mohrig, B. McElroy, J. Buttles, and C. Pirmez (2008), Interactions between turbidity currents and topography in aggrading sinuous submarine channels: A laboratory study, *GSA Bulletin, 120*, 368-385, doi: 10.1130/B25983.1.

Torres, J., L. Droz, B. Savoye, E. Terentieva, P. Cochonat, N. H. Kenyon, and M. Canals (1997), Deep-sea avulsion and morphosedimentary evolution of the Rhine Fan Valley and Neofan during the Late Quaternary (north-western Mediterranean Sea), *Sedimentology, 44*, 457-477.

Tosca, N. J., S. M. McLennan, B. C. Clark, J. P. Grotzinger, J. A. Hurowitz, A. H. Knoll, C. Schröder, and S. W. Squyres (2005), Geochemical modeling of evaporation processes on Mars: Insight from the sedimentary record at Meridiani Planum, *Earth and Planetary Science Letters*, *240*, 122-148.

Tosca, N., A. Knoll, A., and S. McLennan (2008a), Water activity and the challenge for life on early Mars, *Science, 320*, 1204-1207.

Tosca, N. J., R. E. Milliken, M. B. Wyatt, and S. M. McLennan (2008b), Clay minerals and poorly crystalline silicates: Unraveling paleo-acidity at the Martian surface, Lunar and Planetary Science Conference XXXIX: League City, TX.

Trimble, S. W. (1981), Changes in sediment storage in the Coon Creek Basin, Driftless Area, Wisconsin, *Science*, *214*, 181-183.

Twitchell, D. C., W. C. Schwab, N. H. Nelson, N. H. Kenyon, H. J. Lee (1992), Characteristics of a sandy depositional lobe on the outer Mississippi Fan from SeaMARC 1A sidescan sonar images, *Geology*, *20*, 689-692.

van der Werff, W., and S. D. Johnson (2003), Deep-sea fan pinch-out geometries and their relationship to fan architecture, Tanqua Karoo basin (South Africa), *International Journal of Earth Sciences, 92*, 728-742.

Viseras, C., M. L. Calvache, J. M. Soria, J. Fernández (2003), Differential features of alluvial fans controlled by tectonic or eustatic accommodation space. Examples from the Beltic Cordillera, Spain., *Geomorphology, 50*, 181-202.

Walker, R. G. (1992), Turbidites and Submarine Fans, in *Facies Models: Response to Sea Level Change*, edited by R. G. Walker and N. P. James, Geological Association of Canada, Ontario, 239-263.

Walling, D. E., P. N. Owens, G. J. L. Leeks (1999), Rates of contemporary overbank sedimentation and sediment storage on the floodplains of the main channel systems of the Yorkshire Ouse and River Tweed, UK, *Hydrological Processes*, *13*, 993-1009.

Wellner, R., R. T. Beaubouef, J. C. Van Wagoner, H. Roberts, T. Sun (2005) Jet-plume depostional bodies - the primary building blocks of Wax Lake Delta, *Gulf Coast Association of Geological Societies Transactions*, *55*, 867-909.

Weitz, C. M., T. J. Parker, F. S. Anderson, and J. A. Grant (2001), The interior layered deposits of Valles Marineris: Layering, erosional processes, and age relationships, Lunar and Planetary Science Conference XXXII, Abstract 1629, League City, TX.

Weitz, C. M., T. J. Parker, M. H. Bulmer, F. S. Anderson, and J. A. Grant (2003), Geology of the Melas Chasma landing site for the Mars Exploration Rover mission, *Journal of Geophysical Research, 108*, 8082, doi:10.1029/2002JE002022.

Weitz, C., R. E. Milliken, J. A. Grant, A. S. McEwen, R. M. E. Williams, J. L. Bishop, and B.J. Thompson (2009) Mars Reconnaissance Orbiter observations of light-toned layered deposits and associated fluvial landforms on the plateaus adjacent to Valles Marineris, *Icarus, 205,* 73-102, doi: 10.1016/j.icarus.2009.04.017

Wells, S. G., and A. M. Harvey (1987), Sedimentologic and geomorphic variations in storm-generated alluvial fans, Howgill Fells, northwest England, *GSA Bulletin*, *98*, 182-198.

Whipple, K. X., and T. S. Dunne (1992), The influence of debris-flow rheology on fan morphology, Owens Valley, California, *GSA Bulletin*, *104*, 887-900.

Williams, G. E. (1971), Flood deposits of the sand-bed ephemeral streams of central Australia, *Sedimentology, 17*, 1-40.

Williams-Stroud, S. C., and J. Paul (1997), Initiation and growth of gypsum piercement structures in the Zechstein Basin, *Journal of Structural Geology, 19*, 897-907.

Winston, D. (1978), Fluvial systems of the Precambrian Belt Supergroup, Montana and Idaho, U.S.A., in *Fluvial Sedimentology,* edited by A. D. Miall, Canadian Society of Petroleum Geologists Memoir 5, 343-359.

Witbeck, N. E., K. L. Tanaka, and D. H. Scott (1991), *Geologic Map of Valles Marineris Region, Mars, MAP I-2010,* U. S. Geological Survey, Reston, VA.

Wohletz, K. H., and M. F. Sheridan (1979), Model of pyroclastic surge, Geological Society of America Special Paper, 180, 177-194.

Wood, L. J. (2006), Quantitative geomorphology of the Mars Eberswalde delta, *GSA Bulletin*, *118*, 557-566.

Wynn, R. B., B. T. Cronin, J. Peakall (2007), Sinuous deep-water channels: Genesis, geometry and architecture, *Marine and Petroleum Geology, 24*, 341-387.

Yu, B., A. Cantelli, J. G. Marr, C. Pirmez, C. O'Byrne, G. Parker (2006), Experiments on self-channelized subaqueous fans emplaced by turbidity currents and dilute mudflows, *Journal of Sedimentary Research, 76,* 889-902.

Zegers, T. E., W. Dabekaussen, E. Hauber, K. Gwinner, F. Scholten, F. Fueten, R. Stesky, P. MacKinnon, G. Neukum, and H. C. -I. Team (2006), 3D Structural analysis of Ophir Chasma based on HRSC data and stereo-derived DTM, Lunar and Planetary Science Conference XXXVII, Abstract 1605, League City, TX.